République Algérienne Démocratique et Populaire
Ministère de l'Enseignement Supérieur et de la Recherche Scientifique
Université A. MIRA-BEJAIA

Faculté : Sciences Exactes
Département : Informatique
Laboratoire ou unité de recherche de rattachement : Laboratoire d'Informatique Médicale et des Environnements Dynamiques et intelligents (LIMED)

THÈSE

EN VUE DE L'OBTENTION DU DIPLOME DE DOCTORAT

Domaine : Mathématique et Informatique. Filière : Informatique
Spécialité : Intelligence artificielle et Génie logiciel
Présentée par

Rachida ZEGOUR

Thème

Segmentation d'images par les techniques du Deep Learning, cas des images de la peau sur IRM haute résolution

Soutenue le : 07/03/2024

Devant le Jury composé de :

Nom et Prénom	Grade	Université	Qualité
Mme Soraya ALOUI	MCA	Univ. de Bejaia	Présidente
Mr Ahror BELAID	Professeur	Univ. de Bejaia	Rapporteur
Mr Douraied BEN SALEM	Professeur	Univ. de Brest, France	Co- Rapporteur
Mr Djamel GACEB	Professeur	Univ. de Boumerdes	Examinateur
Mme Houda EL BOUHISSI	MCA	Univ. de Bejaia	Examinatrice

Année Universitaire : 2023 /2024

People's Democratic Republic of Algeria
Ministry of Higher Education and Scientific Research
A.MIRA-BEJAIA university

Faculty : Sciences Exact
Department : **Computer Science**
Research laboratory : **Laboratory of Medical Informatics and Intelligent and Dynamic Environments (LIMED)**

THESIS
IN VIEW OF OBTAINING THE DOCTORAL DEGREE

Domain: Mathematics and Computer Science. Sector: **Computer Science**

Specialty: Artificial Intelligence and Software Engineering

Presented by :
Rachida ZEGOUR

Theme

Image segmentation using Deep Learning techniques, case of skin images on high resolution MRI

Defended on: 07/03/2024

Board of examiners:

First and last name	Grade	University	Quality
Mrs Soraya ALOUI	MCA	Univ. of Bejaia	Présidente
Mr Ahror BELAID	Professeur	Univ. of Bejaia	Examiner
Mr Douraied BEN SALEM	Professeur	Univ. of Brest, France	Co-Examiner
Mr Djamel GACEB	Professeur	Univ. of Boumerdes	Examiner
Mrs Houda EL BOUHISSI	MCA	Univ. of Bejaia	Examiner

Academic year : 2023/2024

Acknowledgment

I extend my heartfelt gratitude to my esteemed supervisors, Professor **BELAID Ahror** and Professor **BEN SALEM Douraied**, for their invaluable guidance, mentor ship, and unwavering support throughout my research journey. Their expertise and dedication have been instrumental in shaping the direction and quality of this work.

I am also thankful to the entire team at the **Laboratory of Medical Informatics and Intelligent and Dynamic Environments (LIMED)** for their collaboration, insightful discussions, and contributions to this research project. Their collective efforts have significantly enriched the outcomes of this study.

Furthermore, I would like to express my deepest appreciation to my family, especially my precious children, for their patience, understanding, and unwavering support during this challenging endeavor. Their love and encouragement have been my driving force.

Dedications

With unwavering support, their mentorship, encouragement, and wisdom have been the guiding beacons that transformed challenges into opportunities, shaping my scholarly pursuits into a rewarding odyssey.

To my esteemed parents, whose boundless love, sacrifices, and unwavering belief in my potential have been the guiding lights on this challenging yet rewarding path.

To my remarkable husband, your unwavering support, understanding, and encouragement have been an unwavering foundation. Your belief in my capabilities has fueled my determination and sustained me through every academic endeavor.

To my cherished children, your laughter, warmth, and patience during late-night study sessions have transformed challenges into cherished memories. You serve as a daily reminder of the profound purpose behind this academic pursuit.

To my brothers and sisters, whose support, understanding, and shared moments of familial strength have been an integral part of my journey. Your presence has added immeasurable value to the tapestry of my academic odyssey.

To my dearest friends and peers, whose camaraderie, understanding, and shared moments of respite have been the much-needed balm during the most demanding phases of this intellectual journey. Your friendship has rendered the challenges more bearable and the successes more celebratory.

I extend my heartfelt appreciation to all of you for being the guiding stars on my academic odyssey.

With deep gratitude,
Dr. Rachida ZEGOUR.

List of publications

International papers

- **R. Zegour**, A. Belaid, and D. Ben Salem. "A Segmentation Method of Skin MRI 3D High Resolution in Vivo: Array". Medical Technologies Journal, vol. 2, no. 3, Sept. 2018, pp. 255-61, doi:10.26415/2572-004X-vol2iss3p255-261.

- **R. Zegour**, A. Belaid, J.Ognard and D. Ben Salem. "Convolutional neural networks-based method for skin hydration measurements in high resolution MRI". Biomedical Signal Processing and Control. Elsevier, 2023. Vol. 81, March 2023, 104491, doi: 10.1016/j.bspc.2022.104491.

List of Contents

Contents

List of Figures

List of Tables

List of Abbreviations

AI	Artificial Intelligence
CNN	Convolutional Neural Network
CT	Computed Tomography
DICOM	Digital Imaging and Communications in Medicine
DL	Deep Learning
DP	Proton Density
DSNet	Dermoscopic Skin Network
DSC	Dice Similarity Coefficient
FCN	Fully Connected Network
fMRI	Functional Magnetic Resonance Imaging
IOU	Union or Jaccard Loss
ISIC	International Skin Imaging Collaboration
KLD	Kullback-Leibler Divergence
LC	Langerhans Cell
MSE	Mean Squared Error
MSD	Mean Squared Difference
MRI	Magnetic Resonance Imaging
NMR	Nuclear Magnetic Resonance
NRRD	Nearly Raw Raster Data
PET	Positron Emission Tomography
PVE	Partial Volume Effects
RF	Radio Frequency
RNN	Recurrent Neural Network
ROI	Region of Interest
SC	Stratum Corneum
SGD	Stochastic Gradient Descent
SNR	Signal to Noise Ratio

List of Abbreviations

T	Tesla
T1	T1 weighted
T2	T2 weighted
TE	Echo Time
TR	Repetition Time
3D	Three-Dimensional
2D	Two-Dimensional

Introduction

The biomedical field has witnessed significant advancements in medical image generation through high-performance imaging modalities such as CT scans, MRI, and ultrasound. Medical imaging is recognized as a crucial component of medical data representation, visually communicating data. Magnetic Resonance Imaging (MRI) is a vital medical application that has seen a substantial increase in medical data over the past decade. MRI allows for the visualization of different human organs with clear discrimination between tissue structures. In dermatology, high-resolution magnetic resonance imaging enables the visualization of various skin layers and provides insights into their physical and biochemical characteristics [1]. This modality is particularly useful for investigating skin hydration levels through various morphological, physical, and chemical features. However, the MRI technique produces a vast amount of data that needs to be organized, displayed, and transmitted quickly and effectively. Extracting information from this big data is hindered by obstacles such as statistical counting noise, systematic biases, image presentation, filtering, feature identification, pattern recognition, exchange, modification, compression, and short-term storage [2]. For these reasons, biomedical applications have made it challenging for doctors to analyze and comprehend this enormous amount of data. Consequently, various scientific research efforts have focused on developing computer-based techniques to process medical images.

Today, Artificial Intelligence (AI) plays a significant role in enhancing healthcare applications for diagnosis, treatment planning, treatment guidance, and disease progression tracking in the biomedical field. Machine Learning (ML) is one key area that has greatly contributed to medical data processing [3]. ML aims to identify and learn patterns from data, and it requires a substantial amount of data to discover hidden patterns or make predictions based on them. Among ML techniques, Deep Learning (DL) methods have been frequently used in image processing tasks. DL applied to medical imaging can improve precision medicine, analyze patient risk factors, enhance medical tests, and reduce the workload for doctors. Convolutional Neural Networks (CNNs), a DL-based technique, are commonly employed in computer vision tasks [4]. Semantic segmentation is a popular task in human skin data, which involves dividing medical images into different classes based on their similar properties. The goal of this method is to

extract features and representations and assign a class label (skin layer) to each pixel in the input image [5].

The research work on which this thesis is based falls within the field of skin layer segmentation using deep learning techniques, specifically the segmentation of high-resolution MRI skin images. The primary objective of this thesis is to measure skin hydration levels before and after the application of a moisturizing cream. To achieve this objective, we propose a deep learning segmentation method based on CNN networks to detect skin layers using high-resolution MRI. Currently, this process is typically performed manually by doctors, requiring precision, considerable time, and resulting in a "rough" estimate due to the lack of precision. Therefore, our work aims to propose an automatic skin segmentation method. After this process, we will quantify the hydration level for each skin layer based on T2 mapping cartographies. Furthermore, we will propose a skin hydration simulation method based on a CNN auto-encoder model.

Clinical motivation

Skin hydration is a fundamental aspect of skin health and appearance, and this is clearly evident from compelling statistics. For example, research indicates that approximately 40% [6] of the world's population experiences issues with skin dryness or reduced hydration at various times, underscoring the widespread importance of this parameter. Precise measurements of skin hydration, including innovative techniques such as MRI (Magnetic Resonance Imaging), assist dermatologists in diagnosing a wide range of skin problems, from simple dryness to more complex dermatological issues. Furthermore, monitoring changes in hydration levels before and after treatments, often through the non-invasive power of MRI, is essential for evaluating treatment effectiveness and adapting them as needed. These data enable doctors to provide personalized recommendations for skincare routines and product choices based on the individual hydration needs of each person. The utilization of MRI in clinical applications not only enhances our clinical understanding of skin health but also aids in providing personalized, effective care plans for patients, addressing both medical and cosmetic concerns. MRI, with its ability to visualize and quantify skin hydration at various depths, has revolutionized our approach to dermatological care, offering insights that were previously unattainable. It exemplifies the synergy between cutting-edge technology and the art of skincare, ultimately benefitting patients in their quest for healthy, radiant skin.

Technical motivation

The core of our research hinges on harnessing cutting-edge techniques to advance the field of skin hydration analysis. T2 mapping segmentation using deep learning, specifically convolutional neural networks (CNNs), stands as a pivotal component. By employing CNNs, we aim to automate and refine the segmentation process, offering unparalleled precision and efficiency. Furthermore, our research extends beyond mere segmentation; we delve into the intricate realm of data registration. Leveraging registration algorithms, we ensure the alignment of multiple imaging modalities, enabling precise visualization of hydration dynamics at different skin layers. This integration not only enhances our understanding of skin hydration but also opens avenues for more accurate clinical assessments. Additionally, we employ regression models for simulation, allowing us to recreate and analyze skin hydration scenarios under various conditions. This simulation capability is invaluable for comprehending the impact of treatments, environmental factors, and skincare products on skin hydration. In summary, our technical motivation revolves around seamlessly integrating T2 mapping segmentation, CNNs, registration algorithms, and regression models. This synergy aims to elevate the accuracy and depth of our skin hydration analysis, ultimately contributing to enhanced clinical insights and the development of more effective skincare solutions.

Contribution of this research

In this context, we will propose a deep learning segmentation approach for skin layers in MRI images. The approach proposed in this work is based on Convolutional Neural Networks (CNNs). CNNs have proven their effectiveness in skin segmentation, as we will discuss in the literature review chapter. This approach encompasses various architectures that enable the automatic segmentation of skin layers. In this study, we will focus on the U-net and Dens-net architectures. The aims of this study consist of:

- **Data preprocessing:** In this work, we will utilize real data collected in a medical laboratory, which, initially, was of a relatively small size, not meeting the requirements for CNNs. Data preprocessing presents a significant challenge in this work to achieve high-performance CNN training with high accuracy. To address this challenge, we will employ various techniques, including One-Hot Encoding and data augmentation.
- **A skin segmentation approach**: Our segmentation approach based on deep learning aims to develop a method for measuring skin hydration using MRI data, both before and after the application of moisturizing cream. The measurement of hydration will be based

on T2 mapping cartographies, which enable the observation of water content in each skin layer. Additionally, we will automate this approach using deep learning techniques, imaging tools such as ImagingFiji, and mathematical morphology to calculate the T2 values based on imaging intensity.

- **A skin regression approach**: Our regression approach based on deep learning aims to simulate the skin hydration phenomena. We proceeded according to this, in order to evaluate the performance of artificial skin hydration. In other word we proposed a CNN model that can predict the hydration effect after the application of hydrated cream on the feet for MRI skin data.

Structure of the research

The dissertation is organized into four chapters.

- **Chapter 1**: Provides an introduction to the principles and concepts associated with skin hydration, as well as an overview of the different physical aspects that describe Magnetic Resonance Imaging (MRI).
- **Chapter 2**: Is dedicated to providing an overview of Convolutional Neural Networks (CNNs). It is divided into three main sections: skin segmentation, skin hydration measurements, and skin registration. Each section discusses the relevant techniques and methodologies employed in these areas.
- **Chapter 3**: We present the proposed approach, which builds upon the foundations established in the previous chapters. This chapter summarizes the work done in skin segmentation, skin hydration measurements, and skin registration, introducing our approach and methodology.
- **Chapter 4**: Focuses on the presentation of the results obtained from the application of our proposed approach. Additionally, we describe the similarity matrices that were used to evaluate the performance of our results.

Finally, the dissertation concludes with a general conclusion, summarizing the findings and contributions of the research. We also provide some perspectives for future work in the field. By structuring the dissertation in this manner, we aim to provide a comprehensive understanding of the principles and concepts of skin hydration, Magnetic Resonance Imaging, and Convolutional Neural Networks. We present the proposed approach and its application in skin segmentation, skin hydration measurements, and skin registration, followed by the presentation and evaluation

of the results. The dissertation concludes with a summary of the findings and potential avenues for future research.

CHAPTER 1

Clinical background and medical concepts

1.1 Introduction

Nowadays, thanks to the advancements in scientific research in the medical field, medicine has made remarkable progress in various clinical applications. Medical imaging plays a crucial role in scientific research as it enables the visualization of different anatomical regions of the human body, providing comprehensive information in the form of medical images. These imaging techniques contribute to a better understanding of diseases and support decision-making for medical professionals. Currently, there are several imaging modalities available in medical applications for various purposes, such as diagnosis, treatment planning, treatment guidance, and disease monitoring, all aimed at enhancing healthcare outcomes.

Our specific research area focuses on the study of the water content of human skin, which is essential for ensuring proper skin hydration and directly influences the mechanical and physical properties of the skin. This chapter aims to provide foundational knowledge and concepts necessary for measuring skin hydration using medical imaging, specifically Magnetic Resonance Imaging (MRI). MRI is an effective method for studying skin hydration due to its ability to capture a multitude of morphological, physical, and chemical properties. The chapter begins by describing the anatomy and physiology of the skin, with a particular emphasis on the skin's hydration function. Additionally, the fundamental components of an MRI system and their parameters are outlined. These concepts serve as the basis for understanding Magnetic Resonance Imaging and skin anatomy, forming the fundamental background for this dissertation. Furthermore, the chapter discusses the benifites and limitations of MRI applications concerning data collection in a clinical setting.

1.2 Skin anatomy and physiology

Skin is the outermost protective covering of the human body, serving as a barrier against external microbial threats. It spans the entire surface area of the body and consists of four main layers, which are described as follows: (Figure 1.2.1):

- **(1) Stratum corneum**: The outermost protective skin layer, is primarily made up of dead keratinocytes. It only appears as a high-signal band separating from the live epidermis at the heel [7] and fingers [8, 9].
- **(2) Epidermis**: The waterproof barrier layer that composed of approximately 95% of keratinocytes, with three sublayers: stratum basal, stratum spinous, stratum granular, and many skin holes, such as hair follicles and sweat ducts. These layers are undergoing continuous transformation and form the remaining (5%) with a set of immune cells such as Langerhans cells (LCs), γδ T cells and resident memory (T) cells that insure the immunological of the skin anatomy [10].
- **(3) Dermis**: Is beneath the epidermis fibrous tissue rich in collagen, which is composed of fibroblasts, dermal dendritic cells, spermatocytes and macrophages (70%). Other components include collagen, elastic fibres and air follicles. The dermis is grouped into two categories: papillary dermis and reticular dermis [10].
- **(4) Hypodermis**: The deeper subcutaneous tissue is made of fat and connective tissue [10]. It is occasionally seen as subcutaneous tissue and other times as a component of the skin [10, 11].

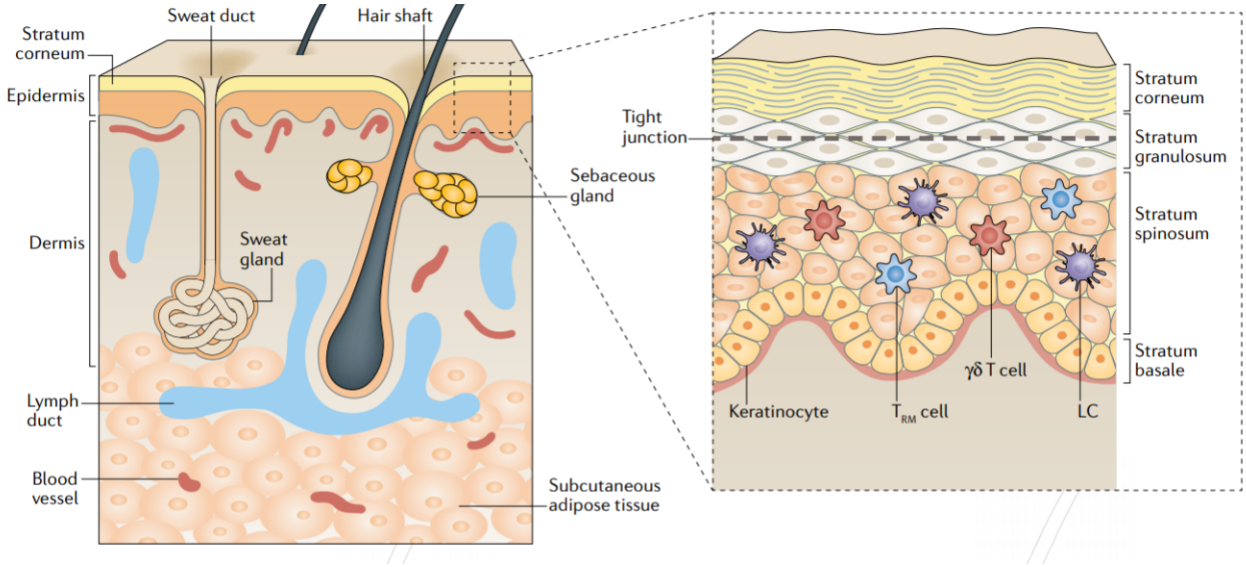

Figure 1.2.1: Anatomical skin structure.

The skin carries out a variety of essential tasks, including safeguarding the body from external physical, chemical, and biological threats, preventing excessive water loss from the body, and aiding in thermoregulation [12]. In the next section, we will discuss the most important function of the skin, which is highly complex and influences the mechanical and physical properties of the skin.

1.3 Skin hydration function

Water has a significant distribution in the human body and plays a crucial role in maintaining normal physiological balance. It serves as the primary component of cells and tissues, accounting for 75% of the body's composition at birth and around 60% in adults. The distribution of water in the layers of the skin plays a key role in various skin functions, including the water "barrier" function and the "envelope" function [13]. Hydration is a necessary function that involves several synergistic mechanisms to maintain body homeostasis [3]. However, skin hydration can be compromised daily due to environmental stressors that the skin is exposed to. To maintain moisturized skin, several techniques have been developed. Some of these techniques are in vitro methods [14] that include water flux analysis, electrical measurements, photo-acoustic spectroscopy, viscoelastic properties, topography, among others. Other techniques are in vivo approaches that utilize confocal Raman microscopy [15]. These techniques

employ newly developed methods for measuring skin hydration, such as silicon image sensor technology, near-infrared spectroscopy, nuclear magnetic resonance spectroscopy, and transient thermal transfer [16]. The measurement of transepidermal water loss is also one of the easiest in vivo methods used to assess skin hydration, as it has an inverse relationship with hydration levels [17]. However, these traditional invasive techniques do not directly monitor water content; rather, they measure changes in specific skin parameters. One major disadvantage of these measurement techniques is that they can temporarily disrupt the barrier function and water-holding capacity of the stratum corneum or increase sweat gland activity [18].

In the late 80s, the proton magnetic resonance technique was proposed as a non-invasive method to provide simultaneous information about various morphological, physical, and chemical parameters of the skin. This technique enables the generation of water cartography, which is an excellent way to observe water distribution in vivo across different skin layers and study hydration. Moreover, in dermatology, MRI techniques are utilized to examine the impact of moisturizing products such as creams, emulsions, and gels on skin hydration. This approach can serve as an alternative to in vivo investigations conducted on humans and animals for evaluating novel dermatological formulations [19]. The following sections will describe medical imaging concepts and explain the proton magnetic resonance technique as a medical tool that helps in assessing water content in human skin.

1.4 Medical imaging

Imaging is a modern diagnostic tool that has been recently introduced in medical applications to enhance and streamline the diagnostic process. It provides a non-invasive means of visualizing the structures of the human body. Nowadays, due to significant advancements in imaging technology across various clinical fields, hospitals and research organizations are equipped with state-of-the-art imaging tools that assist clinicians in making accurate diagnoses, particularly in complex medical cases before surgical interventions.

An important question arises: How are medical images obtained using these different imaging modalities? In essence, these medical tools are based on the physical properties of body tissues. They gather information by interacting with the body and utilize this information to generate medical images. In his book on medical imaging physics, Hendee William [20] provides the following definition of medical images:

> *"Medical images are pictures of tissue characteristics that influence the way energy is emitted, transmitted, reflected, and so on, by the human body. These characteristics*

are related to, but not the same as, the actual structure (anatomy), composition (biology and chemistry), and function (physiology and metabolism) of the body."

This definition provides a comprehensive understanding of the physical principles involved in the creation of medical images. It emphasizes the application of a carefully chosen energy source with distinct physical properties to a specific area of the body. Through this process, valuable information is generated, which is subsequently processed and transformed into a visual representation in the form of an image. The definition also highlights the significance of medical images in providing crucial insights into the internal structures and functions of the body. By enabling visualization and analysis of anatomical and physiological features, medical images play a pivotal role in the diagnostic process and treatment planning. They offer healthcare professionals a non-invasive means to gather detailed and accurate information about the human body, thereby reducing the need for invasive procedures.

The realm of medicine has undergone a paradigm shift through the development and integration of advanced imaging tools, endowing healthcare practitioners with unparalleled diagnostic capabilities. These cutting-edge imaging technologies have ushered in a new era, fundamentally altering the landscape of disease detection, diagnosis, and monitoring. They furnish intricate and accurate insights, fostering elevated standards of patient care and outcomes. Through the utilization of diverse imaging modalities including X-rays, magnetic resonance imaging (MRI), computed tomography (CT), and ultrasound, medical professionals glean invaluable insights into the inner intricacies and functionalities of the human body. Each modality uniquely engages with the body, employing distinct physical principles to capture pertinent information. For instance:

- **X-rays** pass through the body and are absorbed to varying degrees by different tissues, resulting in an image that reflects the differential absorption. This enables the visualization of bones, lungs, and other dense structures [21].

- **MRI** on the other hand, employs powerful magnetic fields and radio waves to generate highly detailed images based on the unique relaxation properties of tissues. By exploiting the inherent magnetic properties of hydrogen atoms in the body, MRI provides exceptional soft tissue contrast [22].

- **CT scans** utilize X-rays from multiple angles to reconstruct cross-sectional images of the body. By rotating the X-ray source and detector around the patient, a series of images are acquired and processed by computer algorithms to create detailed 3D images of internal structures [23].

- **Ultrasound imaging** utilizes high-frequency sound waves that are emitted by a transducer and directed into the body. These sound waves then bounce off tissues, and the returning echoes are used to generate real-time images. This modality is commonly used for imaging organs, blood vessels, and developing fetuses [24].

In medical imaging, each modality boasts distinct strengths and limitations, tailoring them to specific clinical scenarios. Choosing the optimal modality hinges on factors like the area of focus, desired level of detail, and associated risks. In all instances, the energy source interacts with the body, yielding data that is processed, captured, and transformed into images packed with crucial diagnostic insights [25].

The upcoming section provides an in-depth exploration of Magnetic Resonance Imaging (MRI), encompassing its hardware and software elements. A solid grasp of the MRI system's complex hardware and software is essential for effectively using and interpreting MRI images across diverse medical contexts. Within this thesis's framework, this profound understanding of the MRI system lays the foundation for utilizing its potential in evaluating and analyzing skin hydration. By skillfully amalgamating MRI technology with advanced methodologies, our aim is to refine our grasp of skin hydration and measurement, ultimately influencing healthcare outcomes positively.

1.4.1 Magnetic Resonance Imaging (MRI)

Magnetic Resonance Imaging (MRI) is a non-invasive imaging technique that relies on the physical phenomenon of Nuclear Magnetic Resonance (NMR). NMR was initially used to observe and analyze the nuclear structure of atoms by applying a magnetic field and a radio frequency (RF) pulse. This phenomenon utilizes the magnetic properties of certain atoms, such as the hydrogen proton ^{1}H, sodium^{23}Na, carbon ^{13}C ....etc [26]. As the human body is made of 70% water (H_2O). In clinical applications, Magnetic Resonance Imaging (MRI) utilizes the Nuclear Magnetic Resonance (NMR) phenomenon, which is based on the magnetic properties of hydrogen atoms, to generate medical images. The nucleus of a hydrogen atom contains an odd number of protons, resulting in a magnetic moment known as nuclear spin. When there is no external magnetic field, the spins are randomly oriented in space and their magnetization, represented as $M^{\rightarrow}$, is zero [27]. However, when the spins are subjected to an external influence, the following phases describe the creation of the NMR signal [27].:

- **Polarizing field phase** β_0: When an intense magnetic field β_0 is applied to hydrogen protons, some spins align parallel to the magnetic field while others align antiparallel. When the number of parallel spins is greater than the number of antiparallel spins, resulting in a non-zero magnetization ($M^{\rightarrow} \neq 0$), the spins reach an equilibrium state and

exhibit a precessional motion around β_0. The speed of precession is determined by the strength of the magnetic field and is characterized by the angular frequency of precession, denoted as $f_0 = \gamma\beta_0$, where γ is the gyromagnetic ratio of the atom (for hydrogen, $\gamma = 42.58 :: MHz/T$) (Figure 1.4.1).

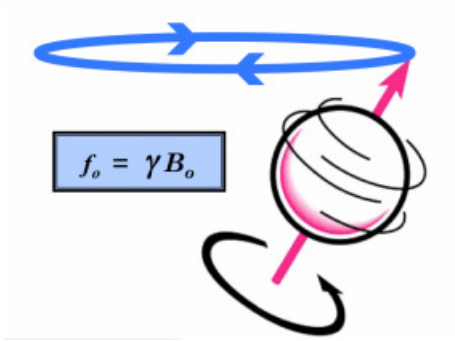

Figure 1.4.1: Polarizing phase

- **Magnetic resonance phase**: When a radio frequency (RF) pulse β_1 is applied to hydrogen protons, it disrupts the equilibrium of the protons through a phenomenon called resonance. This application of the RF field causes a reorientation of the global magnetization $M^{\rightarrow}$ in the direction of the RF field β_1. As a result, the global magnetization can be decomposed into a longitudinal component $M_z^{\rightarrow}$ and a transverse component $M_{x,y}^{\rightarrow}$ (Figure 1.4.2).

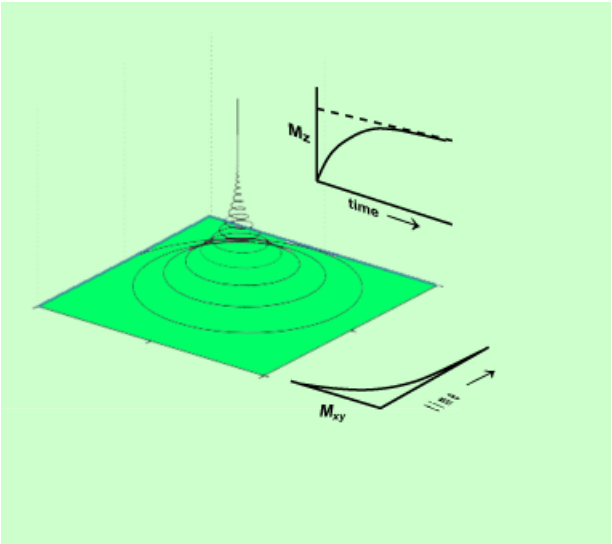

Figure 1.4.2: Resonance phase

- **Relaxation phase**: After the RF pulse is turned off, the system returns to an equilibrium state by releasing the absorbed energy. During this phase, the global magnetization realigns itself with the direction of the β_0 field. Two relaxation times, T1 and T2, exist, which correspond to the time required for the magnetization components ($M_z^{\rightarrow}$, $M_{x,y}^{\rightarrow}$) to return to their equilibrium state.
- **Reading the signal**: The release of energy during the relaxation phase is accompanied by the emission of energy in the form of an RF wave. This RF wave is recorded by a radio-frequency antenna, which then forms the NMR signal. The NMR signal is further transformed into a spectrum through Fourier transformation. Based on these two steps, MRI images are created [28].

– The NMR signal is converted into an image through two steps [29]:

  – **Spatial Encoding**: This step involves the use of gradient coils, which introduce a weak magnetic field to the system. The gradient coils vary the magnetic field strength in different spatial directions, allowing for the localization of the NMR signal in the image. This spatial encoding process enables the recovery of the spatial position of the imaged region.

  – **Image Reconstruction**: After the spatial encoding, the NMR signal contains information about the phase and frequency of the magnetic resonance. In this step,

an inverse fourier transformation is applied to the NMR signal, converting it from the frequency domain to the spatial domain. This transformation reconstructs the image by assigning intensity values to each pixel, resulting in the final MRI image.

Figure 1.4.3 provides a visual summary of the Nuclear Magnetic Resonance process for generating MRI images.

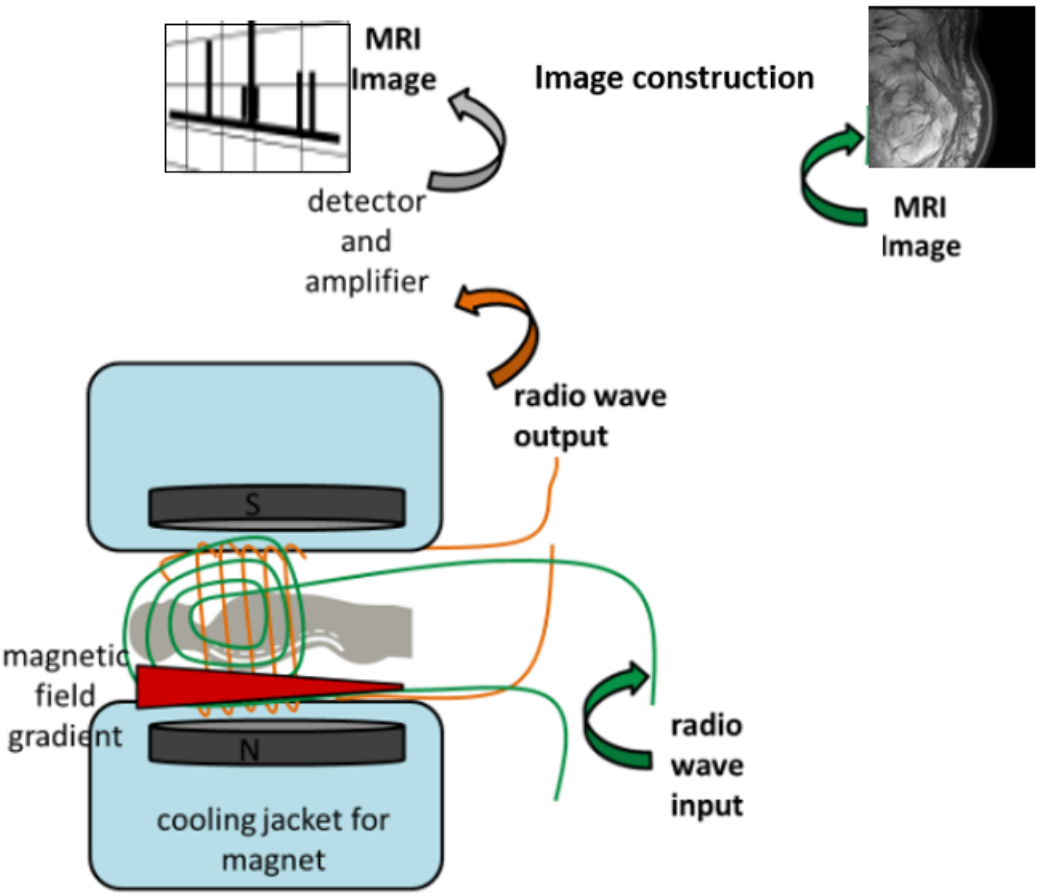

Figure 1.4.3: Nuclear Magnetic Resonance process

This physical process is utilized by the MRI modality in the biomedical field to capture images of various tissues. In the following subsections, we will discuss different MRI parameters, as well as their sequences and components.

1.4.1.1 MRI parameters

MRI utilizes a variety of radio frequency pulses and gradients, governed by distinct parameters, to generate a set of images with specific characteristics [30]. Each parameter-defined configuration in MRI is tailored for a specific medical objective and encompasses various attributes [27]. Several factors contribute to characterizing an MRI configuration, including:

- **Repetition Time (T_R)**: Refers to the time interval between the application of one excitation pulse and the application of the subsequent pulse. It determines the amount of longitudinal magnetization recovery between each pulse. T_R is typically measured in milliseconds [31]. Figure 1.4.4 illustrates the relationship between T_R and the recovery of longitudinal magnetization.
- **Echo Time (T_E)**: Refers to the time interval between the application of the radio frequency excitation pulse and the peak of the signal generated in the coil. It is typically measured in milliseconds [32]. In other words, T_E represents the time between the center of the RF pulse and the center of the spin echo acquisition, which corresponds to the reading of the MRI signal [33]. Figure 1.4.4 illustrates the relationship between T_E and the timing of the spin echo production.

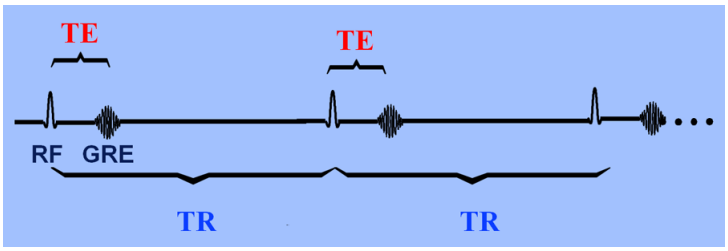

Figure 1.4.4: Repetition time T_R and echo time T_E

- **Relaxation Time (T_1)**: Refers to the longitudinal relaxation time required for the magnetization $M_Z^{\rightarrow}$ to return to its initial maximum value (M_0) parallel to the magnetic field (B_0). The relationship is described by the equation $M_Z^{\rightarrow} = M_0^{\rightarrow}(1 - \exp^{-t/T_1})$, where t represents the time elapsed. T_1 is typically measured in milliseconds [34]. Figure 1.4.5 illustrates the behavior of longitudinal relaxation over time.

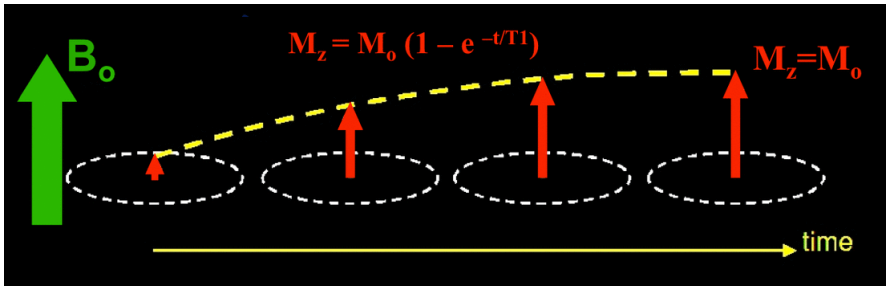

Figure 1.4.5: Relaxation time T_1

- **Relaxation time T_2** : Refers to the time required for the magnetization $M_{x,y}^{\rightarrow}$ to return to its initial maximum value (M_0) in the transverse plane perpendicular to the magnetic field (B0). The relationship is described by the equation $M_{x,y}^{\rightarrow} = M_0^{\rightarrow} \exp^{-t/T_2}$, where t represents the time elapsed. T_2 is typically measured in milliseconds [34]. Figure 1.4.6 illustrates the behavior of transverse relaxation over time.

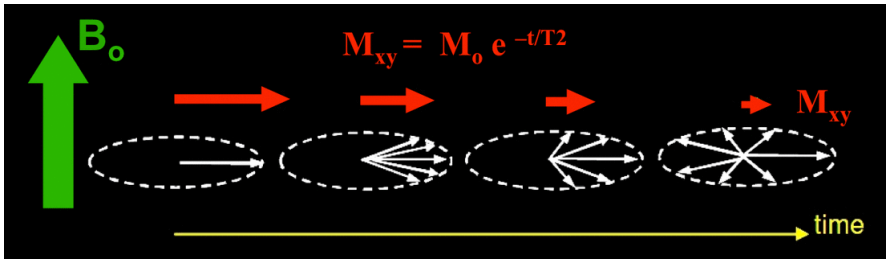

Figure 1.4.6: Relaxation time T_2

Each MRI sequence and its corresponding parameters are carefully selected based on the specific clinical requirements and the desired image characteristics for a particular medical application. The variation of these parameters allows clinicians to create different MRI sequences for skin imaging, each tailored for specific applications. The following section provides an overview of some common MRI sequences that are commonly used in skin imaging.

1.4.1.2 MRI sequences

An MRI sequence is a set of pulses with adjusted T_R and T_E parameters to generate images with specific weightings, such as T1-weighted (T1), T2-weighted (T2), T2 FLAIR, DP (Proton

Density), diffusion-weighted, functional MRI, and others [35]. These sequences play a crucial role in clinical practice and provide essential information related to the considered pathology. Some sequences are routinely used and offer initial insights into the pathology, while others are employed based on the clinician's request during the MRI examination [35]. In this research, the following description presents the MRI sequences utilized.

- **The "spin-echo" pulse** is a fundamental category in MRI that plays a crucial role in quantifying the spin-lattice relaxation. It involves adjusting the repetition time (T_R) and echo time (T_E) parameters. This category includes three sequences:

  – **T1 weighted (T1)**: The T1 sequence utilizes short repetition time (T_R) and echo time (T_E) to measure spin-lattice relaxation. In clinical applications, the T1 sequence is used to detect various conditions such as edema, infection, tumors, hyperacute or chronic hemorrhage, infarction, and inflammation. It is characterized by a decrease in signal, indicating a higher water content in these conditions [34]. On the other hand, the T1 sequence provides a high signal for the detection of fat [36] as well as for enhancing the visibility of MRI contrast agents.

  – **T2 weighted (T2)**: The T2 sequence is characterized by longer repetition time (T_R) and echo time (T_E) compared to the T1 sequence, resulting in a reverse contrast. In the context of skin hydration, the MRI image obtained with the T2 sequence shows a higher signal intensity for the water content in the stratum corneum (SC) layer, which appears hyperintense (white) due to the significant magnetization of the tissues in this sequence [21]. On the other hand, the fat layer of the skin appears hypointense (black), while the gray matter represents the other skin layers in varying shades of gray.

  – **Proton density weighted(PD)**:Proton density (PD) weighted images differ from T1 and T2 weighted images as they do not primarily display the magnetic properties of the hydrogen nuclei, but rather the number of nuclei present in the imaged area [37]. Proton density weighted images are obtained by minimizing the contribution of both T1 and T2 contrast. This is achieved by using a long repetition time (T_R) to minimize T1 contrast and a short echo time (T_E) to minimize T2 contrast. As a result, proton density weighted images exhibit a large signal with little T1 and T2 contrast.

Indeed, these parameters, including T_R and T_E, are crucial in determining the image contrast and characteristics in MRI. The machine settings are adjusted according to the specific

imaging protocol and the desired outcomes for the examination. For instance, a T1-weighted image with short T_R and T_E values can enhance the contrast of tissues with short T1 relaxation times, while a T2-weighted image with long T_R and T_E values can highlight tissues with long T2 relaxation times. Other parameters related to the tissue properties, such as T1 and T2 relaxation times, can also influence the image contrast. These values vary depending on the type of tissue and can be measured or estimated prior to the imaging procedure. By optimizing these parameters and considering the specific tissue characteristics, the MRI machine can generate the necessary data to construct the 'Nearly Raw Raster Data' (NRRD) image, which is a multi-dimensional representation of the acquired image data in the Digital Imaging and Communications in Medicine (DICOM) format [38].
In the following section, we will provide an overview of the components of an MRI machine.

1.4.1.3 MRI components

MRI machines come in various sizes and shapes. Older designs were often compact and enclosed, providing limited space. This confined environment could cause discomfort and fear for patients undergoing examinations. However, in recent years, engineers have made significant improvements to MRI machine design. One notable enhancement is the introduction of more open configurations. These modern designs feature expanded sides and increased space within the scanner compared to the original models. The larger and more open design of these newer MRI machines has a positive impact on patients. It helps alleviate feelings of claustrophobia and creates a more comfortable and inviting atmosphere during the scanning process. Patients are less likely to experience anxiety, which can improve cooperation and the overall quality of the examination. Moreover, the increased space in the scanner benefits healthcare providers by allowing better access to patients. It facilitates easier positioning and monitoring, enhancing the efficiency and accuracy of the imaging procedure. The advancements in MRI machine design have transformed the patient experience, making it less intimidating and more accommodating. These improvements have helped alleviate patient concerns and ensure a smoother and more successful examination. Today, an MRI machine consists of four main components, each playing a crucial role in the imaging process. These components are: [39]:

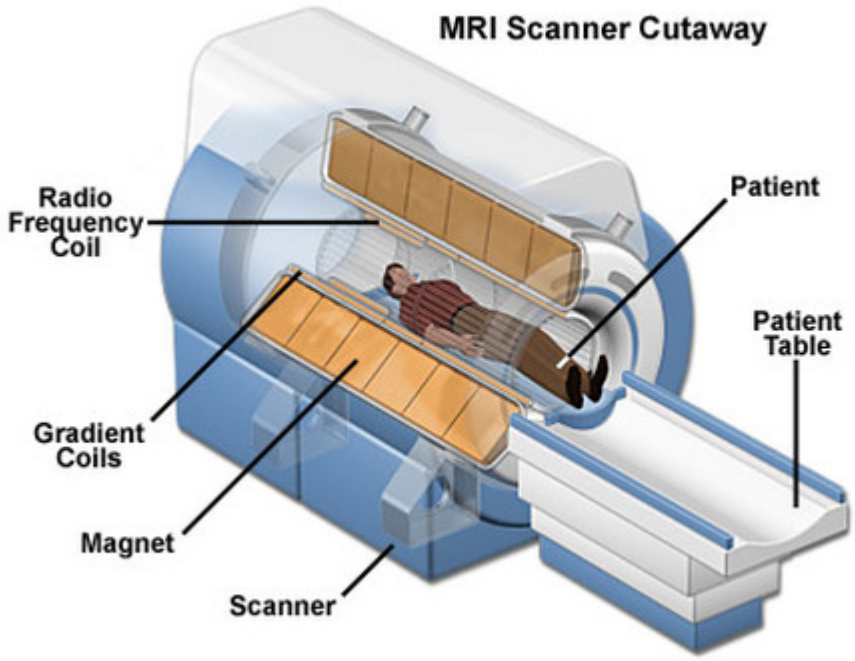

Figure 1.4.7: MRI system

1. **Magnet**: The magnet system is the core component of an MRI machine. It generates a strong and uniform magnetic field, typically using superconducting magnets or permanent magnets. The magnetic field aligns the hydrogen atoms in the patient's body, which is essential for the imaging process.

2. **Gradient coil**: The gradient system consists of gradient coils that create varying magnetic fields in different directions. These gradient fields are superimposed onto the main magnetic field and allow for spatial encoding of the MRI signal. By manipulating the gradient fields, the MRI machine can determine the location of signal sources within the patient's body, enabling the reconstruction of detailed spatial information.

3. **RF coil**: The RF system consists of coils and antennas that transmit and receive radiofrequency pulses. These pulses are used to manipulate the hydrogen atom alignment and stimulate the emission of radiofrequency signals. The RF system is responsible for transmitting the RF pulses during the imaging process and receiving the resulting signals for image reconstruction.

4. **Computer system**: The computer system controls and coordinates all the components of the MRI machine. It generates the necessary pulse sequences, adjusts the parameters of the magnet, RF, and gradient systems, and collects and processes the acquired data. The computer system also performs image reconstruction and provides the final MRI images to the radiologist or healthcare professional for interpretation.

These four components work together seamlessly to acquire, process, and generate high-quality MRI images. The magnet system creates a strong magnetic field, the RF system transmits and receives RF pulses, the gradient system provides spatial encoding, and the computer system controls the entire process and produces the final images. The combination of these components enables the visualization of anatomical structures and pathological conditions inside the patient's body, providing valuable diagnostic information for medical professionals.

In the following section, we will delve into the various parameters and techniques employed by MRI to visualize and analyze the human skin in detail. We will explore how different MRI sequences and imaging parameters can provide valuable information about the structure, composition, and hydration of the skin. Additionally, we will discuss the challenges and advancements in skin imaging using MRI, as well as the potential applications of this modality in dermatology and skincare research.

1.5 MRI skin applications

Since the skin has low water content compared to other tissues, its signal on an MRI scan is generally weak, which can limit its usefulness for diagnostic purposes in routine cases. As a result, other imaging modalities such as dermatoscopy, ultrasound, or visual examination are often preferred for evaluating skin conditions and lesions. However, there are specific scenarios where MRI can be valuable in assessing certain skin conditions. For instance, MRI can be utilized to evaluate:

- **Soft tissue tumors**: In rare cases, when a skin lesion extends deep into the underlying soft tissues, an MRI scan may be performed to evaluate the extent and involvement of adjacent structures [40].
- **Inflammatory conditions**: MRI can be useful in assessing inflammatory skin conditions like cellulitis, where the infection spreads to the underlying tissues [41].
- **Skin cancer staging**: MRI can be employed to assess the involvement of deeper structures in cases of advanced skin cancers, such as melanoma [42].

- **Skin hydration**: MRI has been widely used in skin hydration applications to assess and monitor the water content and distribution within the skin. It provides valuable insights into the hydration levels of different skin layers, offering a non-invasive and quantitative approach to evaluate skin health [43].

The next section focuses on the visualization of the skin using MRI and explores the use of multiple parameters to enhance the understanding of skin anatomy and pathology.

1.6 MRI skin visualisation

MRI has proven to be an excellent imaging modality for visualizing the anatomy of skin layers, thanks to its ability to provide high-resolution images with special soft tissue contrast [44]. It allows for the differentiation and validation of the distinct layers within the skin structure [26]. Recent advancements in MRI technology have introduced the use of small coils placed directly on the skin to capture images with exceptionally high spatial resolution. This level of spatial resolution, typically reaching 100 micrometers or less, enables detailed analysis and study of even the thinnest organ, such as the skin. By utilizing these advanced techniques, MRI offers valuable insights into the structure and composition of skin layers (Figure 1.6.1), contributing to improved understanding and diagnosis in dermatology and related fields.

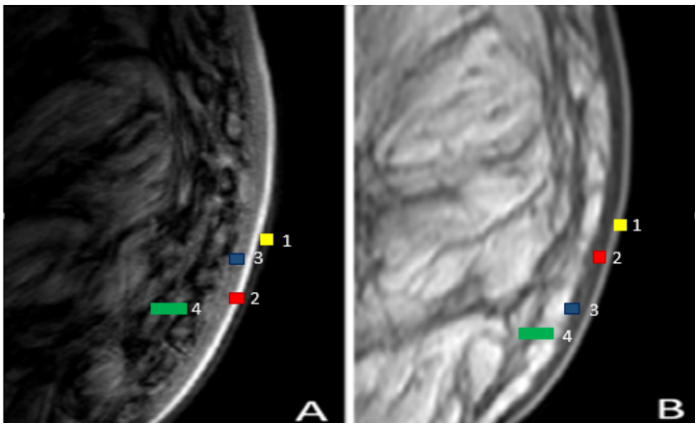

Figure 1.6.1: MRI sequences. (A) T1 sequence, (B) T2 sequence. 1: Stratum Corneum, 2: Epidermis, 3: Dermis, 4: Hypodermis

In dermatology, skin imaging studies have been conducted using various magnetic field strengths, including 0.5 T, 1.5 T, 2 T, and 2.4 T. These studies have focused on vivo imaging, capturing images of the skin in living subjects. Recently, a feasibility study involving 36

participants was reported, specifically investigating skin imaging at 3 T [45]. To achieve high-resolution skin imaging, small surface receiver coils with a diameter typically around 1 inch are employed. These coils are placed directly on the skin to capture detailed images with improved spatial resolution. It's important to note that the maximal gradient amplitude, which determines the strength and precision of the magnetic field gradients used in the imaging process, poses limitations on the achievable resolution when imaging tissues with short T2 relaxation times, such as the dermis. To optimize skin imaging, a short echo time (T_E) is preferred. The T_E refers to the time between the excitation pulse and the collection of the MRI signal. Since the dermis has a relatively short T2 relaxation time, using a short T_E helps to minimize signal decay and improve the visibility and clarity of the skin structures during imaging [45]. In addition, High-resolution skin imaging requires immobilization and motion correction. Small voxels and lengthy scans are needed for high-resolution imaging; even minute motion can cause the picture to be considerably degraded; The specific clinical needs and constraints will inform the choice of one sequence over the others. When imaging the dermis, increasing the field strength from 1.5 T to 3 T provides a substantial increase in signal-to-noise ratio (SNR) Which is required in the separation between water and fat in clinical applications field [46].

Utilizing MRI provides the ability to visually and quantitatively assess the impact of skincare interventions on skin hydration, leading to a better understanding of their efficacy and potential benefits for individuals. Furthermore, MRI-based skin hydration assessment offers valuable information for diagnosing and monitoring dermatological conditions. Abnormal water content in the skin is associated with certain skin disorders, and MRI can aid in visualizing and characterizing these changes. This can contribute to early detection, treatment planning, and evaluating the effectiveness of therapeutic interventions. Additionally, MRI can assess the functional aspects of the skin by utilizing specific imaging techniques and sequences. It enables the evaluation of parameters related to skin function, including blood flow, perfusion, oxygenation, and temperature distribution [47]. These functional measurements provide valuable insights into the physiological processes occurring within the skin, such as hydration regulation, circulation, and tissue metabolism.

In summary, MRI provides a comprehensive approach to visualize and assess the morphological and functional aspects of the skin. By employing MRI for skin hydration assessment, researchers and clinicians can evaluate the effects of skincare interventions, diagnose dermatological conditions, and gain valuable insights into skin structure and function.

- **Morphological imaging of the human skin**: This type of imaging focuses on capturing the anatomical details of the skin. It provides high-resolution images that allow for the

visualization of skin layers, hair follicles, sweat glands, blood vessels, and other structural components. Structural imaging techniques include T1-weighted imaging, T2-weighted imaging, and proton density imaging. These techniques provide valuable information about the skin's architecture and can help identify abnormalities or changes in tissue structure. [48]. For studying skin hydration, structural MRI takes advantage of subtle differences between voxels (3D pixels) to distinguish between different types of tissue and compare two tissues or layers with varying water content. By acquiring high-resolution images of the skin, MRI can capture the fine details and variations in tissue composition, allowing for the visualization and analysis of water distribution within different skin layers. These minute variations in signal intensity or contrast between voxels provide valuable information about the hydration status of the skin and can be used to assess the effectiveness of moisturizers or hydration treatments.

- **Functional imaging of the human skin**: Functional imaging aims to understand the activity and functioning of the skin, in contrast to anatomical imaging which focuses on producing anatomical maps of the skin. It allows for the investigation of various skin systems and processes. For example, functional imaging techniques such as T2 mapping can be used to detect and measure the water content of the skin, providing valuable information about skin hydration. Functional imaging differs from anatomical imaging in that it requires a fast and sensitive acquisition process, often at the expense of resolution. Any anatomical imaging technique can potentially be used to acquire the signal used in functional imaging, as there is nothing fundamentally different about it. However, the primary focus of functional imaging is not on anatomical details, but rather on capturing changes in tissue characteristics over time. This allows researchers to study dynamic processes and functional aspects of the skin [48].

1.7 MRI skin hydration measurement

MRI can be used to indirectly assess skin hydration by evaluating changes in water content within the deeper layers of the skin. Although the skin itself has low water content and does not generate strong MRI signals, the underlying structures and tissues can be informative. One technique used to evaluate skin hydration with MRI is called T2 mapping. T2 relaxation time refers to the time it takes for the hydrogen atoms to return to their original alignment after being perturbed by the magnetic field. It is influenced by the water content within tissues. In

the case of the skin, T2 mapping can be used to measure the water content in the underlying dermis, which indirectly reflects skin hydration. By performing T2 mapping MRI scans, changes in T2 relaxation times within the dermis can be observed. Higher T2 relaxation times indicate higher water content, suggesting better skin hydration, while lower T2 relaxation times may indicate decreased hydration levels. This information can be useful in assessing skin conditions, evaluating the efficacy of moisturizers, and studying the effects of environmental factors on skin hydration. It's important to note that while MRI can provide insights into skin hydration, there are other non-MRI techniques that are more commonly used for direct measurement of skin hydration, such as corneometry and impedance measurements. These methods directly assess the water content of the outermost layer of the skin (stratum corneum) and provide more accurate and specific hydration measurements [49].

However, T1-weighted imaging is a commonly used MRI technique that provides excellent anatomical detail. It is particularly useful for visualizing skin structures, including the epidermis, dermis, and subcutaneous tissues. T1-weighted images offer valuable information about tissue composition, thickness, and overall morphology. This imaging modality is often employed in dermatology and skincare research to assess the structural integrity of the skin and identify abnormalities or changes in tissue architecture.

On the other hand, T2-weighted imaging is highly sensitive to water content. It allows for the visualization of skin hydration levels, edema, and inflammatory processes. T2-weighted images are widely used in the study of skin pathologies, as they can provide insights into the presence and extent of edema, inflammation, and other water-related changes in the skin. This imaging technique is valuable for evaluating skin lesions, diagnosing skin conditions, and monitoring the response to interventions aimed at addressing hydration and inflammation issues. By employing both T1-weighted and T2-weighted imaging techniques, clinicians and researchers can obtain comprehensive information about the structural and functional characteristics of the skin. This combined approach enables a more thorough understanding of skin conditions, facilitating accurate diagnosis, treatment planning, and monitoring of treatment efficacy in dermatology and skincare applications. Indeed, Changes in T2 values within the skin layers play a crucial role in research focused on skin hydration. T2 refers to the relaxation time of the MRI signal and is influenced by the amount of water present in a particular skin layer. Specifically, T2 values are longer when there is a higher water content in the layer. Therefore, measuring T2 values serves as a practical and accurate approach in assessing skin hydration levels.

MRI plays a significant role in the field of dermatology, offering valuable insights and applications in various aspects of skin assessment and diagnosis. In the next section, we will provide an overview of some notable research studies related to MRI in the field of dermatology. These

studies highlight the advancements and potential applications of MRI in understanding and diagnosing various dermatological conditions.

1.8 MRI skin background

The goal of MRI in the majority of clinical applications is to distinguish between different types of skin tumors and determine their extent prior to surgery in situations where surgical resection should be reduced, such as in the case of a face tumor. Moreover, it aids in the diagnosis, localization, and delineation of some cancers that, due to their topography, may be challenging to identify, such as subungual glomus tumors. It also enables measuring the size and thickness of malignant tumors as well as their level of infiltration into deeper soft tissues. Many benign and malignant skin cancers' most prevalent MRI findings were listed in a review written in 2008 [46].

The utilization of MRI in examining the impact of dehydration on human skin is relatively uncommon, as mentioned in previous studies [45, 50, 51, 52, 53]. However, MRI offers a wide range of acquisition parameters that characterize water properties, including T1 and T2 relaxation times and proton density. These biochemical parameters provide valuable insights into skin physiology, hydration levels, and the effects of cosmetic products. They also contribute to the evaluation of morphological, physical, and chemical parameters, enabling the generation of water cartography maps [54]. Furthermore, MRI serves as an appropriate method to observe the behavior of water molecules in vivo, allowing for the visualization of changes in water distribution and dynamics within different skin layers. This imaging technique provides information about the location, concentration, and chemical environment of skin water protons. By understanding how these parameters change, researchers and clinicians can gain insights into maintaining adequate hydration levels in the skin. In addition, the interactions between water molecules and soluble macromolecules in the immediate surroundings influence the T1 and T2 relaxation times of water within the skin layers [19]. These variations in interaction dynamics contribute to the overall understanding of water behavior and hydration status within the skin.

In addition, MRI techniques have proven to be valuable in experimental research for assessing the penetration of exogenous substances into the skin and evaluating the health and hydration of the skin [19]. In vitro studies have demonstrated the capability of MR to differentiate between the stratum corneum and viable epidermis of human skin samples. The use of magnetic resonance in skin research was first introduced in 2003 by [43], enabling the examination of both in vivo and in vitro skin moisture. It was found that in vitro skin samples from a single donor can be used with high repeatability, and there is a good correlation between the signal strength and equilibrium moisture content of the skin. MRI technique allows

researchers to quantify the impact of moisturizing creams on skin water levels over time in vivo. In vitro investigations are preferred by the beauty and pharmaceutical sectors due to their cost-effectiveness compared to in vivo trials. The technique facilitates the study of skin structure, its biochemical properties, and the behavior of water within its layers. Magnetization transfer is another metric used to quantify skin hydration levels. According to prior research by [55], MRI with magnetization transfer enables the direct, quantitative, and non-invasive evaluation of skin hydration by examining signal intensity and the thickness of the stratum corneum, which increases with moisture. The application of two-dimensional diffusion-weighted MRI was pioneered by [56], who investigated the behavior of water in the live epidermis and dermis. By assessing the tissue's apparent diffusion coefficient, they were able to elucidate several characteristics of these two skin layers. The impact of cosmetic care products on skin moisture has been studied in both in vivo and in vitro skin MRI experiments by [57]. High-field MRI has indeed proven to be a valuable tool in biomedical applications, particularly in studying skin morphology and characteristics, including the evaluation of skin moisture content and the effects of skincare products. However, High-field MRI offers several benefits in biomedical applications, but it also has its limitations. Let's explore both aspects in the following sections.

1.9 MRI applications benefits

MRI offers a plethora of benefits in healthcare applications, making it a versatile and indispensable tool for medical professionals. Its advantages stem from its unique imaging capabilities, safety profile, and ability to provide both structural and functional information without invasive procedure. Following the description of some benefits [58, 59]:

1. **Detailed Imaging**: MRI provides highly detailed and precise images of the internal structures of the body. It can produce images of organs, soft tissues, muscles, joints, blood vessels, and the brain with exceptional clarity, aiding in accurate diagnosis and treatment planning.

2. **Non-Invasive and Safe**: MRI is a non-invasive imaging technique that does not use ionizing radiation like X-rays or CT scans. It relies on strong magnetic fields and radio waves to generate images, making it a safer option for patients, especially those who require frequent or repeated imaging.

3. **Multi-Planar Imaging**: MRI allows imaging in multiple planes, including axial, sagittal, and coronal views. This capability enables comprehensive visualization of anatomical

structures from different angles, aiding in a more thorough assessment of the patient's condition.

4. **Functional Imaging**: In addition to structural imaging, MRI can also provide functional information about the body. Recently,Techniques such as functional MRI (fMRI) can map brain activity, helping in the study of cognitive processes, language, and sensory functions.

5. **Contrast Enhancement**: MRI can employ contrast agents to enhance the visibility of specific tissues or abnormalities. Contrast agents can help highlight areas of inflammation, tumors, or blood flow abnormalities, enabling better detection and characterization of certain conditions.

6. **Evaluation of Soft Tissues**: MRI excels at imaging soft tissues, such as muscles, tendons, ligaments, and organs. It is particularly useful in assessing joint and musculoskeletal disorders, sports injuries, spinal conditions, and abdominal or pelvic abnormalities.

7. **Real-Time Monitoring**: MRI can be performed in real-time, allowing the monitoring of certain procedures or interventions. For example, MRI-guided biopsies or minimally invasive treatments can be precisely targeted and monitored during the procedure.

8. **Pediatric Imaging**: MRI is considered safe for children and infants, as it does not involve radiation exposure. It is often the preferred imaging modality for evaluating pediatric conditions, including brain disorders, congenital anomalies, and musculoskeletal abnormalities.

Overall, the benefits of MRI in healthcare applications include its excellent image quality, non-invasiveness, multi-planar imaging capabilities, functional assessment, and the ability to evaluate a wide range of conditions in various anatomical regions. While MRI is a preferred technique for studying skin anatomy, it does come with certain limitations that practitioners must address when acquiring images. The following section describe the most common limitation of MRI applications.

1.10 MRI applications limits

Despite its non-invasive nature and remarkable ability to provide detailed structural and functional information, MRI does have certain limitations that can impact its clinical applications. The following are three common limitations that can introduce inaccuracies and degrade the quality of the acquired MRI image and their interpretation [60]:

1. **Noise**: In MRI, noise refers to unwanted random variations or distortions in the acquired images, which can affect image quality and interpretation. The sources of noise in MRI include the radiofrequency antenna, patient motion during image acquisition, and physiological processes such as blood circulation or respiration. The Signal-to-Noise Ratio (SNR) is a measure that quantifies the strength of the signal relative to the background noise level in an image. A higher SNR indicates a stronger signal compared to the noise, resulting in a clearer and more reliable image. Conversely, a lower SNR indicates that the noise level is relatively high compared to the signal, which can reduce image quality and make it more challenging to discern fine details or subtle anatomical features.

   In the context of MRI skin imaging, noise is often observed in consistent regions that correspond to a single anatomical feature. This can be due to various factors, such as variations in tissue composition, susceptibility effects, or other sources of noise mentioned earlier. The presence of noise in specific regions can affect the accuracy of measurements and the interpretation of anatomical features within those regions. To mitigate the effects of noise and improve SNR in MRI images, several approaches are utilized [61]:

   (a) **Higher field strength**: Using higher field strength MRI scanners can improve the SNR as the signal received from the tissue increases proportionally with the field strength.

   (b) **Sequence optimization**: Choosing appropriate imaging sequences and parameters can optimize the SNR. Certain sequences may provide better SNR for specific applications, and optimizing parameters like repetition time (T_R) and echo time (T_E) can improve image quality.

   (c) **Motion control**: Minimizing patient motion during image acquisition is essential to reduce motion-related artifacts and noise. Recent echniques such as patient immobilization, patient coaching, and gating can be employed to minimize motion artifacts.

   (d) **Advanced noise reduction techniques**: Various image denoising algorithms and filtering methods can be applied to reduce noise while preserving important anatomical details. These techniques aim to enhance the SNR by suppressing noise components while preserving the underlying signal.

   It is important to note that achieving a suitable SNR depends on several factors, including the specific MRI protocol, hardware capabilities, and patient-related factors. The SNR can vary in different imaging scenarios and may require optimization for specific

applications, including skin imaging. Figure 1.10.1 shows a noisy MRI skin image.

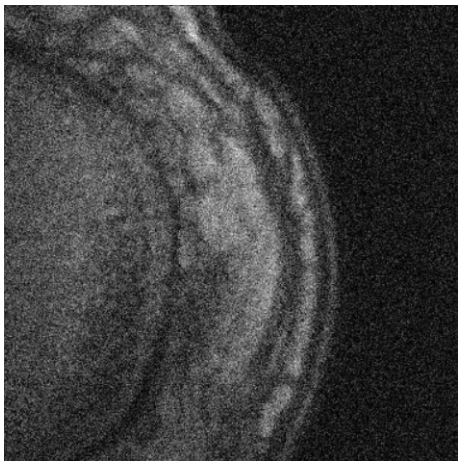

Figure 1.10.1: Noisy MRI skin image

2. **Intensity value change (bias)**: This phenomena occurs when the intensity value change, in MRI images refers to systematic variations in the signal intensity across the image that are unrelated to the underlying tissue properties. It occurs due to various factors, including technical imperfections, instrumental artifacts, and image acquisition or processing errors (Figure 1.10.2). These intensity value changes can impact the accuracy and reliability of quantitative analysis and interpretation of MRI images.The sources of intensity value change can include:

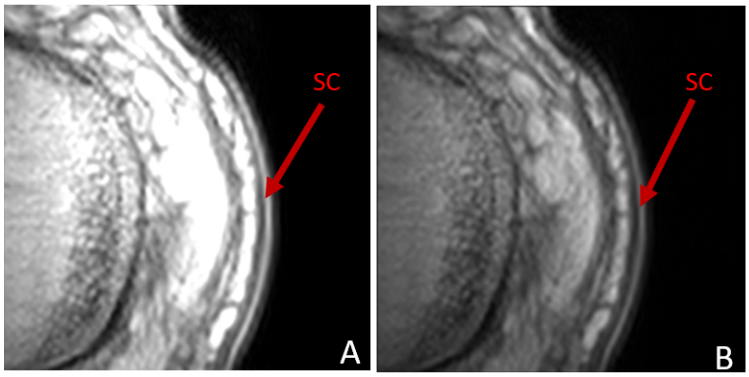

Figure 1.10.2: Intensity value change in SC layer of MRI image

3. **Magnetic field inhomogeneity**: Imperfections in the magnetic field can cause intensity variations across the image. These variations may arise from system-related factors, such as variations in the magnetic field strength or non-uniformity in the magnetic field across the imaging region. Magnetic field inhomogeneities can lead to intensity biases that affect the overall image appearance [62]. To address the challenges posed by intensity variations, various strategies can be employed, such as [63]:

   (a) **Intensity normalization**: Applying intensity normalization techniques can help reduce bias and standardize the intensity values across the image or within specific regions of interest. Normalization methods aim to equalize the intensity distributions, improving comparability and facilitating accurate quantitative analysis.

   (b) **Calibration scans**: Including calibration scans with known intensity values can provide reference standards for correcting intensity biases. These calibration scans can be used to establish correction factors or calibration curves to adjust the intensity values in the acquired images.

   (c) **Post-processing correction**: Image post-processing techniques, such as bias field correction algorithms, can be used to remove intensity variations caused by magnetic field inhomogeneities or RF coil sensitivity differences.

   Through the systematic correction of intensity variations, researchers and medical practitioners can enhance the exactitude and dependability of MRI image analysis. This proactive approach enables more precise interpretations, quantitative measurements, and an enriched comprehension of the underlying biological composition of tissues [33].

4. **The partial volume effect (PVE)**: PVE is associated with the discrimination of space. When the interface between many objects is located in a single discrete volume element, or voxel, the measurement of this voxel will contain a variety of distinct materials [64]. The restricted spatial resolution of the camera and the sampling of the reconstructed images into the matrix result in partial volume effects (PVE). The observed intensity will be less than the source's real intensity because of the restricted spatial resolution. Moreover, high activity regions will spread into surrounding low activity areas, and low activity areas will spread into high activity areas. When a voxel contains more than one tissue (such as at the borders of organs), the intensities of the two tissues are combined into that voxel and cannot be differentiated due to sampling of the activity into a matrix (Figure 1.10.3).

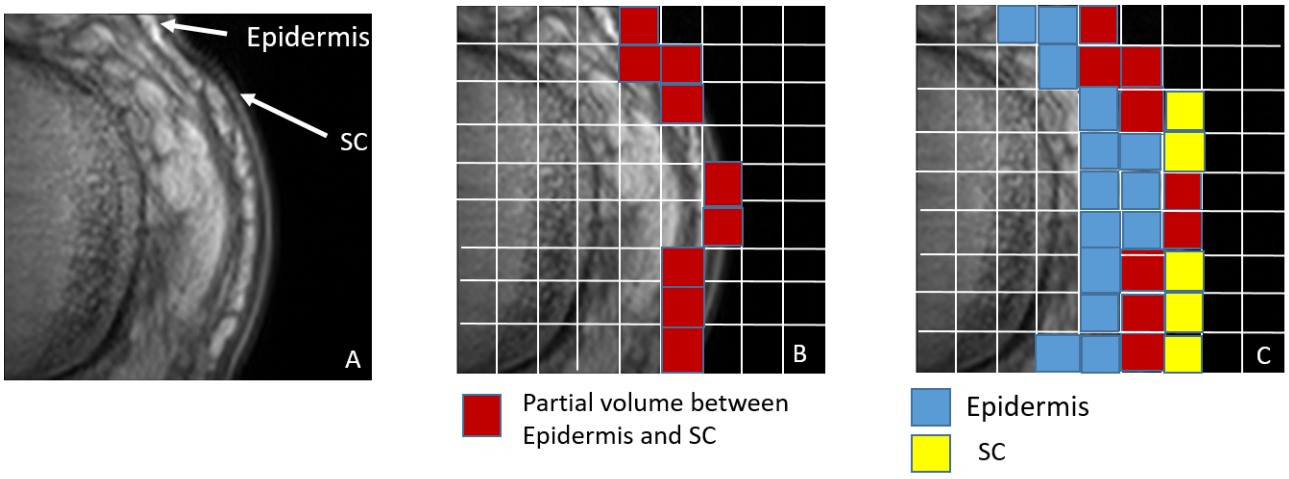

Figure 1.10.3: A schematic explanation of the partial volume effect in the context of skin magnetic resonance imaging. (A): Skin MRI image, (B):Measured image.(C): Spill out.

Nevertheless, the dimensions and morphology of the imaged tissue, the distinction between adjacent objects, the spatial resolution of the imaging device, and the size of voxels collectively influence Partial Volume Effect (PVE). PVE becomes negligible for larger organs such as the liver, while it becomes more conspicuous for smaller organs like the heart or in cases of malignancies [65].

1.11 Conclusion

This chapter, we have embarked on a comprehensive exploration of the skin and its vital role in maintaining hydration. We've delved into the intricate mechanisms that govern skin physiology, highlighting its dynamic nature and the critical importance of adequate hydration. Additionally, we've introduced the indispensable role of medical imaging, specifically MRI, in quantifying skin hydration with precision. This foundational knowledge serves as the bedrock upon which our subsequent chapters will build, providing a solid understanding of the fundamental concepts. The forthcoming chapter promises to provide an illuminating overview of intelligent image processing methods, firmly grounded in the realm of Convolutional Neural Networks (CNNs). We will delve into the world of cutting-edge image analysis techniques, with a particular emphasis on their application in processing skin images. This includes techniques for segmenting and analyzing different skin layers, which are crucial for understanding hydration dynamics. Furthermore, we will conduct an exhaustive review of existing methodologies for processing skin images, shedding light on their strengths and limitations. This comprehensive review will set the stage for a deeper dive into the intricacies of CNN-based approaches, offering a glimpse into the state-of-the-art in skin image processing. As we look ahead to the chapters to come, we anticipate an enriching exploration of the synergy between skin physiology, medical imaging, and advanced image processing techniques. This journey holds the promise of unveiling novel insights into the dynamic nature of skin hydration and innovative methods for its precise quantification. It is a testament to the ever-evolving landscape of interdisciplinary research, where technology and healthcare converge to enhance our understanding and promote healthier, well-hydrated skin.

CHAPTER 2

Literature review on skin MRI processing

2.1 Introduction

In the field of medical imaging, the combination of Artificial Intelligence (AI) and Machine Learning (ML) has opened up exciting possibilities in various domains, including image classification [66], and semantic segmentation [67]. Within this landscape, Deep Learning (DL) has seen remarkable growth, often achieving or even surpassing human performance in complex tasks [68]. Among deep learning architectures, Convolutional Neural Networks (CNNs) have gained prominence due to their ability to automatically detect important features without manual feature engineering [69]. While CNNs have been widely used in various applications, their impact in medical imaging, especially in the context of Magnetic Resonance Imaging (MRI), is remarkable. MRI plays a crucial role in healthcare by providing detailed anatomical and physiological information. In skin analysis, MRI offers a non-invasive and highly detailed approach to studying skin properties and conditions. This literature review embarks on an exploration of the intricate interplay between AI, CNNs, and MRI within the context of skin imaging and analysis.

In the ensuing sections of this chapter, we commence with an introduction to the foundational concepts of CNNs, Subsequently, we delve into the intricate anatomy of CNNs, dissecting the various layers and mechanisms underpinning their functionality. To provide a holistic view, we also address the myriad applications and challenges associated with CNNs within the broader medical imaging domain.our focus shifts to the specific applications of CNN-based techniques within the existing literature, followed by an exploration of their pivotal role in the medical field, with a particular focus on their applications in dermatology and skin analysis. with a keen eye on their relevance to the objectives of our dissertation. This review is thoughtfully structured into three principal segments: Skin Segmentation, which examines segmentation methods

in the context of skin clinical applications; Skin Hydration Measurement, presenting various techniques for quantifying skin hydration; and Skin Registration, which focuses on registration approaches within skin medical imaging. In summary, this introduction lays the foundation for our literature review journey, setting the stage for a comprehensive exploration of CNN-based methodologies within the context of skin MRI processing. Our ultimate goal is to advance our understanding of skin hydration and contribute to the field of dermatology and clinical practice.

2.2 Convolutional Neural Network (CNN)

Artificial Intelligence (AI) has gained significant popularity in research and has been successfully applied in various domains using Machine Learning (ML) techniques, including text mining [70], image classification [66], and semantic segmentation [67]. Deep Learning (DL) approaches, such as recursive neural networks (RvNNs), recurrent neural networks (RNNs), and convolutional neural networks (CNNs), have emerged as prominent architectures within the field of DL.

In recent years, DL has rapidly become the most popular computational approach in ML, achieving remarkable results on challenging cognitive tasks that rival or even surpass human performance [68]. Among the different DL networks, CNNs are considered particularly powerful and find widespread application across various domains [68]. One of the fundamental advantages of CNNs over their predecessors is their ability to automatically identify relevant features without human intervention [69]. CNNs have found extensive use in clinical applications, particularly for analyzing medical images obtained from diverse modalities.

The specific context of this dissertation revolves around the semantic segmentation of skin MRI images for measuring skin water content. In the literature chapter of this dissertation, the focus is on introducing CNNs, their background, and their applications in the medical field, with an emphasis on skin-related applications. Subsequently, the different layers of CNNs are explained, followed by a discussion of their applications and associated challenges.

The subsequent sections of the literature chapter provide an overview of CNN-based techniques found in the existing literature for analyzing skin medical images, aligning with the perspective of the dissertation. The review is structured into three principal parts: skin segmentation, which explores previous segmentation methods applied in skin clinical applications; skin hydration measurement, which introduces existing approaches for quantifying skin hydration; and skin registration, which offers a review of registration methods used in the field of skin medical imaging.

2.2.1 Background of CNN

The origins of CNNs can be attributed to the groundbreaking work of Hubel and Wiesel [71] on the visual cortices of primates and birds. In the 1980s, [72] further advanced CNNs with the development of the Neocognitron, a convolutional algorithm that drew inspiration from the findings of Hubel and Wiesel. [73] made significant contributions to CNNs by introducing the 7-level convolutional network known as LeNet-5, which incorporated backpropagation and adjustable weights. LeNet-5 has served as a foundational architecture for many subsequent CNN designs. In 2012, researchers from the University of Toronto made a breakthrough in computer vision by creating an AI model that surpassed existing image recognition algorithms. This model, known as [66], achieved an impressive 85 percent accuracy in the ImageNet computer vision competition.

Since 2012, CNNs have continued to evolve and have become indispensable not only in computer vision but also in various other domains, including the medical field. Their applications extend to areas such as natural language processing, hyperspectral image processing, and medical image analysis. The following sections delineate all concepts related to CNN, commencing with an exploration of the architecture of Convolutional Neural Networks (CNNs).

2.2.2 CNN structure

The main objective of a Convolutional Neural Network (CNN) is to compress images into a more manageable format while preserving important components necessary for accurate predictions. This capability is crucial for developing architectures that can effectively learn features and handle large-scale data-sets. In a CNN, there are three primary types of layers [68] (Figure 2.2.1):

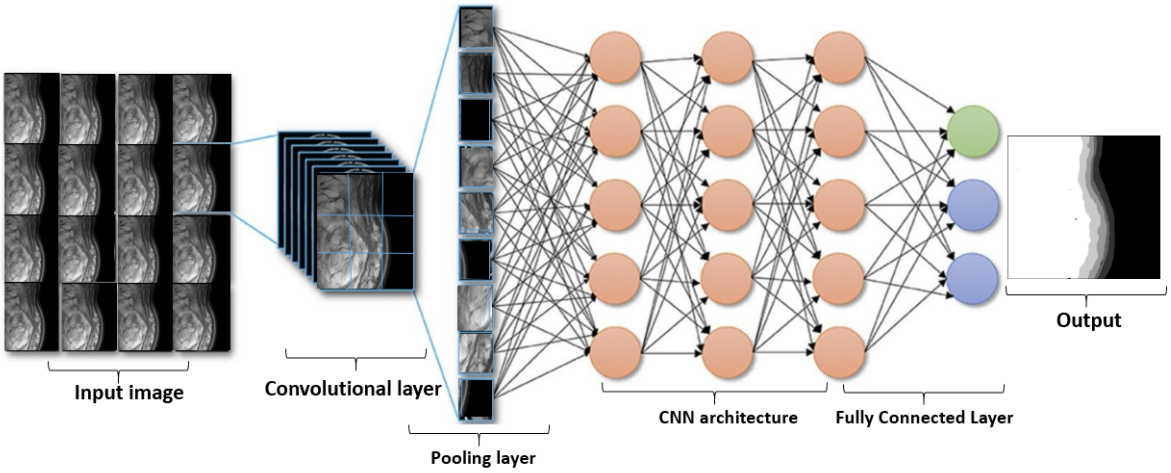

Figure 2.2.1: Convolutional Neural Network structure

- **The convolutional layer (ConV)**: Is the most important part of CNN architecture that made up of a number of convolutional filters, or "kernels." In this layer the output feature map is produced by convolving the input image expressed as N-dimensional metrics. concepts below help to understand the convolution technique:

  - **The kernel**: In a Convolutional Neural Network (CNN) is indeed defined as a grid of values, and each value represents the kernel weight. However, the weights of the kernel are not randomly chosen at the beginning of training. During the initialization phase of a CNN, the kernel weights are typically initialized using specific techniques such as Xavier [74] or [75]initialization. These techniques help set the initial weights to appropriate values, considering the network's architecture and activation functions, to facilitate effective learning. And during the training process, the kernel weights are iteratively updated using an optimization algorithm like gradient descent, Optimization Algorithms for Neural Networks, Adam Optimizer, or Momentum Optimizer [76]. The network learns to adjust these weights through back propagation, which involves calculating the gradients of the loss function with respect to the kernel weights and updating them accordingly. This learning process allows the kernel to extract important features from the input data.
  - **Convolutional operation**: In a CNN, the input is typically a multi-channeled

image, and the convolutional operation involves moving the kernel over the entire image. The convolution process starts by sliding the kernel horizontally and vertically across the input image. At each position, a dot product operation is performed between the kernel and the corresponding region of the image. This dot product is calculated by multiplying the corresponding values of the input image and the kernel together and then summing them up. This computation is performed simultaneously for all positions in the image.

The mathematical formula that represents the convolutional operation is as follows:

$$y[m,n] = x[m,n] * k[m,n] = \sum_{i}^{k} \sum_{j}^{k} x[i,j] * k[1-i, n-i]. \tag{2.2.1}$$

In this formula:

* $y[m,n]$ Represents the output value at position (i,j) in the feature map.
* $\sum_i^k \sum_j^k x[i,j]$ Denotes the input value at position (i+m,j+n) in the input image.
* $k[1-i, n-i]$ Refers to the kernel weight at position (m,n).

By applying this formula at each position, the convolutional operation produces a single scalar value for each position (i,j) in the output feature map. This process is performed for all channels of the input image simultaneously.

For example, let take the following input with initial kernel below (Figure 2.2.2):

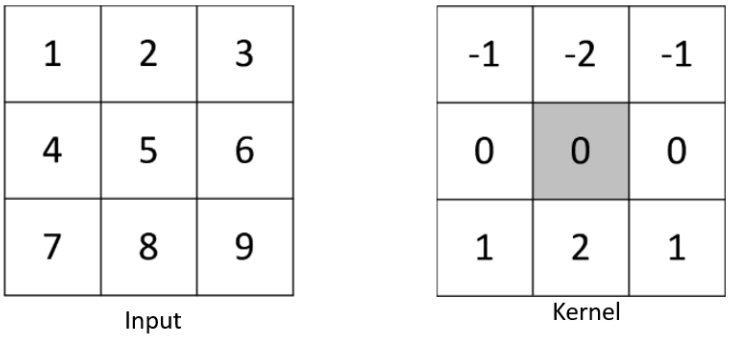

Figure 2.2.2: Input and initial kernel of convolutional operation example

Convolutional operation present in Figure 2.2.3 that graphically illustrates the primary calculations executed at each step. And Figure 2.2.4 outline the final outcome following the addition of the product values; each value represents an entry into the output feature map.

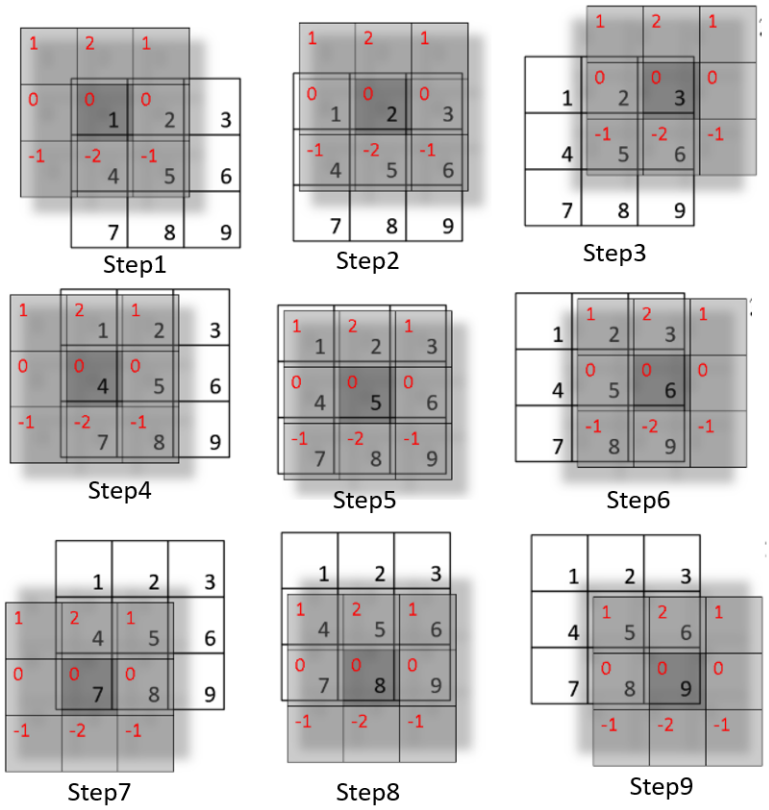

Figure 2.2.3: Convolutional operation steps

-13	-20	-17
-18	-24	-18
13	20	17

Output

Figure 2.2.4: Output of convolutional operation example

- **Pooling layers**: Pooling layers are often inserted after convolutional layers in the design of Convolutional Neural Networks (CNNs) to reduce dimensionality and computational requirements. Pooling layers work by subsampling the feature maps produced by the convolutional layer. They accomplish this by applying a pooling operation, such as max pooling or average pooling, to local regions of the feature maps. These operations condense the information within each region into a single value, effectively reducing the spatial dimensions of the feature maps. By reducing the dimensionality, pooling layers help in controlling the computational complexity of the network and preventing overfitting. Additionally, pooling layers can help retain the dominant features while discarding some of the less important details.

  However, it's important to note that pooling layers do not perform a "convolutional procedure" in the sense of convolutional operations. Instead, they apply a specific pooling operation within local regions of the feature maps.

  When selecting a pooling operation for feature maps in a pooling layer, it is common to use a filter size of 2x2 pixels with a stride of 2 pixels. This means that the pooling operation or filter is smaller than the feature map in size. By using a 2x2 pooling filter with a stride of 2, each feature map is compressed by a factor of 2. This results in each dimension being halved, reducing the feature map to contain only a quarter as many pixels or values. For example, a 4x4 feature map (16 pixels) would produce a 2x2 output pooled feature map (4 pixels), when the pooling layer is applied. Pooling layers help in producing a condensed version of the features found in the input. They achieve this by downsampling or pooling the feature maps. By reducing the spatial dimensions, pooling layers help ensure that slight changes in the position of a feature in the input, detected by the convolutional layer, still result in the pooled feature map having the feature in the same general location. It's worth noting that while a 2*2 pooling filter with a stride of 2 is commonly used, other configurations can also be chosen, such as using larger or smaller filter sizes or strides depending on the requirements of the network and the specific task at hand.

  There are several sorts of pooling techniques that may be used in various pooling layers [77]. Figure 2.2.5 illustrates the most pooling types used of the same example taken in convolutional layer.

  - **Average Pooling**: Average pooling calculates the average value within each pooling region. It provides a smoothed representation of the features and helps reduce the

impact of noise or minor variations.

– **Maximum pooling**: Max pooling selects the maximum value within each pooling region. It helps retain the most prominent feature in a particular region while reducing spatial dimensions.

– **Global Average Pooling**: is a pooling technique commonly used in convolutional neural networks (CNNs) as an alternative to traditional pooling layers. It is particularly effective in reducing the spatial dimensions of feature maps while preserving important information. Unlike traditional pooling layers, which use fixed-size pooling regions, Global Average Pooling computes the average value across the entire feature map. It replaces the spatial dimensions of the feature map with a single value per channel. This operation effectively collapses the spatial information into a global representation.

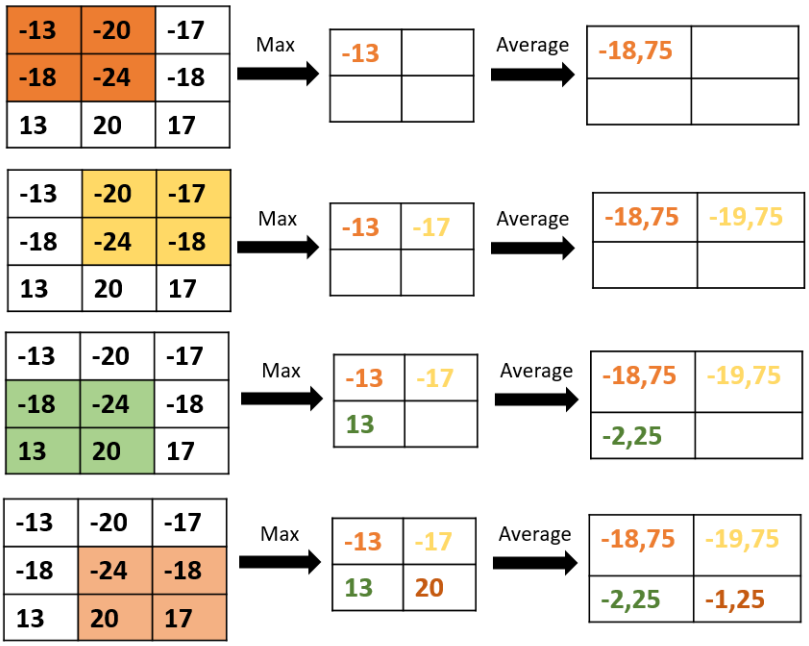

Figure 2.2.5: Pooling operations types

Where, the Global Average Pooling of the example is equal to Max(-13,-17,13,20)=20.

- **Fully Connected Layers (FCN)**: Fully Connected Layers are often located at the end of CNN architectures and play a crucial role in the categorization or classification process. In a Fully Connected Layer, also known as a Dense Layer, every neuron is indeed connected to every input from the previous layer. Each neuron in the layer receives input from all the neurons in the preceding layer. After the convolutional and pooling layers in a CNN, the feature maps are typically flattened into a 1-dimensional vector. This flattened vector is then passed through one or more Fully Connected Layers. In these Fully Connected Layers, traditional mathematical operations are performed, including matrix multiplication and activation functions. These operations transform the input vector through a series of weights and biases, allowing the network to learn complex patterns and relationships in the data. The final Fully Connected Layer often corresponds to the output layer of the CNN. The number of neurons in this layer typically matches the number of target classes or categories for classification. Each neuron in the output layer represents a specific class, and the output values from these neurons are often interpreted as the probabilities or scores for each class.

  By applying mathematical operations and learning from the data during training, the Fully Connected Layers enable the network to perform the categorization or classification process, producing the final predictions or outputs.

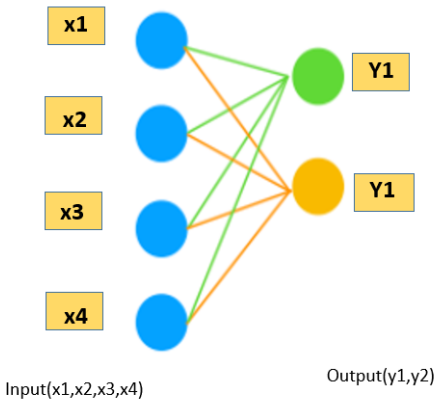

Figure 2.2.6: Fully Connected Layer (FC)

- **The activation function**: Is an important component in neural networks, including CNNs, as it introduces non-linearity and helps the network learn complex patterns and make decisions. However, the activation function is typically applied after the convolutional and fully connected layers, rather than specifically after the pooling phase. In a typical CNN architecture, the sequence of operations is as follows: convolutional layers, activation function, pooling layers, fully connected layers, and finally, the output layer [68].

  Regarding the spectrum of activation functions commonly employed in Convolutional Neural Networks (CNNs) and other deep neural networks, the following enumeration highlights some prevalent choices [78]:

  - **Sigmoid**: The sigmoid activation function squashes the input values into the range (0, 1). It is commonly used in binary classification tasks. The mathematical representation of the sigmoid function , which has a S shape, is Eq 2.2.2

$$\underset{sigm}{f(x)} = 1/(1 + \exp^{-x}) \tag{2.2.2}$$

  - **Rectified Linear Unit**: ReLU is one of the most widely used activation functions. It sets all negative input values to zero and leaves positive values unchanged. Eq 2.2.3 has a mathematical representation of it.

$$\underset{ReLU}{f(x)} = \max(0, x) \tag{2.2.3}$$

  - **Leaky ReLU**: Leaky ReLU is similar to ReLU but allows a small, non-zero gradient for negative input values. This helps address the "dying ReLU" problem Eq. 2.2.4.

$$f(x) = \begin{cases} x, & \text{if } x > 0 \\ \alpha x, & \text{otherwise} \end{cases} \tag{2.2.4}$$

    Where, "x" is the input, and α (alpha) is the small positive slope (usually a small constant like 0.01) that determines how much the function leaks when the input is less than or equal to zero.

– **Softmax**: Softmax is often used in the output layer for multi-class classification tasks Eq2.2.1. It normalizes the output values into a probability distribution over the classes.

$$\text{Softmax}(x)_i = \frac{e^{x_i}}{\sum_{j=1}^{N} e^{x_j}} 2.2.1 \tag{2.2.5}$$

where, x_i represents the $i-th$ element of the input vector, and N is the total number of elements in the vector.

These are just a few examples of activation functions used in CNNs. The choice of activation function depends on the nature of the problem, the network architecture, and the desired properties of the network. Different activation functions may be suitable for different layers within the network.

- **Loss Functions**: The output layer in a CNN architecture is indeed where the final categorization or prediction is obtained. The output layer typically consists of one or more neurons, depending on the number of target classes or categories.

  To measure the error or discrepancy between the predicted output and the actual output, a loss function is used in the output layer. It quantifies how well the CNN model is performing on the training samples, and compares the predicted output with the ground truth or target output 2.2.7.

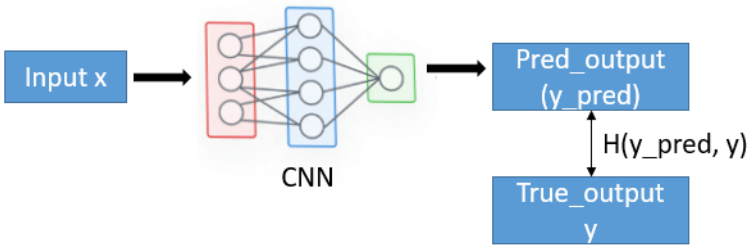

Figure 2.2.7: Loss function

The loss function is a fundamental component that necessitates two crucial parameters:

the predicted output generated by the CNN and the target or actual output. The predicted output signifies the network's result for a specific input sample, while the target output embodies the genuine label or anticipated output pertaining to that very sample. This function serves as a pivotal guide, quantifying the dissimilarity between the network's predictions and the ground truth, ultimately steering the optimization process during training. By comparing the predicted output with the target output, the loss function computes the error or discrepancy between them. This error value serves as a measure of how well the network is performing and guides the optimization process during training.

Different types of loss functions are used depending on the nature of the problem, the fellow paragraphs denote a several loss function types that exist with a succinctly explained [68].

– **Binary Cross-Entropy (sigmoid)**: Binary cross-entropy is commonly used for binary classification problems Eq 2.2.6. It measures the dissimilarity between the predicted and actual binary labels. It is particularly effective when dealing with imbalanced data sets or tasks where different classes have varying importance.

$$L(y, \hat{y}) = -\left[y \log(\hat{y}) + (1 - y) \log(1 - \hat{y})\right] \tag{2.2.6}$$

Where,
- $L(y, \hat{y})$ represents the binary cross-entropy loss.
- y is the true label (0 or 1).
- $\hat{y}$ is the predicted probability that the input belongs to class 1.

– **Categorical Cross-Entropy(Softmax)**: Categorical cross-entropy is used for multi-class classification tasks. It calculates the dissimilarity between the predicted class probabilities and the true class labels. It encourages the model to assign high probabilities to the correct class and low probabilities to others. Eq 2.2.7 is a mathematical expression of Cross-Entropy loss function:

$$h(p, y) = \sum_{i=1}^{N} y_i \log p_i \tag{2.2.7}$$

Where the probability distribution p is represented by the following formula Eq 2.2.8:

$$p_i = \frac{\exp_i^a}{\sum_{k=1}^{N} \exp^a \exp_k K} \tag{2.2.8}$$

With, N stands for the number of neurons in the output layer, and $\exp^a_i$ stands for the non-normalized output from the preceding layer.

– **The Euclidean Loss Function**: Is frequently utilized in regression issues. Eq 2.2.9 is a mathematical formula that expresses the estimated Euclidean loss.

$$H(p, y) = \frac{1}{2n} \sum_{i=1}^{N} (p_i - y_i)^2 \tag{2.2.9}$$

Where,
- $H(p, y)$ Euclidean Loss value, measuring the dissimilarity between predicted values (p) and actual observations (y).
- N Number of data points in the data set.
- p_i True or actual value of i^{th} data point.
- y_i Predicted value of i^{th} data point.

– **Hinge Loss Function**: This function finds prominent utility in the realm of binary classification tasks, particularly in contexts that involve maximum-margin-based classification. It holds notable significance, especially within Support Vector Machines (SVMs) that leverage the hinge loss function. In such cases, the optimizer's objective revolves around maximizing the margin surrounding the dual objective classes, aligning well with the Euclidean Loss Function's role in guiding classification tasks. Its mathematical equation is Eq.2.2.10.

$$H(p, y) = \sum_{i=1}^{N} \max(0, m, (2(y_i - 1)p_i) \tag{2.2.10}$$

Where,
- H represents the loss value.
- p is the true label or actual output (-1 or 1) of the sample.
- y is the predicted output, signifying the signed distance from the decision boundary.
- The max function ensures that the loss value is zero for correctly classified samples

and a positive value is incurred for misclassified samples.

– **Mean Squared Error (MSE)**: MSE is a widely used loss function for regression problems. It computes the average squared difference between the predicted and actual values. It penalizes larger errors more heavily, making it suitable for tasks where minimizing overall distance or deviation is important Eq 2.2.11.

$$MSE(y, \hat{y}) = \frac{1}{n}\sum_{i=1}^{n}(y_i - \hat{y}_i)^2 \tag{2.2.11}$$

Where,
- MSE represents the Mean Squared Error.
- n is the number of data points in the data-set.
- y denotes the true or actual value of the i^{th} data point.
- $\hat{y}$ indicates the predicted value for the i^{th} data point.

– **Kullback-Leibler Divergence (KL Divergence)**: KL divergence is a measure of dissimilarity between two probability distributions Eq2.2.12. It is often used in tasks such as variational auto encoders (VAEs) and generative models. KL divergence quantifies how much information is lost or gained when approximating one distribution with another.

$$D_{\mathrm{KL}}(P \,||\, Q) = \sum_{i} P(i) \log\left(\frac{P(i)}{Q(i)}\right) \tag{2.2.12}$$

Where,
- $D_{\mathrm{KL}}(P \,||\, Q)$ represents the KL Divergence between P and Q.
- $P(i)$ and $Q(i)$ represent the probabilities of the event i under the distributions P and Q.

– **Jaccard Loss or Union (IoU) Loss**: Is a commonly used loss function in various computer vision tasks, including image segmentation. It measures the similarity or overlap between the predicted and ground truth segmentation masks. The Jaccard Loss is computed by dividing the intersection of the predicted and ground truth regions by their union. Mathematically, it can be defined as Eq 2.2.13:

$$Jaccard\_Loss = 1 - (Intersection/Union) \tag{2.2.13}$$

The Jaccard Loss aims to maximize the IoU between the predicted and ground truth regions, encouraging accurate segmentation by penalizing false positives and false negatives. It is particularly useful when dealing with imbalanced classes or when the foreground and background regions have significantly different sizes.

– **Mean Squared Difference (MSD)** Is a similarity metric used in image processing and image registration. It measures the average squared difference between corresponding pixel intensities in two images. The lower the MSD value, the more similar the images are in terms of pixel intensity. MSD is commonly used to evaluate the quality of image alignment and registration algorithms. Mean Squared Difference (MSD) is calculated by measuring the pixel-wise intensity differences between corresponding pixels in the reference image and the transformed image, squaring those differences, and then taking the mean over all pixels. Mathematically, it can be defined as Eq 2.2.14:

$$MSD = (1/n) * \sum (Iref - Itransform)^2 \tag{2.2.14}$$

where, $\sum$ represents the summation over all n pixels, Iref is the intensity value of a pixel in the reference image, and Itransform is the intensity value of the corresponding pixel in the transformed (registered) image.

2.2.3 How does CNN work ?

A Convolutional Neural Network (CNN) is a deep learning architecture widely used for image processing tasks due to its ability to automatically learn and extract relevant features from input images. The input images are divided into three dimensions: height (m), width (n), and depth (r). In most cases, the height and width are equal, representing square input images. Gray scale images have a depth of 1, while RGB images have a depth of 3, with each channel representing color information. Each convolutional layer consists of multiple kernels (filters) denoted by the letter k, with dimensions (n * n * q). Here, n must be smaller than or equal to the height/width of the input (m), and q must be less than or equal to the depth (r). The kernels act as small windows that slide over the input image during the convolution operation [79]. The convolution operation between the kernels and the input image is represented by the

following equation:

$$\overset{k}{h} = f(\overset{k}{w} * x + \overset{k}{b}) \tag{2.2.15}$$

where:

- $\overset{k}{h}$ represents the feature map produced by the k-th kernel.
- f is the activation function, such as ReLU, sigmoid, or tanh, applied element-wise to the output.
- $\overset{k}{w}$ denotes the weight parameters associated with the k-th kernel.
- x is the input image or feature map.
- $\overset{k}{b}$ represents the bias term associated with the k-th kernel.

After the convolution operation, the resulting feature maps highlight specific patterns or features present in the input image. To reduce computational complexity and prevent overfitting, subsequent layers often include pooling layers, which down-sample the feature maps. Common pooling operations are max-pooling and average-pooling, where the maximum or average value within a small window (usually of size p * p) is retained while discarding the others. The feature maps from the convolutional and pooling layers serve as input to fully connected (FC) layers, which provide high-level abstractions and correspond to the last layers in a standard neural network. The FC layers are followed by a finishing layer, which can be a softmax layer for classification tasks. The softmax function produces categorization scores for each class, reflecting the likelihood of the input image belonging to a particular class [79].

In summary, a CNN learns and extracts meaningful features from images through the use of convolutional layers, pooling layers for downsampling, and fully connected layers for high-level abstraction. This hierarchical process allows the CNN to effectively perform various computer vision tasks, such as image classification, object detection, and image segmentation.

2.2.4 CNN supervised and CNN unsupervised

Convolutional Neural Networks (CNNs) exhibit remarkable versatility, finding utility in a spectrum of learning scenarios encompassing both supervised and unsupervised contexts. The choice between these paradigms hinges upon the nature of the problem at hand and the nature of the data available.

In supervised learning, CNNs shine when presented with data sets that are meticulously labeled, offering input-output pairs for training. This manifests in tasks like image classification, where CNNs meticulously predict the categorical class of images; object detection, wherein the networks deftly localize and label objects in images; semantic segmentation, facilitating pixel-level object segmentation; and even regression tasks, where continuous predictions, such as age estimation from facial images, come into play. The training process in supervised learning engenders optimization that seeks to minimize the discord between predicted outputs and the ground truth labels. Through this iterative process, CNNs learn to discern patterns in the data, ultimately acquiring the capacity to extrapolate these patterns to hitherto unseen instances [80].

In unsupervised learning, CNNs navigate a distinctive realm where labeled data is eschewed, and the emphasis pivots toward autonomous pattern extraction. Here, tasks such as auto encoders, a neural network architecture for dimensionality reduction and feature discovery, shine. Through an encoder-decoder setup, the network captures a compact latent representation of input data. Additionally, CNNs flourish in clustering tasks, where they organize akin data points into clusters based on learned features. Anomaly detection also emerges as a forte, as CNNs, trained on regular data, can discern deviations that mark anomalies. Crucially, the underpinning of unsupervised learning for CNNs involves their training on unlabeled data, a process oriented towards distilling meaningful patterns without relying on explicit labels [80].

2.2.5 CNN architectures

Over the past ten years, the architecture of Convolutional Neural Networks (CNNs) has undergone significant changes and improvements. These advancements encompass various aspects, such as regularization, parameter optimization, and structural reformulation, as highlighted in a study by [68]. However, the most substantial improvement in CNN performance can be attributed to the restructuring of processing units and the creation of new blocks. One of the groundbreaking developments in CNN design has been the exploration of network depth. Increasing the depth of CNNs, i.e., adding more layers, has led to innovative breakthroughs in improving their performance. Deeper networks have demonstrated enhanced ability to capture and learn intricate features from the input data, enabling CNNs to excel in complex visual tasks. In this section, we will review the most prominent CNN designs, each with its unique architectural properties. These architectures represent the state-of-the-art approaches that have pushed the boundaries of CNN capabilities in image processing tasks. By examining their design characteristics and successes, we gain valuable insights into the evolution of CNNs and their application to various real-world problems.

2.2.5.1 LeNet-5 (1998)

The most well-known CNN architecture is the LeNet-5 network, introduced in 1998 by [81]. LeNet-5 was a pioneering model that marked the beginning of deep CNN development. During that time, CNNs were primarily used for tasks related to handwritten digit recognition. LeNet-5 consists of three fully connected layers and two convolutional layers. The architecture of LeNet-5 is illustrated in Figure 2.2.10. Despite its relatively simple structure, LeNet-5 was able to achieve impressive results in digit recognition tasks.

However, as the complexity of visual tasks increased, higher-resolution images demanded more and larger CNN convolutional layers to effectively capture intricate features. Consequently, subsequent CNN architectures were developed to accommodate the growing requirements of various image processing tasks. These advancements in CNN architecture have paved the way for the remarkable progress seen in the field of computer vision in recent years.

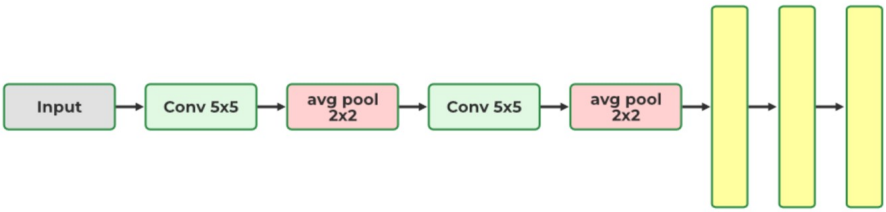

Figure 2.2.8: LeNet-5 architecture

2.2.5.2 AlexNet (2012)

The groundbreaking advancement in CNN architecture came with Alex Krizhevsky's introduction of AlexNet, which revolutionized the stacking of convolutional layers directly on top of each other, as opposed to adding a pooling layer on top of each convolutional layer. This change significantly improved the model's ability to capture intricate features from images.

In the 2012 ImageNet ILSVRC challenges, AlexNet's CNN architecture achieved a remarkable feat, winning with a significant margin and achieving a top-5 error rate of 17%. The architecture comprised a total of eight layers, including five convolutional layers and three fully connected layers. AlexNet's activation functions were initially based on Rectified Linear Units (ReLUs), as shown in Figure 2.2.9. Due to its groundbreaking results in image recognition and classification tasks, AlexNet became highly regarded in the field of deep CNN architecture

[82]. Since then, researchers have continued to enhance CNNs' learning capacity by deepening the network, incorporating various parameter optimization techniques, and exploring new architectural modifications.

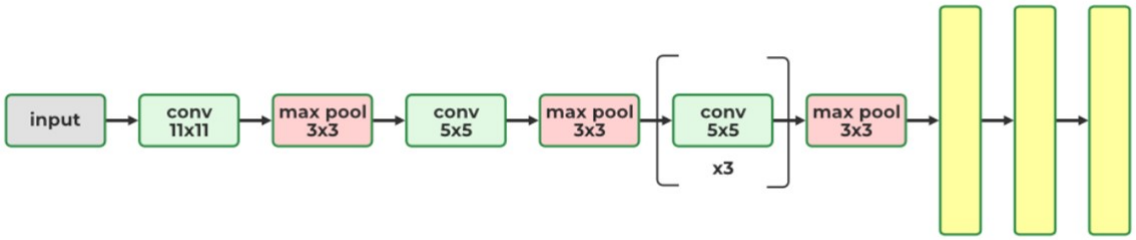

Figure 2.2.9: AlexNet architecture

2.2.5.3 ResNet (2015)

ResNet, short for "Residual Network," is a deep convolutional neural network architecture introduced by [83] ResNet was designed to address the vanishing gradient problem that arises in very deep neural networks, making it possible to train and optimize models with hundreds or even thousands of layers. The key innovation in ResNet is the use of residual blocks, also known as skip connections or shortcut connections. These skip connections allow the network to learn residual mappings instead of directly trying to learn the desired underlying mapping. By propagating the input directly to the deeper layers through these skip connections, ResNet can learn the residual information, making it easier for the network to optimize and avoid degradation in performance as the network becomes deeper. The core building block of ResNet is the residual block, which is typically composed of two or more convolutional layers with a skip connection. The skip connection adds the input to the output of the convolutional layers, allowing the network to learn the difference (residual) between the input and output.

The general formula Eq2.2.16 for the output of a residual block can be represented as follows:

$$\text{Output} = F(\text{Input}) + \text{Input} \tag{2.2.16}$$

where, F(Input) represents the output of the convolutional layers.

ResNet comes in various depths, with the most popular versions being ResNet-18, ResNet-34, ResNet-50, ResNet-101, and ResNet-152, denoting the number of layers in each variant. The deeper variants have shown superior performance in various image recognition tasks and have won several competitions, including the ImageNet Large Scale Visual Recognition Challenge (ILSVRC). ResNet has found widespread use in a wide range of computer vision tasks, including image classification, object detection, semantic segmentation, and medical image analysis. Its ability to train very deep networks effectively, along with its excellent performance and efficiency, has made it a fundamental architecture in the field of deep learning.

2.2.5.4 U-net (2015)

U-Net is a convolutional neural network architecture designed for semantic segmentation tasks, particularly in biomedical image segmentation. It was introduced by[84] The name "U-Net" comes from the U-shaped architecture of the network. The U-Net architecture is characterized by its encoder-decoder structure with skip connections. It is designed to effectively capture both local and global features while preserving spatial information during the downsampling and upsampling process. The skip connections are used to connect corresponding encoder and decoder layers, allowing the network to combine high-resolution features from the encoder with the low-resolution features from the decoder. The U-Net architecture can be broken down into two main parts:

- Encoder: The encoder part of the U-Net consists of a series of down-sampling layers, typically achieved through convolutional layers followed by max-pooling. The purpose of the encoder is to extract hierarchical features from the input image, reducing the spatial dimensions while increasing the number of feature maps.
- Decoder: The decoder part of the U-Net consists of a series of up-sampling layers, typically achieved through deconvolution (transpose convolution) layers followed by concatenation with the corresponding feature maps from the encoder through skip connections. The decoder's goal is to reconstruct the original input size while retaining detailed information from the encoder.

The skip connections allow U-Net to pass both local and global contextual information to the decoder, helping the network make more accurate segmentation predictions. These connections aid in overcoming the information loss that typically occurs during down-sampling. U-Net has found widespread use in various medical image segmentation tasks, such as cell segmentation,

organ segmentation, and tumor segmentation. Its effectiveness in handling limited data and its ability to produce accurate segmentation masks have made it a popular choice in the medical imaging community.

The architecture of U-Net has also inspired the development of many variations and extensions, such as 3D U-Net for volumetric data, attention U-Net that incorporates attention mechanisms, and cascaded U-Net for iterative refinement of segmentation masks. The versatility and adaptability of the U-Net architecture have contributed to its success in various segmentation applications.

2.2.5.5 SegNet (2015)

SegNet is a convolutional neural network architecture specifically designed for semantic segmentation tasks. It was introduced by [85]. SegNet is especially well-suited for scenarios with limited data and computational resources, making it popular in applications such as medical image segmentation and real-time scene understanding. The SegNet architecture consists of an encoder-decoder structure with skip connections, similar to U-Net. However, unlike U-Net, SegNet primarily focuses on reducing memory consumption while maintaining segmentation accuracy.

Key features of the SegNet architecture:

- Encoder: The encoder in SegNet performs down-sampling using convolutional layers and pooling operations to capture hierarchical features from the input image. The encoder's primary role is to extract informative features for segmentation.
- Decoder: The decoder part of SegNet is designed to up-sample the feature maps to reconstruct the segmentation mask. Unlike traditional deconvolution (transpose convolution) layers used in the decoder, SegNet employs "max-pooling indices" from the encoder. These indices indicate the location of the maximum activation during the pooling operation in the corresponding encoder layer. By using these indices, SegNet avoids learning additional parameters in the decoder, reducing memory requirements.
- Skip Connections: SegNet incorporates skip connections between the corresponding encoder and decoder layers. These skip connections help in preserving spatial information and facilitate the precise localization of segmented objects.
- Softmax Layer: The output of the decoder is passed through a softmax layer to produce class probabilities for each pixel, enabling pixel-wise segmentation.

The use of max-pooling indices instead of traditional deconvolution layers helps SegNet achieve significant memory savings, making it suitable for deployment on resource-constrained devices and handling large-scale image segmentation tasks. However, it is essential to note that SegNet may produce rough boundaries for segmented objects due to the pooling operation's inherent loss of spatial information.

SegNet has been successfully applied to various medical image segmentation tasks, such as brain tumor segmentation, cell segmentation, and organ segmentation. Its lightweight and efficient architecture make it an attractive choice for scenarios where computational resources are limited or real-time performance is crucial .

2.2.5.6 Dense-net (2017)

Dens-Net, short for "Densely Connected Convolutional Network," is a deep neural network architecture introduced by [86]. Dens-Net is designed to address the vanishing gradient problem in very deep neural networks while promoting feature reuse and efficient parameter usage. The key innovation in Dens-Net is its dense connectivity pattern, where each layer is connected to every other layer in a feed-forward manner within the same dense block. In traditional CNN architectures, feature maps are concatenated only at certain stages or layers. In contrast, Dens-Net directly concatenates feature maps from all preceding layers, creating dense connections between layers. This densely connected architecture ensures that each layer has access to the feature maps of all preceding layers, promoting feature reuse and facilitating the flow of gradients during backpropagation. The core building block of Dens-Net is the dense block, which consists of a series of convolutional layers followed by concatenation of their outputs. By densely connecting each layer to all previous layers, Dens-Net effectively encourages feature propagation and enables better information flow throughout the network. Additionally, Dens-Net's dense connectivity pattern allows it to be highly parameter-efficient, reducing the number of parameters required compared to traditional architectures. Dens-Net comes in various depths, such as Dens-Net-121, Dens-Net-169, Dens-Net-201, and Dens-Net-264, with the number indicating the total number of layers in each variant. Deeper Dens-Nets have shown impressive performance in image classification and other computer vision tasks, often outperforming other architectures with similar numbers of parameters. One of the challenges of dense connectivity is the potential increase in memory consumption during training. To address this, Dens-Net often employs transition layers between dense blocks to reduce the number of feature maps before passing them to the next dense block. Transition layers typically consist of convolutional layers followed by pooling or strided convolution operations to downsample the feature maps. Dens-Net has become a popular architecture due to its ability to effectively learn

from limited data, its parameter efficiency, and its impressive performance on various image classification and segmentation tasks. It has become a valuable tool in computer vision and has spurred further research in dense connectivity and network architectures.

2.2.6 CNN limitations and challenges

The inherent deep architecture of Convolutional Neural Networks (CNNs), facilitating the extraction of a multitude of discriminative features across various levels of abstraction, constitutes a formidable strength of the system. However, constructing a deep CNN from the ground up is not without its drawbacks, as highlighted by Nima et al. [87].

To begin, the medical field grapples with challenges arising from the cost of expert annotations and the scarcity of illness-related data, such as lesions. Consequently, assembling a substantial repository of labeled training data for CNNs becomes a formidable task. The healthcare domain frequently contends with the issue of underrepresented clinical or demographic categories, limiting the model's potential for effective generalization. Notably, this predicament is mitigated by the advent of transfer learning. The capability to repurpose a model trained on extensive data sets to serve as the foundation for a new model with distinct objectives has alleviated the need for copious labeled data [88]. Furthermore, training deep CNNs entails substantial computational and memory resources, necessitating prolonged training durations. The process is susceptible to challenges like fatigue, overfitting, and convergence concerns. Addressing these demands recurrent alterations to the network's architecture and learning configurations to ensure consistent learning across all layers. Consequently, the process of deep learning from scratch mandates a significant commitment of time, patience, and expertise. Despite the marked advancements witnessed in specific domains, deep learning remains far from emulating human-like performance across all AI endeavors. Owing to the intricate interplay of numerous training parameters, deep learning models are often referred to as "black boxes," wherein the decision-making process is obfuscated. Weights and features are intricate to interpret, rendering it intricate for researchers to grasp the inner workings of the model and the rationale behind its performance [88].

In culmination, the efficacy of Deep Learning (DL) and CNNs in precisely diagnosing skin cancer and dermatological disorders has been well-established. Within this context, digital learning (DL) emerges as a potent technology with the potential to guide therapeutic decisions. The nexus of computer science and dermatology is propelling the development of avant-garde techniques for dermatological diagnosis. However, while DL holds promise in medical treatments, further substantiation through data and perspectives is requisite [89].

2.2.7 Skin processing in CNNs applications

In recent years, the utilization of Deep Learning (DL) and Convolutional Neural Networks (CNNs) has witnessed a significant upsurge in medical image analysis, notably within the dermatology domain. An area of substantial focus involves the detection of skin cancer using dermoscopic images, considering the global prevalence of skin malignancies [91]. The International Skin Imaging Collaboration (ISIC) [92] has taken the initiative to establish a repository of dermoscopic images, facilitating research and the development of automated melanoma diagnosis techniques. This organization also orchestrates an annual competition centered on the analysis of skin lesion images [93, 94]. Notably, during the 2016 International Symposium on Biomedical Imaging (ISBI Melanoma Detection Challenge), all participating teams harnessed DL techniques for this task [95]. DL's prowess extends to diverse dermatological areas, encompassing ulcer classification, onychomycosis detection, and monitoring wound healing processes [96]. Furthermore, DL-based models have been adeptly crafted not only for classification objectives, but also for the intricate task of segmenting skin lesions and ulcers [97]. During 2021, a study conducted by [89] presented an interactive computer program along with a comprehensive description of the procedures involved in setting up and fine-tuning a CNN for the categorization of dermatological images. Regarding the study of skin hydration effects, [91] utilized the AlexNet architecture as a classification model to examine skin moisture in images. While this work did not directly assess hydration levels, it incorporated hydration as a categorization label in the training data to improve the performance of complex methods for skin image analysis, considering features such as skin texture and color.

Table 2.2.10 summarizes various related works in the biomedical field related to skin applications, categorized by the medical task, and the primary loss functions employed for each task, along with their associated limitations:

Medical task	Loss function	Applications	Limitations	Related work
Skin lesion segmentation	Jaccard loss	- Skin cancer segmentation. - Melanoma detection	- Class imbalance sensitivity. - Fuzzy boundaries.	- (Norsage et al, 2023) - (Mirikharaji et al, 2023) - (Lei et al, 2018)
Skin disease classification	Cross Empty Loss	- Eczema classification. - Psoriasis classification.	- Noisy/ mislabeled data sensivity.	- (Brinker et al, 2020) - (Tschandl et al, 2019) - (Codella et al, 2018)
Skin registration	MSD (Mean Squared Difference)	- Image alignement. - Skin image registration.	- Intensity shifts. - Artificat sensitivity.	- (Balakrishnan et al, 2019) - (Wang et al, 2018) - (Vu et al, 2013)
Skin hydration	MSE(Mean Square Error)	- Skin hydration level estimation. - Skin care assecement.	- Noise/ outlier sensitivity	- (Pan et al, 2017) - (Beradesca et al, 2012) - (Pillia et al, 2005)
	L1 loss(Mean Absolute Error)	- Skin moisture contenet prediction. - Hydration mapping.	- Less sensitivity to outliers.	
	Huber loss	- Skin water contenet measurments. - Skin barrier evaluation.	- Balances behavier MSE and MAE.	

Figure 2.2.10: Loss types for skin biomedical tasks.

These studies underscore the extensive application of Deep Learning (DL) and Convolutional Neural Networks (CNNs) in dermatology, encompassing tasks such as skin cancer diagnosis and the analysis of various dermatological conditions, including the evaluation of skin hydration levels. The subsequent section offers a comprehensive review of CNN-based processing methods applied to skin data within this clinical context.

2.3 CNN for skin processing methods

In this section, we provide an overview of relevant work pertaining to the current investigation. We begin with a discussion of current research on skin investigations that employ image segmentation techniques. Image segmentation is a crucial step in computer vision tasks, including dermatology, as it allows for the precise delineation and identification of regions of interest within skin images. Next, we highlight investigations that have utilized deep learning techniques to evaluate skin moisture. Deep learning has shown great promise in various medical imaging applications, and its application to skin moisture assessment can provide valuable insights into skin health and hydration. Finally, we present a comparable approach for

skin research registration. Skin research registration involves aligning and registering images from different sources or time points to facilitate meaningful comparisons and analyses. Such registration techniques are essential for longitudinal studies and tracking changes in skin conditions over time. By discussing these areas of research, we aim to provide a comprehensive understanding of the current state of skin investigations, the advancements made through deep learning, and the significance of image registration in dermatological studies. These collective insights will inform and contribute to the current investigation's objectives and pave the way for further advancements in skin health assessment and research.

2.3.1 Skin segmentation

Segmentation is an essential task in image processing applications. We can define it as the mechanism that allows dividing an image into regions, according to similar properties such as gray level, texture, brightness, and color, etc [98].

In the medical imaging field, High precision, low bias segmentation techniques are used to characterize anatomical structure, identify aberrant regions like tumors and lesions. In medical imaging processing, the segmentation problem is often characterized as locating the collection of voxels that comprise either the interior or the contour of the object(s) of interest. The most often discussed topic in articles utilizing deep learning in medical imaging is segmentation, which has also led to the creation of distinctive CNN-based segmentation architectures. Among these novel CNN architectures, U-net [84] combines equal amounts of upsampling and downsampling layers, which is one of its two primary architectural innovations. Despite the fact that learnt upsampling layers have previously been suggested, Opposing convolution and deconvolution layers are combined by U-net via so-called skip connections. The U-net design has also been modified by other authors. For instance, [68] introduced the V-net, a 3D variation of the U-net architecture that does 3D image segmentation using 3D convolutional layers with an objective function that is directly dependent on the Dice coefficient. In addition to the lengthy skip-connections in a typical U-net, [99] looked at the usage of short ResNet-like skip connections.

Now days, Deep learning-related techniques for segmentation in medical imaging have become quite popular. To specifically address the segmentation challenge, unique structures have been developed. Related to skin applications, [100] accomplished an effective segmentation method on skin benchmark data sets using DensNet architecture. The fundamental idea employed in their work is to link the outputs of the Dens block of the decoder component with its corresponding decoder at each feature resolution. Skin lesions were primarily sought after in investigations on skin segmentation. Using Fully Convolutional Networks (FCN), [101] sugges-

ted a multi-class semantic lesions segmentation for the investigation of melanoma, seborrheic keratosis, and nevus . In studies done before this one, [102] and [103] presented deep residual convolutional neural networks with various techniques for segmenting skin lesions, but only for a single class. [104], also used FCN to generate plausible segmentation maps of images from their surroundings and their background. [105] proposed a skin segmentation method, which allows to integrate the prediction scores of the intermediate network layers. More details about these methods can be found in the review by [106] which gives an overview of algorithms and techniques of conventional deep learning approaches for skin segmentation lesions. Recently, [107], presented also an automatic semantic segmentation network (Dermoscopic Skin Network (DSNet)) for robust skin lesion segmentation.

Recently, Deep learning approaches recently do well in skin segmentation. While lesion segmentation is the first stage in analysis, the bulk of scientific researchers employed a deep learning framework to find skin lesions. As an illustration, [108]assessed three deep learning models to build a fully-fledged automated solution for skin lesion segmentation. Using a CNN model to precisely extract lesion locations, [109] examined melanoma. [110] then introduced a deep learning technique for automated skin lesion segmentation, with the same goal in mind. [111] developed the skinNet model, which was a modified version of the U-Net framework, as a deep learning framework for skin lesion segmentation. Due to the U-net model superior performance with medical data, it has lately taken the lead in CNN models as the model most frequently employed in medical semantic segmentation applications. It is employed in several research as a result. For instance, [112] suggested an effective segmentation technique for assisted computer diagnostic systems employing convolution separable block and U-net architecture. [113] also employed U-net architecture and DCNN-SVM classifier to classify skin cancers. On the same subject, [114] presented U-net architecture based on contour detection and boundary distance map. Earlier this year, [115] introduce a CLNet modelthat fuses a fusion module feature of skin lesions with a classification and segmentation model. Their new study's objective is to completely use the segmentation and classification approaches' performance utilizing the fusion feature that was generated using the two models.

2.3.2 Skin hydration measurements

Measurement of skin hydration is crucial for several clinical research studies, as it plays a vital role in understanding skin health and various dermatological conditions. In recent years, deep learning architectures have been employed to investigate and explore the hydration level of the skin, aiming to provide more accurate and efficient methods for assessment. However, despite the potential benefits of deep learning in skin hydration analysis, the literature on the study of

skin hydration effects using deep learning approaches remains relatively limited compared to the extensive research conducted on skin lesion studies. This underscores the need for further exploration and development in this specific area.

For instance [116], conducted a study on in vivo skin hydration images using AlexNet as a classification model. Their work focused on extracting skin image characteristics such as skin texture and color, which are crucial factors affecting skin hydration. While hydration level was not explicitly measured in the study, it was considered as a classification label for the AlexNet training data to enhance the performance of deep learning methods for skin images. More recently, [117] proposed a skin capacitive imaging technique utilizing deep learning GoogLeNet. Their method can measure skin hydration in vivo based on the permittivity measuring approach, which provides a non-invasive and efficient means of evaluating skin moisture levels. Following their work, [118] provided a comprehensive overview of state-of-the-art machine learning and deep learning methods for atrial fibrillation detection and skin hydration level estimation. Their study not only described the relationship between AF and skin moisture but also addressed the benefits and drawbacks of various AF detection methods and strategies used to evaluate skin hydration levels in the literature. This informative review serves as a foundation for future research advancements in this field. Building upon these studies, [119] introduced a novel non-invasive method for measuring skin hydration based on the body's skin resistance. They collected data from three distinct body positions, considering different hydration states. To improve the estimation accuracy, they proposed a hybrid (ML+DL) model consisting of four distinct deep learning algorithms and eight different machine learning algorithms. In another related work, [120] explored the use of Convolutional Neural Networks (CNNs) for skin hydration assessment. They employed a multi-scale CNN architecture to analyze skin images captured at different depths, enabling a more comprehensive understanding of skin hydration patterns.

These studies collectively demonstrate the growing interest in employing deep learning techniques for skin hydration measurement and provide valuable contributions to the advancement of dermatological research. As researchers continue to explore the potential of deep learning in this domain, it is expected that novel and robust methodologies will emerge, leading to improved diagnostic and therapeutic approaches in dermatology.

2.3.3 Skin registration

Skin registration, also known as image registration or medical image registration, is a fundamental process used in medical imaging to align or match different images of the same patient or anatomical region. The primary goal of skin registration is to find a transformation that can

spatially align one skin image with another, ensuring that corresponding anatomical structures or features in the images are accurately superimposed.

To summarize, the canonical technique for image registration typically involves four basic phases, as described by [68]:

- Target selection: This phase involves selecting the input image that needs to be appropriately aligned with the second counterpart input image.
- Feature Extraction: In this step, the algorithm computes a collection of features extracted from each input image. These features act as distinctive landmarks that help in comparing and aligning the images.
- Feature matching: The feature matching process compares the previously acquired features from both input images. It aims to find corresponding features between the two images, which enables the algorithm to determine the spatial relationship between them.
- Optimization: The optimization phase seeks to minimize the gap between the two input images by finding the best geometric transformation that aligns the images effectively. The goal is to achieve an optimized overlaying level, which means reducing the distance between the aligned images as much as possible.

Overall, the output of the image registration process is the appropriate geometric transformation that places both input images within the same coordinate system, ensuring that they are properly aligned with an optimized overlaying level. This transformation allows for accurate comparison and analysis of the images, benefiting various applications in medical imaging, computer vision, and other fields.

In the context of skin imaging, registration plays a crucial role in various applications. One important use is in follow-up examinations, where healthcare professionals can monitor changes in skin conditions, such as wound healing or disease progression, by registering images from different time points. Moreover, skin registration is essential for accurate comparison and analysis. By aligning skin images acquired through different imaging modalities or techniques, researchers can perform more reliable quantitative analysis and make more informed comparisons between different data sets. Additionally, skin registration aids in treatment planning in dermatology. Physicians can evaluate the effectiveness of interventions over time by registering images taken before and after treatments, helping them to devise and adjust treatment plans for better patient outcomes. There are several methods for skin registration, each with its own advantages and limitations. Some common techniques include intensity-based, feature-based, and deformable registration methods. The choice of registration method depends on the specific clinical or research application and the characteristics of the skin images being processed.

In recent years, significant progress has been made in the field of skin image registration, leading to the development of diverse techniques that cater to specific challenges and applications. For instance, Jahanifar et al proposed a deep learning-based approach for the registration of dermoscopic images, utilizing a convolutional neural network (CNN) to learn feature representations from images and performing deformable registration using the learned features. Their method achieved highly accurate and efficient registration results, particularly in cases with substantial variations in skin lesion shapes and sizes. To address the challenges of non-rigid registration in skin images, [121] presented a framework based on finite element modeling. Their method incorporated mechanical properties of the skin and used a bio-mechanical model to guide the registration process, enabling accurate alignment of skin surfaces in the presence of deformations. In the context of wound healing assessment, [109] introduced a multi-modal registration approach to align thermal images with RGB images of wounds. Their method combined intensity-based and feature-based techniques, taking advantage of complementary information in thermal and RGB images to enhance wound healing evaluation. Moreover, for skin image registration involving multiple imaging modalities, Shi et al proposed a multi-atlas-based method. They built a library of atlases representing different skin conditions and employed a label fusion technique to achieve accurate registration and segmentation of skin lesions. Furthermore, to address the challenges of aligning skin images acquired at different time points and under varying illumination conditions,[122] introduced a robust illumination-invariant registration method. Their approach utilized a combination of illumination normalization and feature-based registration to achieve reliable alignment in challenging lighting conditions. In addition to traditional 2D image registration, 3D skin image registration is gaining traction. [123] developed a deformable 3D skin surface registration technique based on a Markov random field model. Their method effectively aligned 3D skin surface scans, enabling accurate volumetric analysis and visualization of skin changes. These advancements in skin image registration demonstrate the ongoing efforts to improve the accuracy, efficiency, and applicability of registration techniques in dermatology and related fields. As medical image registration continues to evolve, it holds great promise for advancing clinical practice and research, ultimately leading to better healthcare outcomes and a deeper understanding of skin health and diseases.

2.4 Conclusion

This chapter provides a comprehensive introduction to Convolutional Neural Networks (CNNs), explaining the fundamental concepts and showcasing the main architectures that can be utilized to construct Deep Learning (DL) models. Additionally, the chapter delves into semantic

segmentation, a popular task in CNN clinical applications, which plays a crucial role in image analysis. Moreover, the chapter presents an overview of previous techniques employed to measure skin hydration, with a specific focus on registration techniques in the medical field. These registration techniques are utilized to align and integrate medical images, facilitating comprehensive analysis and accurate measurement of skin hydration. From a CNN perspective, it is evident that medical imaging benefits significantly from DL applications, encompassing tasks like image segmentation and analysis. This dissertation particularly concentrates on three primary tasks: semantic segmentation, regression task, and registration task. In the following chapter, we outline the proposed approach for each task, leveraging CNN techniques and utilizing real MRI data with high resolution to achieve precise and reliable results.

CHAPTER 3

Proposed approaches for MRI skin processing

3.1 Introduction

Accurately determining the physical properties and structural arrangements of skin layers, along with their MRI imaging characteristics, plays a pivotal role in several clinical applications. In this study, we specifically focus on the measurement of skin hydration, where the choice of MRI modality is crucial for investigating this case with utmost reliability and robustness. Deep learning approaches have demonstrated great potential in medical imaging, making them a natural fit for addressing the challenges associated with skin hydration assessment. Our proposed approaches in this chapter not only highlight the significance of the problem at hand but also provide a tailored strategy to overcome the various anticipated limitations. By utilizing advanced deep learning techniques, we aim to revolutionize skin hydration measurement and simulation in clinical settings. The potential implications of accurately assessing skin hydration extend to improved diagnosis, personalized treatment planning, and a deeper understanding of skin health.

The first section of this chapter delves into the motivations driving our research contribution, exploring the pressing need for accurate and efficient skin hydration assessment methods. Subsequently, we present our novel deep learning-based approaches, which encompass both the measurement of skin hydration and the simulation of this crucial clinical phenomenon. Through these innovative methodologies, we anticipate substantial advancements in dermatological research and clinical practice. Our deep learning-based strategies have the potential to pave the way for a new era of precision medicine, where dermatologists can make well-informed decisions based on accurate and reliable skin hydration data. Ultimately, this could lead to enhanced patient care, improved treatment outcomes, and a deeper understanding of skin biology, benefiting a wide range of medical applications.

3.2 Motivations

Skin hydration is a complex task that is deeply intertwined with the mechanical and physical properties of the skin, relying on the distribution of water across different skin layers. Therefore, it is crucial to develop a method that can accurately measure the water content of human skin to study the effects of hydrated creams on these skin layers.

Traditional methods for measuring skin hydration are time-consuming and limited when it comes to studying complete surface layers or multiple skin layers. This presents a challenge that calls for the development of methods that can accurately measure skin layer hydration using large MRI data sets. Some researchers have explored the effects of deep learning architectures on skin moisture. For example, [98] utilized the AlexNet as a classification model to examine skin moisture images. While their work focused on skin image feature extraction, such as skin texture and color, it did not formally assess hydration. However, they incorporated hydration as a categorization label in the training data to improve the performance of complex methods for skin images. Other researchers [124] were interested in measuring skin hydration and employed semi-automatic and fully automatic ML-based methods. They used local regression, boundary selection, and a Canny edge detector to measure T2 values over the region of interest (ROI) and the entire segmented skin layer. Their method showed a good correlation with manual measurement techniques, but it was highly sensitive to noise and intensity fluctuations [125]. Moreover, the boundary selection phase in their approach could lead to incorrect boundaries. The application and generalization of such techniques for MRI segmentation may yield inaccurate results. In contrast, deep neural networks effectively address issues related to intensity and noise. Furthermore, unlike the approach used by [124] the semantic segmentation nature of convolutional neural networks (CNNs) allows for an extension of the method while eliminating the need for the boundary selection phase.

However, the first challenge we face on this work is detecting and defining the structures and properties of each skin layer. For this purpose, we have chosen to employ Resonance Magnetic Imaging (MRI) with high resolution, taking into consideration existing literature on skin segmentation from MRI images. This approach enables us to capture intricate details of the skin layers, facilitating a comprehensive analysis. The second challenge lies in tracking the distribution of water content in each skin layer, which we achieve through the creation of T2 map cartographies. These cartographies provide valuable insights into the hydration levels of different skin regions, facilitating a thorough understanding of skin hydration patterns. Our contribution lies in proposing an automatic approach that utilizes deep learning methods to segment skin layers automatically. This innovative technique allows for precise quantification of water content in each layer, and the subsequent study of hydration changes before and after

the application of hydrated cream, as evidenced by the T2 map cartographies. Additionally, we introduce a simulation approach for studying hydration using deep learning methods. This simulation technique serves to model and predict hydration phenomena, providing valuable insights into how the skin responds to various treatments and environmental factors. The remainder of this chapter provides a detailed exposition of these two proposed approaches, outlining the methodologies and potential impact on advancing dermatological research and clinical practice. Through these approaches, we aspire to make significant contributions to the field of skin hydration analysis, offering valuable tools for assessing skincare product efficacy and guiding personalized treatment approaches.

3.3 A Deep learning segmentation proposed method for MRI skin hydration measurements

This research introduces a state-of-the-art deep learning-based segmentation method specifically tailored for MRI skin hydration measurements. In MRI, a modality that relies on physical and biomedical properties, it is possible to detect and visualize the water content in different skin layers through the generation of water cartographies. However, MRI comes with inherent challenges, including fluctuations in noise levels and variations in image intensity, which can adversely affect the accuracy of traditional segmentation methods that rely on intensity gradients in medical imaging. To address these complex challenges and enhance the precision of skin layer segmentation in MRI images, a comprehensive literature review on skin MRI image segmentation was conducted. This rigorous analysis led to the selection of deep learning as a promising solution due to its ability to handle intricate image data and learn complex patterns from large data sets. The primary focus of this research is to design and evaluate deep learning models based on advanced architectures such as U-net and Dense-net, both of which are variants of Convolutional Neural Networks (CNNs). These CNN models are specifically tailored to exploit the capabilities of deep learning and learn from real MRI data sets to accurately segment skin layers. The incorporation of deep learning techniques enables the models to adapt and capture intricate features and patterns in MRI images, making them well-suited for the complexities involved in skin hydration measurements.

One of the significant challenges addressed in this research is the limited availability of labeled MRI data for training deep learning models. To overcome this obstacle, a data augmentation strategy is employed, generating additional synthetic data by applying various transformations to existing MRI images. This augmentation technique allows the CNN models to learn from a more diverse dataset, resulting in improved generalization and performance. Through

extensive experimentation and optimization, the proposed deep learning models are trained and fine-tuned on real MRI data, enabling them to achieve high levels of accuracy and robustness in segmenting skin layers. The trained models are then validated on independent data sets to ensure their reliability and generalizability in practical clinical settings. The potential impact of this research on dermatological research and clinical practice is substantial. Accurate segmentation of skin layers in MRI images paves the way for more precise and reliable assessment of hydration levels in the skin. This, in turn, can significantly contribute to the diagnosis, monitoring, and treatment of various skin conditions. Moreover, the automation of skin layer segmentation through deep learning methods can streamline and expedite the analysis process, allowing healthcare professionals to focus more on patient care and treatment planning.

Overall, this research represents a significant step forward in the field of medical image analysis, and it has the potential to revolutionize how skin hydration measurements are performed using MRI. By leveraging the power of deep learning, this work contributes to advancing our understanding of skin health and disease, ultimately leading to improved patient outcomes and more effective skincare interventions.

3.3.1 U-net model

Convolutional Neural Networks (CNNs) are powerful deep learning models designed for image processing tasks. They have revolutionized computer vision applications, including image classification, object detection, and image segmentation. CNNs use convolutional layers with small filters to automatically learn hierarchical features from input images, enabling them to detect relevant patterns and features.

In this research, we employ the U-Net architecture, a widely acclaimed deep learning model specifically designed for image segmentation tasks, particularly in the context of medical image analysis. The U-Net's unique U-shaped design allows it to effectively capture fine details and contextual information while performing image segmentation. By leveraging the power of U-Net, we aim to achieve highly accurate and context-aware segmentation of skin layers from MRI images, focusing on skin hydration measurements. Figure.3.3.1 depicts the total U-net architecture.

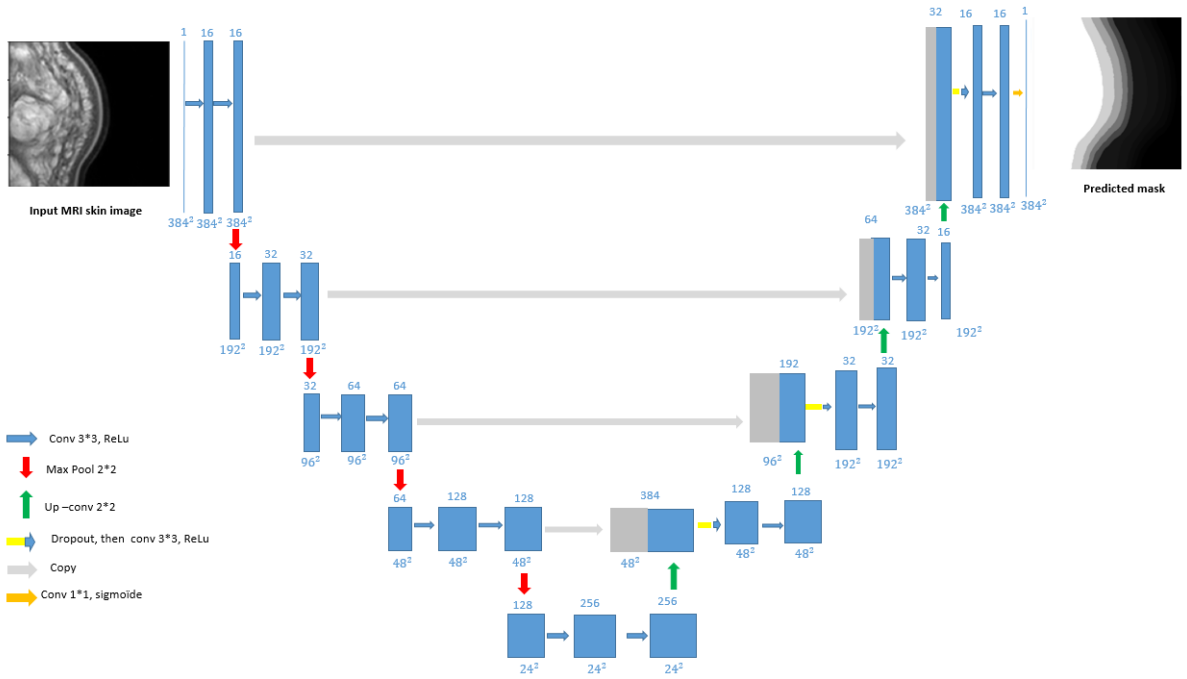

Figure 3.3.1: CNN: U-net model.

The main function of the U-net model is given by:

$$E = \sum w(x) \log p_{k(x)}(x). \tag{3.3.1}$$

where p is the pixel-wise SoftMax activation function applied over the final feature map, defined as:

$$p_k = \exp(a(x)_k) \sum_{k=1}^{k} \exp(a(x)_k)^{'} x \tag{3.3.2}$$

and a denotes the activation in channel k. The U-Net architecture plays a crucial role in addressing the challenges of skin hydration analysis using MRI data. Its ability to efficiently propagate contextual information throughout the network is essential for precisely identifying and delineating skin regions with varying hydration levels. This deep learning-based approach offers a robust and sophisticated solution to the complexities involved in skin hydration analysis, allowing for more reliable and comprehensive assessment of skin hydration patterns before and after the application of hydrated cream. Furthermore, by customizing the U-Net model to our specific real MRI data sets, we can overcome the limitations of limited available data

through data augmentation techniques. This ensures that the U-Net model generalizes well to new, unseen data, making it a valuable tool for advancing dermatological research and clinical practice. Overall, the integration of CNNs and the U-Net architecture in this research represents a significant advancement in the field of skin hydration measurements using MRI. This innovative approach opens up new possibilities for understanding skin health and optimizing skincare interventions, ultimately leading to improved patient outcomes and more effective dermatological treatments.

3.3.2 Dense-net model

Dense Convolutional Neural Networks (Dense-Net) is a recent architecture proposed based on collective knowledge, as mentioned in the previous chapter. In our segmentation approach for skin MRI images, we evaluate the performance of this model. The main concept behind Dense-Net's architecture is that each layer in the model receives inputs from all preceding layers and then transforms its own feature-maps, which are then passed on to all subsequent layers. This design enables the network to have a dense connection, where each layer has access to the collective knowledge learned from all preceding layers.

The collective knowledge in Dense-Net plays a crucial role in enhancing the computational efficiency and memory usage of the network. By reusing feature-maps from previous layers, Dense-Net reduces the number of parameters needed to be learned and allows the model to extract more informative features efficiently. This dense connection also facilitates gradient flow during the training process, addressing the vanishing gradient problem and promoting better convergence.(Figure 3.3.2).

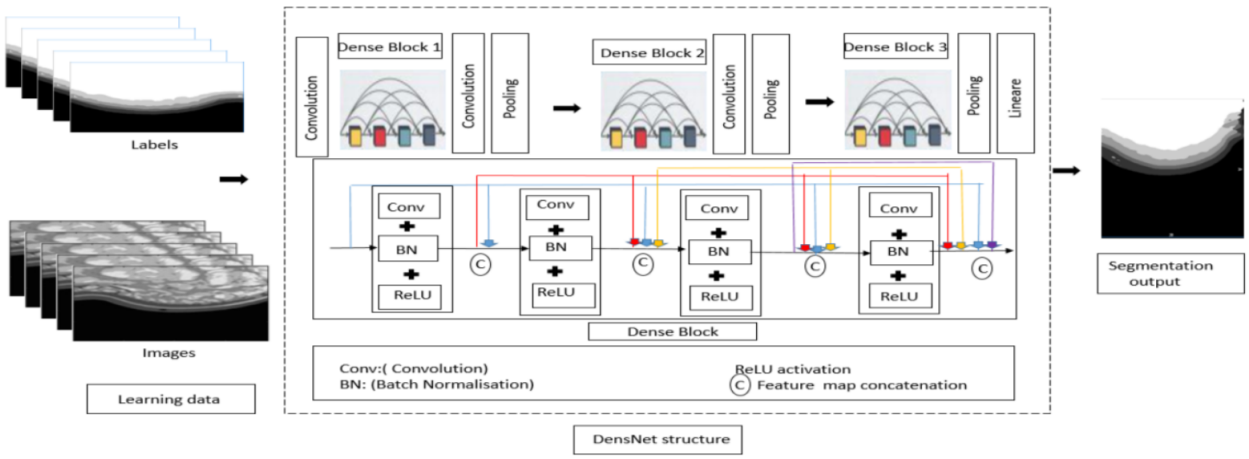

Figure 3.3.2: Dens Net architecture

The Dense-Net model is composed of L layers. Each layer, denoted by an index l, implements a non-linear transformation denoted as $H_l(.)$. This transformation $H_l(.)$ is a composite function that can include various operations such as Batch Normalization (BN), rectified linear units (ReLU), Pooling, or Convolution (Conv). These operations are designed to extract and transform relevant features from the input data at each layer. The distinctive feature of Dense-Net lies in its dense connections. Each layer in the model is directly connected to all subsequent layers (0, l-1). This design enables the current layer (l) to access and utilize the feature maps obtained from all preceding layers, enhancing the information flow and leveraging the collective knowledge learned throughout the network.

$$x_l = H_l([x_0, x_1, ..., x_{l-1}]), \tag{3.3.3}$$

where x_l represents the feature maps at layer l, and $x_{l-1}, x_{l-2}, ..., x_0$ denote the feature maps from all preceding layers.

The dense connections in Dense-Net promote efficient feature reuse, reducing the number of parameters and enhancing the overall computational efficiency and memory utilization. This architecture allows for better gradient flow during training, leading to more stable and faster convergence.

In the context of skin MRI image segmentation for skin hydration measurements, the Dense-Net's dense connections are particularly advantageous. They allow the model to efficiently capture and propagate essential contextual information throughout the network, leading to more

precise and context-aware segmentation of skin layers. By leveraging the collective knowledge from all layers, the Dense-Net model excels in handling complex skin structures and patterns, making it a powerful tool for dermatological research and clinical practice. Once we obtain segmented MRI images using deep learning models, we proceed to measure skin hydration before and after the application of a hydrated cream based on T2 map images using the following formula:

$$T2\_value = (\sum intensity\_value \neq 0)/(\sum number\_pixel). \tag{3.3.4}$$

Here, T2 represents the T2 relaxation time, a parameter acquired from the T2 mapping technique in MRI. The T2 relaxation time is sensitive to the water content in the skin and varies based on the hydration level of different skin layers. By comparing the T2 values before and after applying the hydrated cream, we can quantitatively measure the percentage change in skin hydration. This approach allows for a comprehensive analysis of skin hydration patterns and variations, offering valuable insights into the effects of hydrated creams on different skin layers. The combination of deep learning-based segmentation and T2 mapping in MRI provides a robust and precise method for studying skin hydration in both clinical and research settings. In addition, this integrated approach has the potential to advance dermatological research and clinical practice by providing accurate and objective measurements of skin hydration, enabling personalized skincare treatments, and enhancing our understanding of skin health. The main idea of the measuring phase is to get the intensity values of each segmented image by multiplying segmented and T2 map matrices. Once we have multiplications matrices of each segmented skin layer, we apply the formula and calculate T2 value for each one before and after the application of hydrated cream. These values will be after compared to study the hydration effect.

The measuring phase aims to obtain the intensity values for each segmented image by performing element-wise multiplication between the segmented skin layer and the corresponding T2 map matrices. After obtaining the multiplication matrices for each segmented skin layer, we proceed to calculate the T2 values for each layer before and after the application of the hydrated cream. These T2 values provide crucial information about the hydration level of the skin layers at different stages. By comparing the T2 values before and after the application of the hydrated cream, we can study the hydration effect on the skin. The percentage change in T2 values gives us insights into how the hydration level of each skin layer has been altered due to the application of the cream. This analysis is essential for understanding the impact of the hydrated cream on different skin layers. By quantifying the changes in T2 values, we can assess the effectiveness of the cream in moisturizing the skin and improving its hydration levels. Additionally, this approach allows us to study the spatial distribution of hydration changes

in various skin layers, providing valuable information for personalized skincare treatments and research in dermatology. Overall, the combination of deep learning-based segmentation with T2 mapping and the application of the hydration formula facilitates a comprehensive and accurate assessment of skin hydration before and after the use of the hydrated cream. This methodology contributes to advancements in dermatological research, providing valuable insights into skin health and optimizing skincare interventions for improved patient outcomes.

3.4 A Deep learning regression method for MRI skin hydration simulation

The second significant contribution of this dissertation revolves around the simulation of skin hydration phenomena through the application of deep learning techniques. Understanding skin hydration is a complex process, and accurate simulation can offer valuable insights into dermatological research and skincare practices. To achieve this, we designed and implemented a specialized Convolutional Neural Network (CNN) model tailored explicitly for skin hydration simulation. We have thoroughly evaluated our CNN model for simulation, as described below.

3.4.1 Auto encoder model

An auto encoder model is a crucial component of unsupervised convolutional neural networks, playing a fundamental role in feature learning and data compression. Comprising two main parts, the encoder (W) and the decoder (W'), this architecture is designed to effectively map input data to a lower-dimensional latent space and then reconstruct the original data from this compressed representation. The encoder, also known as the compression part, takes the input data and extracts essential features, compressing the information into a condensed latent representation. On the other hand, the decoder, or the decompression part, reverses the process, aiming to reconstruct the original data from the compressed representation.

$$x = W'\emptyset(W_x) \tag{3.4.1}$$

In the auto encoder model, the activation function $\emptyset$ is a crucial element used in the encoder part. The choice of activation function can significantly impact the model's ability to learn complex patterns and representations from the input data. Commonly used activation functions in the encoder include sigmoid, which maps the input values to a range between 0 and 1, tanh, which maps the input values to a range between -1 and 1, and rectified linear units (ReLU), which sets all negative input values to zero. The activation function $\emptyset$ is applied to the output of

each layer in the encoder, introducing non-linearity to the model. This non-linearity is essential as many real-world data sets contain intricate and non-linear relationships between the input features, and the activation function allows the model to capture these complex relationships effectively. On the other hand, in the decoder part of the auto encoder, there is no activation function applied to the output layer. This is because the data space is assumed to be the space of real numbers. Without an activation function, the decoder can directly output continuous real values, ensuring that the reconstructed data remains in the original data space. By using an appropriate activation function in the encoder, the auto encoder can learn to efficiently compress and encode the input data into a meaningful and lower-dimensional latent space. Then, during the decoding process, the decoder can reconstruct the original data from this compressed representation without the need for any additional transformations. Overall, the choice and use of activation functions in the auto encoder model play a crucial role in its ability to effectively learn and reconstruct meaningful representations of the input data, making it a powerful tool for various applications, including skin MRI image analysis for skin hydration measurements.

The primary training step of an auto encoder model is to learn the encoding weights (W) and decoding weights (W') by minimizing the Euclidean cost or reconstruction error. The Euclidean cost, also known as the mean squared error (MSE), measures the difference between the original input data and the reconstructed output. The goal of the training process is to find the optimal values for the weights that minimize this reconstruction error and produce accurate reconstructions of the input data. Mathematically, the Euclidean cost can be represented as follows:

$$Euclidean\_Cost = \frac{1}{N}\sum_{i=1}^{N}(x_i - x_i')^2 \tag{3.4.2}$$

where:
- N is the total number of training samples,
- x_i represents the i^{th} input data sample,
- x_i' represents the reconstructed output of the i^{th} input data sample.

During the training process, the model iteratively adjusts the values of the encoding and decoding weights to minimize the Euclidean cost (Eq. 3.4.2). This is typically done using optimization algorithms such as stochastic gradient descent (SGD) or its variants. The optimization algorithm calculates the gradients of the cost function with respect to the weights and updates them accordingly to move towards the minimum of the cost function.

$$\arg_{w,w'} \min ||X - W'\emptyset(WX)||^2{}_F. \tag{3.4.3}$$

By minimizing the Euclidean cost, the auto encoder learns to capture the most essential features and patterns from the input data and creates a meaningful and compact latent representation. This latent representation can then be used for various tasks, such as data compression, denoising, and even generation of new data samples.

In our contribution, we propose to train the auto encoder model using a set of paired MRI skin images, consisting of images before hydration and corresponding images after hydration. By providing this paired data to the model, it learns to encode the essential features of the skin images and decode them back to reconstruct the original images. Once the model is trained, we test it with new skin images captured before hydration. The auto encoder predicts the corresponding hydrated images and also reconstructs the images to simulate the hydration effect. This evaluation process allows us to observe how well the model can simulate the clinical hydration phenomena. The advantage of using the auto encoder for this task is that it can learn to capture the subtle differences and patterns in the skin images before and after hydration. By encoding and decoding the images, the model can effectively generate simulated hydrated images that closely resemble the actual hydrated skin images. This simulation capability of the auto encoder opens up new possibilities for dermatological research and clinical applications. It can aid in understanding the impact of hydration on the skin's appearance and properties, and it can also be valuable for assessing the efficacy of skincare products or treatments.

In summary, the trained auto encoder model allows us to simulate the clinical hydration phenomena by predicting the hydrated skin images and reconstructing the images with the hydration effect, offering a valuable tool for exploring skin hydration dynamics and its implications. (Figure 4.5.13).

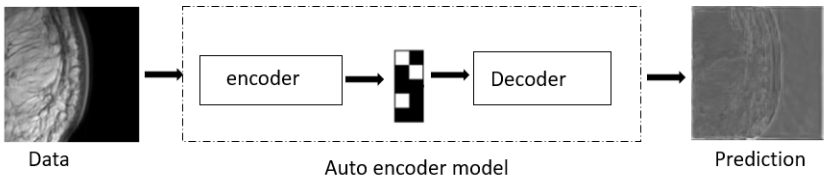

Figure 3.4.1: Auto encoder model

3.5 A registration presentation method for skin MRI images

As mentioned earlier in the literature review section of this dissertation, image registration is a highly valuable technique in medical image processing, as it enables the spatial overlay of anatomical or functional structures between different images. Due to its significance, we have incorporated image registration in both the segmentation and regression aspects of our research.

In the segmentation approach, we utilize image registration to align the ground truth image with the segmented image generated by our deep learning-based segmentation model. This registration method allows us to visualize and validate the alignment of skin layers, providing concrete evidence of the effectiveness of our segmentation approach. By overlaying the ground truth and segmented images, we can visually assess the accuracy of our segmentation results and ensure that the segmented regions accurately correspond to the ground truth.

In the regression task, image registration is employed to align the ground truth image of the skin before hydration with the reconstructed images produced by the auto encoder model after hydration simulation. This registration process enables us to directly compare and visually assess the results of our regression approach. By aligning the ground truth and reconstructed images, we can visually inspect the quality of the hydration simulation and evaluate how well the auto encoder model reproduces the skin's hydration effect. The image registration workflow comprises essential components, including pre-processing steps, image alignment, and feature extraction. Additionally, the registration algorithm estimates the transformation parameters required to bring the images into alignment. Once registered, these images are used for visualization and analysis purposes, providing valuable insights into the performance of our segmentation and regression methods.

The schematic below illustrates the key steps of our image registration workflow (Figure 3.5.1):

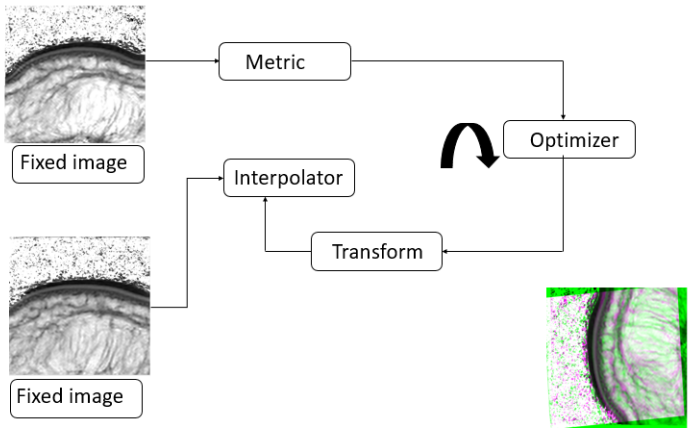

Figure 3.5.1: Image registration workflow

By incorporating image registration in both segmentation and regression tasks, we ensure a comprehensive and context-aware evaluation of our proposed methods, enhancing the accuracy and reliability of skin MRI image analysis and hydration simulation. Image registration plays a pivotal role in aligning and comparing different images, allowing us to effectively integrate information from multiple sources and gain deeper insights into the complex structures of the skin.

In the segmentation approach, image registration enables us to visually validate the alignment of segmented skin layers with the corresponding ground truth images. This visual validation is crucial for ensuring the accuracy of our deep learning-based segmentation models, as it provides tangible evidence of the model's ability to correctly identify and delineate different skin layers. By overlaying the segmented images with the ground truth, we can visually assess any discrepancies and refine the segmentation model to achieve more precise and contextually relevant results.

For the regression task, image registration allows us to align the ground truth images with the simulated hydrated images generated by the auto encoder model. This alignment facilitates a direct comparison between the simulated and actual skin hydration states, providing a qualitative assessment of the hydration simulation's fidelity. Additionally, by quantitatively evaluating the similarity between the registered images using metrics such as mean squared error or structural similarity index, we can objectively measure the accuracy of the hydration simulation.

Furthermore, image registration aids in understanding the spatial relationships between different skin structures, such as epidermis, dermis, and subcutaneous tissue, in the context

of skin hydration. By aligning these structures across multiple images, we can study how hydration affects the different skin layers and explore any variations in hydration patterns.

Beyond the research domain, the integrated approach of using image registration in skin MRI image analysis and hydration simulation holds significant potential for advancing dermatological practice. The accurate segmentation of skin layers and the faithful simulation of hydration effects can have practical applications in diagnosing and monitoring various skin conditions. Dermatologists can use this technology to assess skin hydration levels non-invasively, track the effectiveness of skincare treatments, and develop personalized treatment plans for patients.

In conclusion, the thoughtful integration of image registration into our research enhances the depth and applicability of our findings. It empowers us to gain comprehensive insights into skin health, from accurate segmentation of skin layers to faithful simulation of hydration dynamics. By bridging the gap between research and clinical applications, this integrated approach holds promise in revolutionizing dermatological research and patient care.

From a mathematical point of view, image registration involves finding a transformation that aligns two matrices representing images of the same object. Let I (x,y) and J(x,y) be the two matrices representing the pixel intensities of the images. The image registration process seeks to find a transformation T(X,Y) that maps the coordinates of pixels in one image to the corresponding pixels in the other image. The formula below defines the registration process:

$$J(x; y) = I(T(x, y)) + \epsilon(x, y) \tag{3.5.1}$$

where:

- J(x; y) is the pixel intensity value of the registered image at coordinates (x,y).

- I(T(x,y)) represents the transformed pixel intensity value of the source image I at coordinates (x,y) using the transformation T.

- T(x,y) is the transformation function that maps the coordinates (x,y) in the source image to the corresponding coordinates in the registered image.

- $\epsilon(x, y)$ denotes the registration error or residual, which represents the difference between the registered image J and the transformed source image I(T(x,y)).

The transformation T(x,y) can be represented by a set of parameters, such as translation,

rotation, scaling, and deformation. The goal of the image registration process is to estimate the optimal transformation parameters that minimize the registration error, effectively aligning the two images. Image registration is a fundamental process in medical image analysis, computer vision, and various other fields. It plays a crucial role in aligning images acquired at different times, from different angles, or using different imaging modalities. By facilitating the comparison, analysis, and fusion of information from multiple images, image registration enhances our understanding of complex structures and phenomena.

Our image registration method follows several key steps:

- Deformation Model: The method involves defining a deformation model comprising a fixed image and a moving image. The moving image is deformed to align with the fixed image, allowing us to find the best transformation that brings the images into correspondence.
- Similarity Function: A similarity matrix is computed between the fixed and moving images, serving as a measure of correspondence between anatomical features. This similarity matrix guides the registration process to achieve the most accurate alignment.
- Optimization Parameters: The core objective of image registration is to find the optimal model of spatial transformation that minimizes the distance between corresponding points or features in both images. This optimization process involves determining the best parameters for the transformation to achieve the most accurate alignment.

By incorporating these steps into our image registration method, we ensure precise alignment of images, enabling effective analysis and comparison of anatomical or functional structures. The ability to fuse information from different imaging modalities and facilitate longitudinal studies enhances our understanding of complex structures within the human body. Image registration's significance extends to various applications, including medical image analysis, computer vision, and research in medicine and related fields. It allows us to unlock valuable insights from medical images, leading to improved diagnosis, treatment planning, and advancements in medical research. The registration formula and methodology described above serve as the foundation for various registration algorithms and techniques used in image processing and analysis, making it a vital tool in the domain of medical imaging and beyond 3.5.2.

$$T^* = arg_T max\, S\left(F;\, T(M)\right). \tag{3.5.2}$$

3.6 Methodology

The methodology of our research is structured into four key steps: skin segmentation, skin hydration measurements, skin simulation, and skin hydration analysis. In the first step, we employ state-of-the-art deep learning models, specifically U-Net and Dense-Net, to accurately segment the skin MRI images and identify different skin layers. These models are trained on a diverse dataset of skin images to learn intricate features and patterns, enabling precise segmentation. Ground truth images are used for validation to assess the segmentation accuracy. Moving to skin hydration measurements, we focus on quantifying the water content in various skin layers. T2 map cartographies are generated, and pixel-wise multiplication is applied to the segmented images and T2 map matrices. This yields intensity values for each skin layer, both before and after applying a hydrated cream. The comparative analysis of hydration effects on different layers provides valuable insights into skin health dynamics.

The skin simulation stage leverages an auto encoder model, an unsupervised convolutional neural network, to predict hydrated images and reconstruct images with the hydration effect. The auto encoder is trained using paired MRI skin images captured before and after hydration. This simulation process allows us to mimic the clinical hydration phenomenon, facilitating a controlled examination of hydration dynamics. Finally, the skin hydration analysis involves a comprehensive evaluation of the segmentation, hydration measurements, and simulation results. Both quantitative and qualitative assessments are conducted to validate the accuracy and reliability of the proposed approaches. Additionally, image registration techniques are utilized to visualize the alignment of segmented skin layers with the ground truth. The thorough analysis provides deeper insights into skin health and hydration patterns. By integrating deep learning techniques, image registration, and rigorous analysis, our research offers a robust and comprehensive methodology to study skin segmentation, hydration, and simulation. The findings contribute to advancing dermatological research and hold great potential for enhancing clinical applications, such as skin health assessment, diagnosis, and personalized treatment approaches.

3.7 Significance and implications

The key contributions and insights gained from our proposed approaches are of paramount significance in advancing the field of skin MRI image analysis and skin hydration research. Firstly, our automatic skin segmentation method based on U-Net and Dense-Net convolutional neural networks has proven to be a game-changer. By harnessing the power of deep learning, we have achieved remarkable accuracy in identifying and segmenting different skin layers in MRI

images. This not only saves time and effort compared to manual segmentation but also ensures consistency and reproducibility in our analyses. The precise segmentation allows for more reliable measurements and a better understanding of the anatomical and structural variations in the skin. Secondly, our comprehensive approach to skin hydration measurements has provided valuable insights into the dynamics of skin hydration. By employing T2 map cartographies and deep learning techniques, we are able to quantitatively assess the water content in different skin layers before and after the application of hydrated cream. This level of detailed analysis allows us to study the hydration effect on the skin at a granular level, identifying variations in hydration patterns and their potential implications for skin health. Additionally, our skin hydration simulation approach using auto encoder models is a novel contribution to the field. By training the models with paired MRI skin images, we can accurately predict hydrated images and reconstruct images with the hydration effect. This simulation capability enables us to study the effects of different hydration scenarios on the skin and gain insights into how hydration impacts various skin structures. Such simulation-based analyses have the potential to aid in the development of personalized skincare regimens and treatment strategies. Moreover, the incorporation of image registration in our proposed approaches enhances the reliability and interpretability of our results. Image registration allows us to spatially align different images and compare them accurately. By overlaying segmented and truth images, we can visualize the accuracy of our segmentation approach and validate the effectiveness of our simulation models. This registration-based analysis strengthens the robustness of our research findings and facilitates better comparisons with ground truth data. Overall, the insights gained from our proposed approaches hold significant potential for advancing dermatological research and clinical applications. The accuracy, efficiency, and context-awareness of our methods contribute to a deeper understanding of skin health and hydration dynamics. This research can serve as a valuable resource for dermatologists, skincare specialists, and researchers in developing personalized treatment plans and interventions for various skin conditions.

3.8 Conclusion

In this chapter, we have laid the foundation for our research by presenting the segmentation approaches for skin MRI images. The automatic segmentation method based on convolutional neural networks represents a significant advancement in the field, as it streamlines and enhances the segmentation process compared to traditional manual methods. The ability to accurately measure the hydration effect on skin layers using deep learning techniques opens up new possibilities for studying skin health and understanding the impact of hydration on different skin

structures. Moreover, the proposed artificial simulation method for studying skin hydration is a novel contribution to the field. By leveraging the power of deep learning, we can now simulate the hydration phenomenon with greater accuracy and realism, providing valuable insights into the dynamic changes that occur in the skin with hydration. Moving forward, the next chapter will be dedicated to presenting and discussing the results obtained from our segmentation and simulation approaches. We will conduct a comprehensive analysis of the outcomes, comparing them with ground truth data and previous studies. This detailed evaluation will allow us to assess the strengths and limitations of our methods and shed light on areas for further improvement and refinement. Additionally, the quantitative evaluation in the upcoming chapter will provide objective measurements of the performance of our approaches, ensuring robustness and reliability in our findings. We will present various metrics and statistical analyses to validate the accuracy and generalizability of our models, supporting their potential application in clinical settings and dermatological research.

In conclusion, this chapter sets the stage for an in-depth exploration of our segmentation and simulation methods, highlighting their significance and potential contributions to the field of skin MRI image analysis. The results and evaluations presented in the next chapter will further strengthen the validity of our research and pave the way for advancements in skin health assessment and personalized treatment approaches.

CHAPTER 4

Experimental design and Results

4.1 Introduction

Recently, Magnetic Resonance Imaging (MRI) has emerged as a highly effective method for quantifying water behavior and content in live tissues in real-time. In our research, we sought to evaluate the performance of our proposed approach compared to existing methods by applying it to a set of real skin MRI images. By measuring the mobile water proton density before and after the application of moisturizing cream, we were able to assess in vivo hydration in different skin layers and also simulate skin hydration phenomena. Our research focused on two main objectives: First, measuring skin hydration based on T2 mapping generation and skin segmentation, with a rigorous validation of the results. Second, simulating skin hydration using a CNN auto-encoder model. The details of our contributions were presented in the previous chapter.

This chapter presents the outcomes of our research and offers a comprehensive summary of our findings, which are organized into four sections: Skin segmentation, skin hydration measurements, skin registration method, and synthetic skin hydration simulation. Each section presents detailed results and analyses based on our proposed approaches. We discuss the strengths and limitations of our methods, and how they contribute to the field of dermatological research and clinical applications. Furthermore, the chapter concludes with a comprehensive discussion of our research findings, drawing connections between the results from each section and highlighting their significance. We also address potential areas for improvement and future research directions. In conclusion, this chapter provides a detailed overview of the outcomes of our study, shedding light on the novel insights gained from our proposed approaches and their potential impact on the field of skin MRI image analysis and skin hydration research.

4.2 Development environment

The approach was developed using two main programming environments, MATLAB R2019 and Python 3 with Anaconda Navigator (Jupyter Notebook). The development was carried out on a dedicated workstation equipped with an 12th Gen Intel(R) Core(TM) i7-12700H CPU @ 2.70 GHz 1.80GHz, 32 GB of RAM, and running Windows 11 Professional. MATLAB was employed for calculating T2 measurements and quantifying skin water content before and after the application of moisturizing cream. This step involved processing the MRI images and generating T2 mapping cartographies to obtain water distribution information. The quantification of skin hydration was performed using MATLAB's computational capabilities.

On the other hand, Python was utilized for the evaluation of various deep learning models, including U-net and auto encoder, which were implemented to accomplish skin segmentation and skin hydration simulation tasks. Python's powerful libraries and frameworks, along with Anaconda Navigator, provided an efficient and flexible environment for training and evaluating the CNN models. The final output presentations, such as histograms and visualizations, were also generated using Python. The combination of Python's data visualization libraries and Jupyter Notebook allowed for the clear presentation of results and insights gained from the research. To ensure the accuracy and reliability of the proposed approaches, a validation step was carried out using MATLAB. Various similarity measures were employed to assess the performance of the segmentation and simulation models, validating their ability to accurately predict skin hydration levels and simulate hydration effects. The choice of MATLAB and Python for different aspects of the research allowed us to leverage the strengths of each programming environment, ensuring a comprehensive and robust analysis of skin MRI images and skin hydration phenomena. The dedicated workstation provided the computational power required to process and analyze the large data sets involved in the research, enabling us to achieve meaningful and reliable results.

4.3 Skin MRI data sets

The data utilized in our study was collected at the research center of the Brest Hospital in France, spanning a period from September 2014 to August 2015. The study population comprised 35 healthy volunteers with an average age of 25.3 years, including 17 women and 18 men. Microscopic imaging was conducted in a medical room at a controlled temperature of 21 °C.and humidity of 50% using a 23 mm internal diameter coil (Achieva dStream, Philips, Best, Netherlands). To gather the data, all subjects underwent high-resolution MRI scans targeting their

left heels. The MRI scans were performed before the application of moisturizer and then repeated after one hour of applying a moisturizer called Dexeryl, manufactured by Pierre Fabre. This enabled us to obtain two sets of MRI images for each subject: one representing the skin condition before hydration and the other showing the skin's hydration status after applying the moisturizer. The acquisition of such data allowed us to conduct a comprehensive analysis of skin hydration levels and the effects of moisturizing cream on skin layers. The utilization of high-resolution MRI and controlled imaging conditions ensured accurate and reliable data for our research purposes.

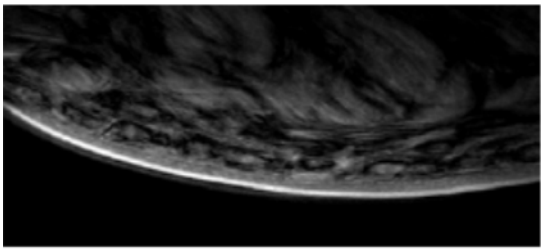

Figure 4.3.1: MRI sequence: Fast Field Echo

To select the most suitable location for T2 mapping acquisition, we initially conducted a T1-sequence scan (Figure 4.3.1). This T1-sequence allowed us to assess the relaxation time of the tissues, providing valuable information about the contrast between different anatomical structures. Following the T1-sequence scan, we proceeded with an eight-echoed Multi Spin Echo (MSE) sequence (Figure 4.3.2). The MSE sequence provided us with multiple echoes, each capturing the signal decay of the tissues over time. By analyzing these echoes, we could derive the T2 relaxation times, which reflect the tissue's water content and hydration levels.

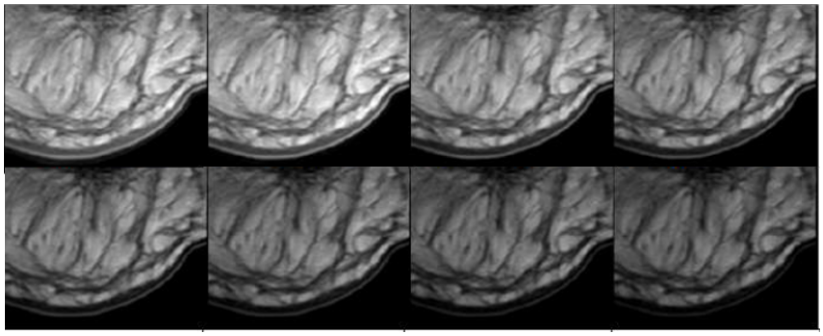

Figure 4.3.2: MRI sequence: Multi Spin Echo(MSE)calculation T2-weighted sequence

The combination of T1-sequence and MSE sequence scans enabled us to identify the optimal location for T2 mapping construction. This process ensured that the T2 mapping data captured relevant and accurate information about the water distribution and hydration characteristics in the skin layers, allowing us to conduct a detailed analysis of skin hydration phenomena.

We summarizes all MRI acquisition parameters in table 1:

For the purpose of this research, the collected MRI data underwent preprocessing to ensure

Parameters	Sequences	
	T1	T2
Echo time (ms)	11	8
Matrix size($pixels$)	432*432	384*384
Repetition time(ms)	58	2000
Time acquisition(min)	10	6
Slice number	13	8
Slice thickness	2	2

Table 4.1: Parameters of MR Image acquisition

its suitability and enhance the quality of analysis. The preprocessing steps involved various techniques, such as noise reduction, intensity normalization, and image alignment, to correct any artifacts or inconsistencies that may have arisen during the acquisition process. Additionally, we performed image registration to align the MRI images acquired before and after the application of moisturizer, ensuring accurate comparison and evaluation of skin hydration levels. The details of the preprocessing techniques used will be described in the next section, outlining the steps taken to prepare the MRI data for further analysis and interpretation.

4.4 Data prepossessing

In the initial phase of our approach, we prepared the data sets using two primary techniques: data augmentation and one-hot encoding. Data augmentation was employed to increase the amount of available data by applying various image transformations, such as rotations, flips, and zooms, to the existing MRI images. This process resulted in a more diverse and extensive data set, which is valuable for training deep learning models and enhancing their performance. These two techniques was described bellow:

4.4.1 One Hot Encoding method

Our method focuses on segmenting MRI skin data into multiple layers, which necessitates the use of the One Hot encoding (OHE) technique. OHE is a popular preprocessing technique that simplifies data treatment for multi-class images. In our case, where we deal with multi-label segmentation tasks, OHE proves to be invaluable. The main objective of this technique is to convert categorical feature inputs into binary feature inputs and create binary images for each segmented label. By employing OHE, we transform the categorical labels of different skin layers or hydration levels into binary vectors. Each element in the binary vector represents the presence or absence of a specific label, effectively converting the multi-class labels into a format that the U-net model can easily understand and process. This conversion allows the U-net model to treat each input feature as a single image, making the learning process more efficient and effective. Instead of learning a set of features within the same image, the model can now focus on learning and distinguishing individual features in each binary image. The benefit of using OHE is that it simplifies the training of our model on the dataset, enabling it to accurately segment the MRI skin data into multiple layers. As shown in Figure 4.5.1, the OHE technique streamlines the data preprocessing phase, improving the overall performance and accuracy of our segmentation approach based on the U-net model. Through this technique, we enhance our ability to obtain reliable and precise segmentation results, contributing to a more comprehensive understanding of skin hydration and its implications for dermatological research and clinical applications.

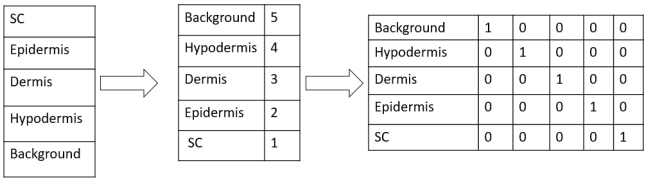

Figure 4.4.1: One Hot Encoding technique.

4.4.2 Data augmentation

Medical image segmentation indeed faces challenges related to the limited availability of training data, which can hinder the performance of deep learning architectures. To overcome this issue, we employed a widely used technique called data augmentation. Data augmentation is a popular approach in deep learning that aims to enhance the capabilities of the models by generating additional training data through small image transformations. In our work, we encountered the problem of having a relatively small data set for training. To address this, we adopted data augmentation to expand our data set artificially. This technique involves applying various image transformations to the existing MRI images during the training process. These transformations can include rotations, reflections, and elastic deformations, among others. By doing so, we create new variations of the original images that closely resemble the ground truth training examples. By augmenting the data set with these transformed images, we effectively increase the diversity and size of our training data. This larger and more varied data set allows the model to learn better and perform more effectively. Each augmented image is considered as an additional data point, which increases the sample size for training the model. The application of data augmentation in our work enables us to train robust models capable of achieving high accuracy, even with a limited initial data set. The augmented data ensures that the model learns from a wide range of examples, leading to improved generalization and performance. As a result, our segmentation and regression approaches are better equipped to handle the complexities of skin MRI images and accurately measure skin hydration levels before and after the application of moisturizing cream. This contributes to a more reliable and insightful analysis of skin health, benefiting dermatological research and clinical applications.

After preparing the data sets using data augmentation and one-hot encoding, we proceed to

Parameters	value
Rotation range	0.2
Width shift range	0.05
Height shift range	0.05
Shear range	0.05
Zoom range range	0.05
Horizontal flip	True
Fill mode	constant

Table 4.2: Parameters of data augmentation technique

discuss the two key models involved in our segmentation process: the U-Net model and the auto encoder model.

The U-Net model is a convolutional neural network architecture that has proven to be highly effective in image segmentation tasks. Its unique "U" shape consists of a contracting path, where the input image is downsampled to capture context and features, and an expanding path, where the features are upsampled to recover the spatial resolution. The U-Net model's dense connections allow it to efficiently capture and propagate relevant contextual information throughout the network, making it well-suited for segmenting skin layers in MRI images. On the other hand, the auto encoder model is an unsupervised neural network that aims to learn a compact representation of the input data. It consists of an encoder, which converts the input image into a latent representation, and a decoder, which reconverts the latent representation back to the data. In our case, the auto encoder is used for skin hydration simulation. By training the auto encoder on paired MRI images before and after the application of moisturizing cream, we can reconstruct the hydrated images and simulate the hydration effect. Both models play crucial roles in our segmentation process, enabling us to accurately segment skin layers in MRI images and simulate skin hydration phenomena. The combination of these two models allows us to achieve a comprehensive analysis of skin health and hydration, providing valuable insights for dermatological research and clinical applications. In the next section, we present the results of our segmentation process and discuss the findings obtained from our research.

4.5 Methodology and findings

In this section, we present a summary of the results obtained in our study, which are organized into three subsections: skin segmentation, skin hydration measurements, and artificial simulation of skin hydration. In the first subsection, we discuss the outcomes of our skin segmentation

approach using the U-Net model. We evaluated the performance of the model on a set of real skin MRI images and compared the segmented results with ground truth labels. The U-Net model demonstrated high accuracy in segmenting skin layers, proving its efficiency in automating the segmentation process and outperforming manual segmentation methods. Next, we focus on skin hydration measurements using T2 mapping in the second subsection. By analyzing the T2 maps generated from MRI images before and after the application of moisturizing cream, we quantified the water content in different skin layers. The results showed significant changes in skin hydration after the cream application, providing valuable insights into the moisturizing effect on the skin. In the third subsection, we present the outcomes of our artificial simulation of skin hydration using the auto encoder model. By training the model on paired MRI images, we successfully reconstructed the hydrated images and simulated the skin hydration phenomena. This approach allowed us to study the hydration effect in a controlled and reproducible manner, providing a valuable tool for future research and experimentation.

Overall, our proposed approaches demonstrated promising results in skin segmentation, skin hydration measurements, and artificial simulation of skin hydration. The integration of deep learning techniques, such as the U-Net and auto encoder models, proved to be effective in enhancing the analysis of skin MRI images and understanding the hydration dynamics of the skin. These findings hold great potential for advancing dermatological research and clinical applications, offering new insights into skin health and personalized skincare treatments. In the following section, we discuss the implications of our results and draw conclusions from our study.

4.5.1 Experiment 1: Skin segmentation

In this section, we present the results of our automatic skin segmentation method, which aims to divide MRI skin images into different layers. To evaluate the performance of our segmentation approach, we compared the results with manual segmentations performed by an expert clinician. The manual segmentation serves as a reference for comparison, allowing us to assess the accuracy and effectiveness of our automatic segmentation method. We start by providing a detailed description of our automatic segmentation method using the U-Net model. We explain the steps involved in the process and discuss the training and validation of the model using our data set. We also present the segmentation results obtained from the U-Net model and compare them with the manual segmentations to assess the level of agreement between the two methods. Next, we delve into the manual segmentation method performed by the expert clinician. We explain the criteria and guidelines used for the manual segmentation and discuss any challenges encountered during the process. We also highlight any discrepancies or difficulties

faced in achieving accurate manual segmentations. Following that, we present the quantitative comparison between the automatic and manual segmentations using similarity measures. We compute various similarity metrics, such as Dice coefficient and Jaccard index, to assess the level of agreement between the two methods. These measures provide insights into the accuracy and reliability of our automatic segmentation approach compared to the manual segmentations. Furthermore, we investigate the effect of moisturizing cream on the skin layers by performing the same segmentation evaluation on MRI images taken before and after the application of the cream. This allows us to observe any changes in the segmentation results and understand the impact of hydration on skin layers. The results obtained from this analysis provide valuable insights into the accuracy and reliability of our automatic skin segmentation approach. By comparing the automatic and manual segmentations, we can evaluate the performance of our method and identify areas for improvement. These findings contribute to the validation of our segmentation approach and its potential applications in clinical settings and dermatological research.

4.5.1.1 Manual segmentation method

In this section, we present the results of our automatic skin segmentation method, which aims to divide MRI skin images into different layers. To evaluate the performance of our segmentation approach, we compared the results with manual segmentations performed by an expert clinician. The manual segmentation serves as a reference for comparison, allowing us to assess the accuracy and effectiveness of our automatic segmentation method. We start by providing a detailed description of our automatic segmentation method using the U-Net model. We explain the steps involved in the process and discuss the training and validation of the model using our data set. We also present the segmentation results obtained from the U-Net model and compare them with the manual segmentations to assess the level of agreement between the two methods. Next, we delve into the manual segmentation method performed by the expert clinician. We explain the criteria and guidelines used for the manual segmentation and discuss any challenges encountered during the process. We also highlight any discrepancies or difficulties faced in achieving accurate manual segmentations. Following that, we present the quantitative comparison between the automatic and manual segmentations using similarity measures. We compute various similarity metrics, such as Dice coefficient and Jaccard index, to assess the level of agreement between the two methods. These measures provide insights into the accuracy and reliability of our automatic segmentation approach compared to the manual segmentations. Furthermore, we investigate the effect of moisturizing cream on the skin layers by performing

the same segmentation evaluation on MRI images taken before and after the application of the cream. This allows us to observe any changes in the segmentation results and understand the impact of hydration on skin layers. The results obtained from this analysis provide valuable insights into the accuracy and reliability of our automatic skin segmentation approach. By comparing the automatic and manual segmentations, we can evaluate the performance of our method and identify areas for improvement. These findings contribute to the validation of our segmentation approach and its potential applications in clinical settings and dermatological research.

4.5.1.2 Automatic segmentation method

Our skin segmentation method is based on the U-Net model, which has proven to be highly effective in accomplishing biomedical image segmentation tasks. In addition to the U-Net, we also utilized the Dens-Net CNN model, implemented on the NiftyNet platform, to compare the performance of the two CNN models with the manual method. While deep learning architectures have demonstrated success in various medical segmentation tasks, training U-Net Convolutional Neural Networks for skin layer segmentation on multi-label MRI skin images is particularly challenging. One of the primary hurdles is the availability of a sufficiently large and diverse dataset for training. To address this issue and improve the model's performance, we employed data augmentation techniques (Figure 4.5.2) to increase the size of our dataset. Data augmentation involves applying various transformations to the existing MRI images, such as rotations, flips, and scaling, to generate augmented versions of the data. These augmented images enhance the diversity and representativeness of the dataset, enabling the model to learn more effectively. Additionally, we used one hot encoding technique (Figure 4.5.1) to simplify the representation of multi-label images. This technique converts categorical features into binary features, creating binary images for each segmented label. By presenting each label as a separate binary image, the U-Net model can learn each feature independently, which improves the efficiency and accuracy of the segmentation process. Through the combination of U-Net and Dens-Net CNN models, data augmentation, and one hot encoding, we aim to achieve accurate and reliable skin layer segmentation results. The comparison between the CNN models and the manual segmentation method will provide valuable insights into the strengths and limitations of each approach. Our ultimate goal is to develop a robust and efficient segmentation method that can be applied in clinical settings and dermatological research, enhancing our understanding of skin health and supporting improved patient care.

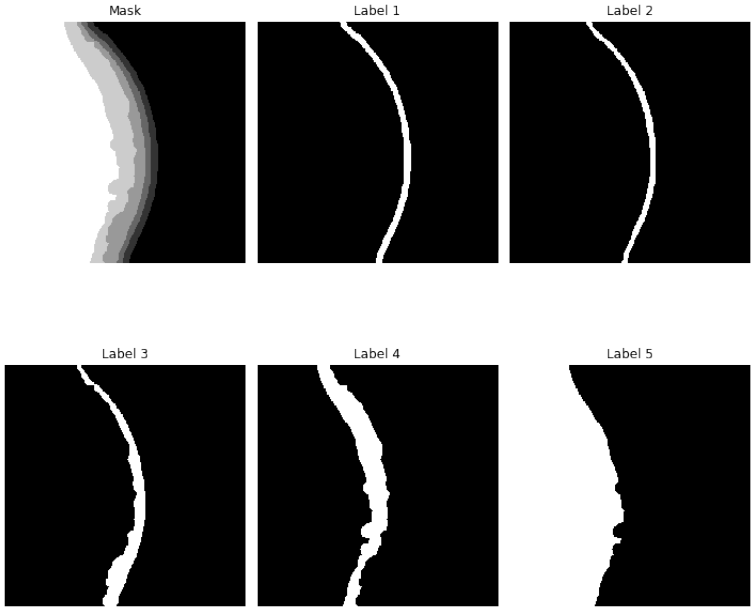

Figure 4.5.1: One Hot Encoding method.

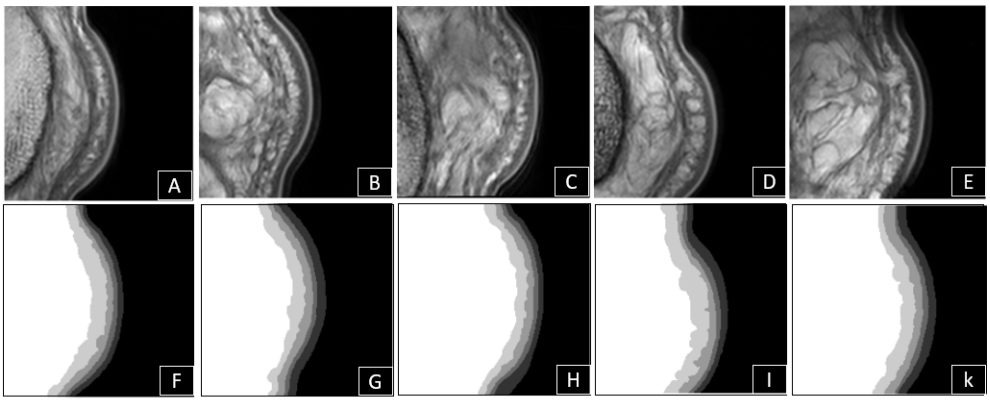

Figure 4.5.2: Augmented MRI images:A, B, C, D, and E augmented images. F,G, H, I and K resp augmented masks.

Once the data was prepared, we proceeded to feed the augmented MRI images data (384x384 pixels) with 8 batches into our CNN models for image segmentation. In the next subsection, we will describe the process of building an image segmentation using both the U-Net and Dens-Net

models.

The U-Net model is a widely used architecture for semantic segmentation tasks. It consists of a contracting path, which extracts features from the input image, and an expansive path, which upsamples the features to generate the segmented output. The U-Net model is designed to capture both local and global information, making it well-suited for skin layer segmentation in MRI images. On the other hand, the Dens-Net model is a more recent architecture that has shown promising results in various image segmentation tasks. It incorporates dense connections, allowing each layer to receive direct inputs from all previous layers. This dense connectivity promotes better feature reuse and propagation, leading to more efficient training and improved performance. For each model, we initialized the weights and biases and used optimization techniques like stochastic gradient descent (SGD) or Adam optimizer to minimize the loss function during the training process. We performed cross-validation to tune hyperparameters and ensure generalization to unseen data. Both the U-Net and Dens-Net models were trained on the augmented dataset with a specific number of epochs to optimize their performance. The training process involved iteratively adjusting the model's parameters to minimize the discrepancy between the predicted segmentation and the ground truth segmentation provided by the expert clinician. After the models were trained, we evaluated their performance using various metrics, such as Dice coefficient, Jaccard index, and pixel-wise accuracy, to measure the similarity between the predicted and ground truth segmentation.

In the subsequent subsection, we will present the results of the image segmentation performed by the U-Net and Dens-Net models, comparing their performance with each other and with the manual segmentation method. This analysis will provide insights into the strengths and limitations of each model and its potential applicability in dermatological research and clinical practice.

- Building an image segmentation using U-Net model

After preparing the data, we proceeded to build the U-Net model using TensorFlow in the Jupyter Notebook environment of Anaconda. The first step was to create standard model blocks, which consisted of two subsequent 3x3 convolutions followed by ReLU activation and max-pooling layers. These blocks were then concatenated to construct the U-Net architecture. The model took an MRI image with a shape of (384x384x1) as input and produced categories (labels) with a shape of (384x384x6) as output. Each category represented a set of pixels with the same class features, corresponding to different skin layers.

As described in detail in Chapter 2, the U-Net model had a contracting path to capture features from the input image and an expansive path to upsample the features and generate

the segmented output. The model was designed to effectively capture both local and global information, making it suitable for skin layer segmentation in MRI images. The evaluation of the U-Net model consisted of three main phases: the training phase, the validation phase, and the test phase. During the training phase, the model was trained on the augmented MRI images dataset using optimization techniques like stochastic gradient descent (SGD) or Adam optimizer to minimize the loss function. The model's parameters were iteratively adjusted to minimize the discrepancy between the predicted segmentation and the ground truth segmentation provided by the expert clinician.

In the validation phase, the trained model was evaluated on a separate subset of data to tune hyperparameters and ensure its generalization to unseen data. The performance was assessed using various metrics such as Dice coefficient, Jaccard index, and pixel-wise accuracy, to measure the similarity between the predicted and ground truth segmentations. Finally, in the test phase, the model's performance was assessed on a completely unseen dataset to evaluate its ability to generalize to new data. The segmentation results were compared with the manual segmentation method as a comparison reference. The test phase provided valuable insights into the accuracy and reliability of the U-Net model in segmenting skin layers in MRI images.

In the next section, we will present the detailed results of the U-Net model's evaluation, including the performance metrics and a comparison with the manual segmentation method. This comprehensive analysis will provide a deeper understanding of the U-Net model's capabilities and its potential usefulness in dermatological research and clinical applications.

- **Training phase**: During the training phase, the U-Net model learned to extract features from the input MRI images and construct segmented masks based on the corresponding manual segmentation labels. We provided the model with a subset of our MRI dataset, consisting of 10 images of size 384x384 pixels, along with their corresponding manual segmented labels, and trained the model using 8 batches of data. The main objective of the training phase was to teach the U-Net model to recognize different skin layers based on the labeled images and learn how to construct masks that accurately represent these layers from the input images. The model iteratively adjusted its parameters during the training process to minimize the discrepancy between the predicted segmentation masks and the ground truth masks provided in the training dataset. The ultimate goal of the training phase was to produce a well-trained model that could generalize well to new, unseen data. To evaluate the accuracy of the trained model in segmenting skin layers, we used a separate set of data called the validation dataset. The validation dataset contained images and their corresponding manual segmentation labels that were not used during the training phase. This ensured that the model was tested on data it had not seen

before, avoiding the problem of overfitting, where the model memorizes the training data and performs poorly on new data. The evaluation of the trained model on the validation dataset provided valuable insights into its performance and generalization capabilities. We used various evaluation metrics such as Dice coefficient, Jaccard index, and pixel-wise accuracy to quantify the similarity between the predicted segmentation masks and the ground truth masks. These metrics allowed us to assess how well the model could accurately segment skin layers in new, unseen MRI images.

In the next section, we will present the results of the training phase, including the performance metrics and a detailed analysis of the U-Net model's ability to segment skin layers in MRI images. This analysis will help us understand the strengths and limitations of the model and guide us in further improving its performance if necessary.

- **Validation phase**: In the training phase, we split the initial dataset into two subsets: the training set and the validation set. The training set was used to train the U-Net model, while the validation set was used to assess the model's performance and make necessary adjustments for optimization. The training set consisted of 8 MRI images, and the validation set had 2 MRI images. We fed batches of data from the training set into the U-Net model, allowing it to learn to extract features and construct segmented masks based on the labeled images in the training set. The model's performance was evaluated using the validation set. By assessing the model's accuracy on the validation set, we could identify if the model was overfitting or underfitting the training data. Overfitting occurs when the model performs well on the training data but poorly on unseen data, indicating that it has memorized the training data and lacks generalization. Underfitting occurs when the model performs poorly on both the training and validation sets, indicating that it hasn't learned enough from the training data. To obtain the most optimized model, we used the outcomes of the validation test. If the model's performance on the validation set was not satisfactory, we adjusted the model's hyperparameters, such as learning rate or batch size, and continued training until we achieved a desirable performance. This process of fine-tuning the model based on the validation set's performance ensured that the model could generalize well to new, unseen data and accurately segment skin layers in MRI images. By splitting the dataset into training and validation sets and utilizing the validation set to optimize the model, we were able to train a U-Net model that achieved high accuracy in segmenting skin layers in MRI images and demonstrated robustness in generalization to new data. The performance of the optimized model will be further evaluated and discussed in the subsequent sections.

- **Test phase**: Once the training phase was completed, we proceeded to test the U-Net

model on the remaining portion of our dataset, which comprised 20 independent MRI images. These test data were not used during the training phase and served as a completely new and unseen dataset for the model. During the testing phase, the test data were fed into the trained U-Net model, and the model produced predicted outputs for each input image. These predicted outputs were then compared with the original MRI images to evaluate the model's performance. To assess the performance of the U-Net model, we used various evaluation metrics, including pixel-wise accuracy, mean intersection over union (IoU), and Dice coefficient. These metrics quantified how well the model's predictions matched the ground truth labels (manual masks) of the skin layers in the MRI images.

Figure (Figure 4.5.3) showcases our skin MRI images alongside their corresponding manual masks and the predicted masks generated by our trained U-Net model. By visually comparing the predicted masks with the ground truth masks, we observed a high level of agreement, indicating that the U-Net model achieved accurate and robust segmentation of skin layers in MRI images. The performance evaluation of the U-Net model on the testing dataset demonstrates its capability to generalize well to new, unseen data, making it a reliable tool for skin MRI image segmentation. These positive results pave the way for further applications of the U-Net model in dermatological research and clinical practice.

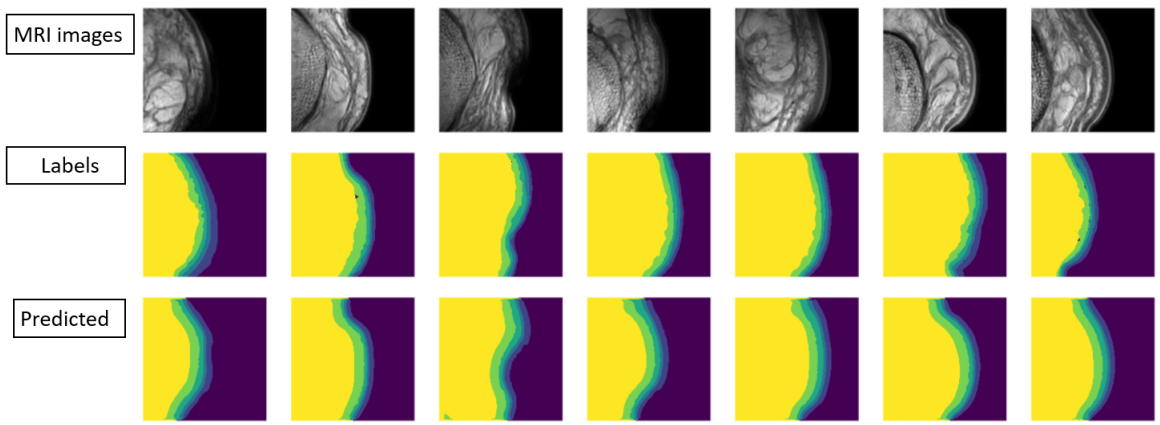

Figure 4.5.3: through MRI images, manual labels, and predicted of MRI images using U-net.

- Building an image segmentation using Dense-Net model

In addition to the U-Net model, we also utilized the Densely Connected Convolutional Network (Dense-Net) architecture for our skin MRI image segmentation task. Dense-Net is a relatively recent and powerful convolutional neural network (CNN) architecture that has shown excellent performance in various medical image segmentation tasks. Its unique design allows each layer to receive inputs from all preceding layers, fostering rich feature reuse and promoting efficient information flow throughout the network. The Dense-Net model comprises L layers, and at each layer, a non-linear transformation Hl(.) is applied to the feature maps obtained from all previous layers. This transformation can include operations like Batch Normalization (BN), rectified linear units (ReLU), pooling, and convolutions. By incorporating these dense connections, the Dense-Net can effectively capture and propagate relevant contextual information throughout the network, leading to more accurate and context-aware segmentation of skin layers. The architecture of the Dense-Net used in this study was presented in detail in chapter 3, where we discussed its advantages and how it addresses the challenges in skin MRI image segmentation. The Dense-Net model was implemented using TensorFlow in the Jupyter Notebook of the Anaconda environment. It took a skin MRI image as input with a shape of (384*384*1) and produced segmented categories (labels) with a shape of (384*384*6) as output. Each category represents a set of pixels that share the same class features, corresponding to the different skin layers. The training of the Dense-Net involved using a subset of our MRI dataset, consisting of 10 images with their corresponding manual segmented labels (masks). The model was trained to recognize different skin layers based on these labeled images and learn how to construct masks from the input MRI images. The goal of this training phase was to produce a well-trained model that can generalize well to new and unseen data. To evaluate the performance of the Dense-Net model, we used a validation set and a test set, which were separate from the training data set, to ensure unbiased evaluation. The validation set, consisting of 2 images, was used during the training phase to estimate the model's accuracy and optimize its performance. Once the training was completed, the model was tested on the test set, comprising 20 images, to assess its ability to accurately segment the skin layers in new and unseen data. The predicted outputs of the trained model were compared with the ground truth images obtained from manual segmentation to evaluate its performance.

The combination of U-Net and Dense-Net models allowed us to perform a comprehensive evaluation and comparison of the two architectures in skin MRI image segmentation, providing valuable insights into their strengths and limitations. The results and findings from these experiments will be further discussed and analyzed in the subsequent sections, highlighting the significance of our proposed segmentation approaches for dermatological research and clinical

applications.

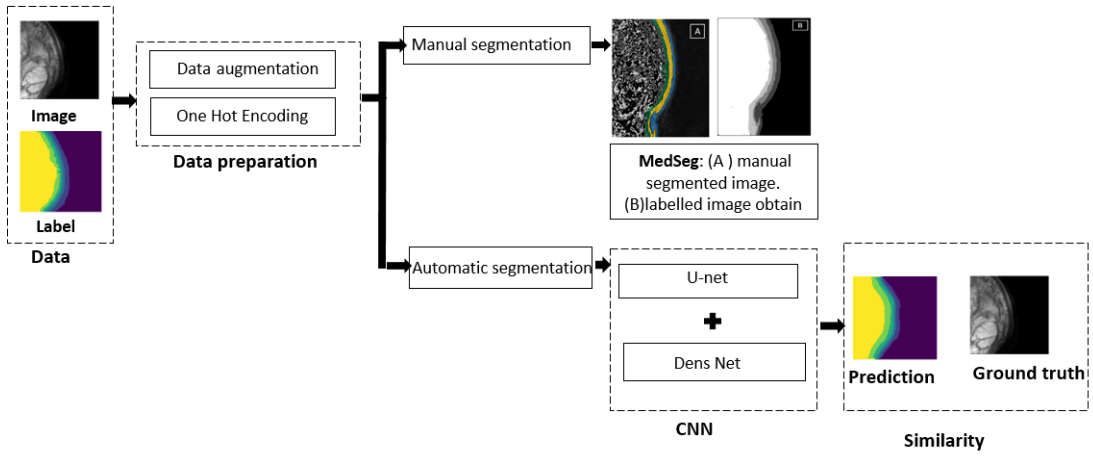

Figure 4.5.4: Segmentation approach.

To summarize the segmentation experiment conducted in this work using skin MRI data sets, figure 4.5.4 presents a diagram describing the segmentation process of our approach. The MRI skin image is fed into the Dense-Net model, which extracts features and predicts the segmented masks representing different skin layers. The predicted masks are then compared with the ground truth masks obtained from manual segmentation to evaluate the performance of the Dense-Net model in accurately segmenting the skin layers. The use of both U-Net and Dense-Net models allowed us to compare and evaluate the performance of each architecture in the skin segmentation task. The results and insights gained from these experiments are presented in the subsequent sections, showcasing the strengths and limitations of each approach and their potential impact on dermatological research and clinical applications.

In the last part of this section, we assess the similarity between the ground truth images (manual masks) and the predicted segmentation results obtained from our U-Net and Dense-Net models. Two commonly used metrics are calculated to validate the segmentation results, providing quantitative measures of accuracy and performance. The first metric used for validation is the Dice coefficient, also known as the Dice similarity coefficient (DSC). The Dice coefficient measures the spatial overlap between the predicted segmentation and the ground truth, quantifying the similarity between the two sets of pixels. It is defined as the ratio of twice the intersection of the two sets to the sum of their sizes. A Dice coefficient of 1 indicates

a perfect overlap between the predicted segmentation and the ground truth, while a coefficient of 0 indicates no overlap at all. The second metric employed for validation is the Jaccard index, also known as the Intersection over Union (IoU). The Jaccard index calculates the ratio of the intersection of the predicted segmentation and the ground truth to the union of their sizes. Like the Dice coefficient, the Jaccard index measures the spatial similarity between the two sets of pixels, with a value of 1 indicating perfect overlap and a value of 0 indicating no overlap. By calculating these two similarity metrics, we can quantitatively evaluate the accuracy of our segmentation models and compare their performance on the skin MRI images. Higher values of the Dice coefficient and Jaccard index indicate better segmentation results and stronger agreement between the predicted and ground truth segmentation.

The results of these similarity measurements provide valuable insights into the effectiveness of our proposed segmentation approaches based on U-Net and Dense-Net models. The comparison between the metrics for both models and the manual segmentation serves as a validation of our method's performance in accurately segmenting skin layers in MRI images. Additionally, the visual representation of the segmentation results supports the strong correlation between the predicted segmentation and the ground truth, confirming the reliability of our proposed approaches for skin MRI image segmentation.

4.5.1.3 Similarity measurements

The Dice similarity coefficient (DSC) is a commonly used metric to assess the accuracy and performance of segmentation results by measuring the spatial overlap between the predicted segmentation and the ground truth. It quantifies the similarity between two sets of pixels and provides a value between 0 and 1, with higher values indicating better segmentation results and stronger agreement between the predicted and ground truth segmentation.

The Dice index is calculated using the following formula:

$$DSC = \frac{2|X \cap Y|}{|X| + |Y|}. \tag{4.5.1}$$

Where, X is a set of images manually segmented and Y is a set of images automatically segmented. The DSC coefficient takes values in the interval in [0; 1]. The closer we get to the value 1, the better the segmentation.

The Hausdorff distance (HD) is a metric used to calculate the spatial dissimilarity between two sets of points or outlines, such as binary images. Huttenlocher et al. introduced this measurement in their work "Comparing images using the Hausdorff distance" published in IEEE Transactions on Pattern Analysis and Machine Intelligence. The HD distance has proven to be a valuable tool for assessing the similarity between images. In our research, we employ

the HD distance to evaluate the accuracy of our U-net model's segmentation. We measure the HD distance between the manually segmented masks (ground truth) and the masks predicted by our U-net model, both before and after the application of moisturization. This allows us to quantify the spatial differences between the two sets of masks [126].

Mathematically, the HD distance is defined as follows:

$$d_{\mathrm{H}}(X,Y) = \max\left\{\sup_{x\in X} d(x,Y), \sup_{y\in Y} d(X,y)\right\} \tag{4.5.2}$$

Where sup represents the supremum, inf the infimum, and $d(a,B) = \inf_{b\in B} d(a,b)$ quantifies the distance from a point $a \in X$ $a \in X$ to the subset $B \subseteq X, B \subseteq X$.

In our experimental evaluation, we calculated the mean Dice index coefficient and the mean Hausdorff distance to assess the performance of our deep automatic segmentation method compared to the manual segmentation method. Before the application of moisturization, the mean Dice index coefficient was found to be 0.79 with a confidence interval (CI) of [0.66-0.88]. This indicates a strong agreement between the ground truth manual segmentation and the segmentation achieved by our U-net model. After the application of moisturization, the mean Dice index coefficient slightly decreased to 0.75 with a CI of [0.61-0.89]. Despite this slight decrease, the Dice index coefficient still demonstrates a significant correlation between the two segmentation methods, affirming the reliability of our deep automatic segmentation approach. Similarly, we evaluated the mean Hausdorff distance, a measure of spatial dissimilarity between the manually segmented masks and the predicted masks by the U-net model. Before moisturization, the mean Hausdorff distance was 0.134, indicating a close spatial proximity between the two sets of masks. After moisturization, the mean Hausdorff distance increased to 0.226. This suggests a slightly larger spatial difference between the predicted and manual masks after the application of moisturization. However, the increase in Hausdorff distance remains within an acceptable range, further confirming the robustness and accuracy of our automatic segmentation method.

In summary, the results obtained from the evaluation of the mean Dice index coefficient and the mean Hausdorff distance demonstrate a significant and strong correlation between the manual and deep automatic segmentation methods. The U-net model shows a high capability to accurately segment skin MRI images and effectively capture the changes in skin hydration before and after the application of moisturization.

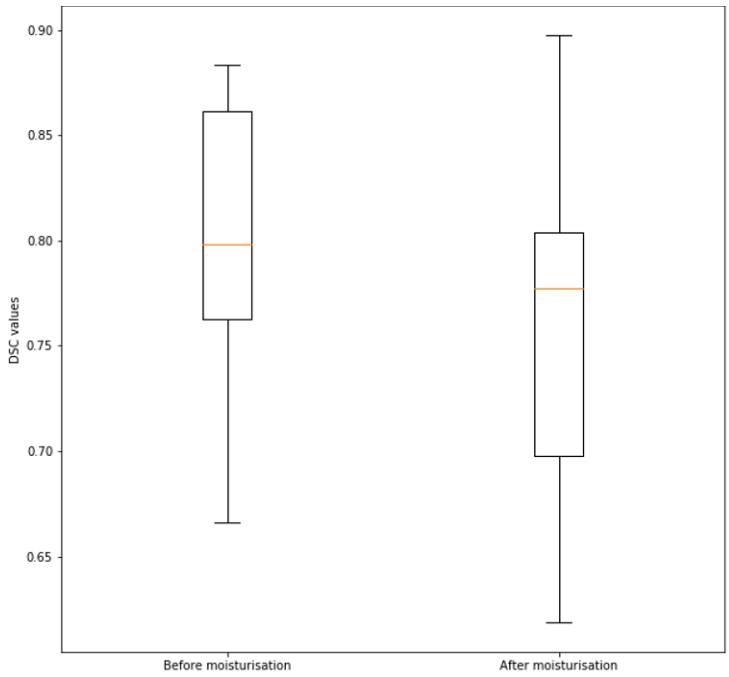

Figure 4.5.5: Box plot of the Dice values for segmented images before and after moisturization.

4.5.2 Experiment 2: Skin hydration measurements

In our skin hydration measurements experiment, the preparation of MRI images was a crucial step to ensure accurate and reliable evaluation of our approach, leading to scientifically valid results. To achieve this, we utilized T2 map cartographies as the basis for our analysis. T2 mapping is a technique used in MRI to quantify the relaxation times of water protons in tissues. In the context of skin hydration measurements, T2 mapping allows us to visualize and quantify the distribution of water content in different skin layers. The T2 map cartographics were generated from the MRI images, providing us with detailed information about the hydration levels in various regions of the skin. By utilizing T2 mapping, we obtained a more comprehensive understanding of the water behavior and content in live tissues, which is crucial for accurately studying the hydration effect in skin layers before and after the application of moisturizing cream. The T2 map cartographies served as a valuable tool for precisely quantifying the changes in hydration and comparing them between different skin regions.

In summary, the preparation of MRI images using T2 map cartographies was essential for the proper evaluation of our approach in skin hydration measurements. It enabled us to obtain

reliable and precise scientific results, facilitating a deeper insight into the hydration phenomena and its response to the application of moisturizing cream on different skin layers.

4.5.2.1 T2 mapping

The generation of T2 map cartographies from our MRI data is a crucial initial step in measuring skin hydration. T2 mapping allows us to detect changes in water content for each skin layer based on the sensitivity of MRI to biophysical properties of the skin. This technique provides a quantitative and noninvasive way to study the water distribution in different skin layers, which is essential for understanding the hydration levels. As discussed in Chapter 1, T2 mapping is a powerful tool in medical imaging, especially in dermatology, where it can be used to assess the skin's hydration status. By analyzing the T2 maps, we can identify variations in water content between different skin regions, and this information is highly valuable in evaluating the effectiveness of moisturizing creams. Figure 4.5.6 presents an example of T2 map generation from our MRI data, both before and after the application of moisturizing cream. These T2 maps visually depict the changes in water content in different skin layers, providing a clear representation of the hydration effect. Through the T2 map cartographies, we gain insights into how the skin responds to moisturization, allowing us to quantify and compare the hydration levels before and after treatment.

In conclusion, the generation of T2 map cartographies plays a crucial role in our skin hydration measurements. It offers a powerful and informative approach to study the water content of skin layers, enabling us to assess the impact of moisturizing creams and validate our proposed methodologies in a quantitative and reliable manner.

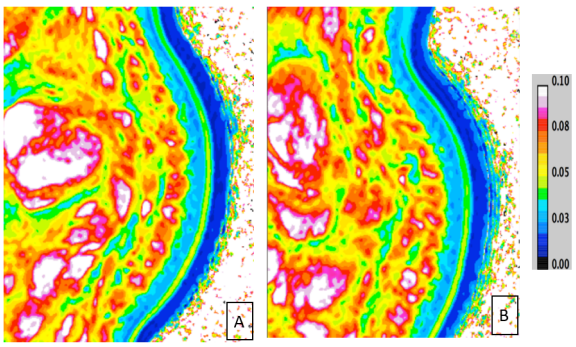

Figure 4.5.6: T2 mapping (seconds) calculation: (A) before and (B) 1 h after moisturizer application.

In our experiment, the main objective is to measure the hydration effect on the skin before and after the application of moisturizing cream. To achieve this, we collected data from twenty subjects and performed T2 mapping on their skin using MRI. The T2 mapping provided us with valuable information about the water content in different skin layers. After generating the T2 maps, we extracted the T2 values from each subject's skin for both the pre-moisturization and post-moisturization conditions. These T2 values represent the water content in various skin layers and serve as a quantitative indicator of the skin's hydration status.

Table 2 presents the collected T2 values for all twenty subjects before and after moisturization. By examining the T2 values, we can observe the changes in water content and assess the effectiveness of the moisturizing cream in maintaining or enhancing skin hydration. The comparison of T2 values before and after moisturization provides crucial insights into the hydration effect. Higher T2 values after moisturization indicate an increase in water content, suggesting improved skin hydration. Conversely, lower T2 values may indicate reduced water content and a potential need for further moisturization.

In summary, the measurement of T2 values through T2 mapping allows us to quantitatively evaluate the hydration effect on the skin. The collected data and comparison between pre-moisturization and post-moisturization T2 values provide valuable information for understanding the impact of moisturizing cream on skin hydration in our study.

Measurement	Layer	Variable	Mean value of T2
Manuel segmentation (whole layer)	S.C	(–)	0.0709
		(+)	0.0716
	Epidermis	(–)	0.0707
		(+)	0.0722
	Dermis	(–)	0.0707
		(+)	0.0730
Dense-Net (whole layer)	S.C	(–)	0.0436
		(+)	0.0599
	Epidermis	(–)	0.0477
		(+)	0.0541
	Dermis	(–)	0.0465
		(+)	0.0508
U-net (whole layer)	S.C	(–)	0.0731
		(+)	0.0745
	Epidermis	(–)	0.0742
		(+)	0.0726
	Dermis	(–)	0.0733
		(+)	0.0750

Table 4.3: T2 values of the different layers of the skin before moisturizer (–), after moisturizer (+), and the difference between before and after moisturizer application

In the T2 mapping process, we utilized the segmentation results from the U-net and Dens-Net models to identify and isolate different skin layers accurately. This allowed us to measure the T2 value for each segmented layer, quantifying the water content within specific regions of the skin.

The primary objective was to compare the T2 values before and after applying moisturizing cream for each skin layer, using both segmentation methods. This comparison enabled us to study the hydration effect at different depths within the skin and evaluate the performance of our segmentation approaches. By conducting this comparative analysis, we gained valuable insights into how the moisturizing cream influenced the water content in various skin layers. It also helped us assess the efficacy of our segmentation methods in measuring skin hydration accurately.

The T2 measurement and comparison of segmented skin layers provided a comprehensive analysis of skin hydration, contributing to our understanding of this phenomenon and the potential benefits of the moisturizing cream. Figure 4.5.7, (resp. 4.5.8, and 4.5.9) presented in box plots shows all T2 measurements obtained using manual method (resp. Dens-Net method, and CNN method) for each segmented skin layer.

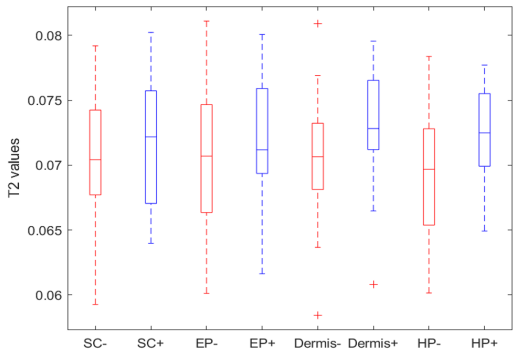

Figure 4.5.7: T2 values of manual segmentation method for each skin layer.

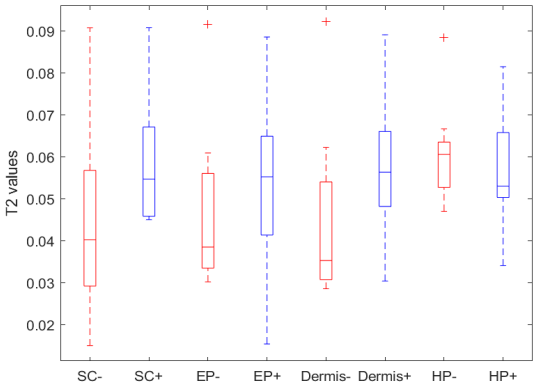

Figure 4.5.8: T2 values of Dens-Net method for each skin layer.

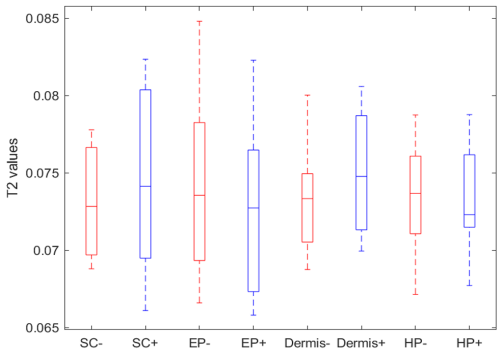

Figure 4.5.9: T2 values of U-net method for each skin layer.

4.5.3 Experiment 3: Skin registration method

The automated affine registration technique employed in our study is a common method used in medical image processing to align images from different time points or modalities. It involves finding the optimal transformation (translation, rotation, and scaling) that best aligns the images, allowing for a direct comparison of corresponding structures. In the context of our research, we used the automated affine registration to align the MRI images captured before and after the application of moisturizing cream. This alignment is essential to ensure that the corresponding skin regions in both images are correctly compared. To visualize the results of the registration and the effect of moisturization, we applied the registration transformation to the segmented image obtained after hydration (Figure 4.5.10B). By overlaying the registered segmented image onto the original MRI image after hydration, we were able to observe any changes or shifts in the skin layers. This visual assessment provided valuable insights into how the moisturizing cream affected the water distribution in different skin layers. It allowed us to see if there were any noticeable changes in the skin's hydration levels after applying the cream. Overall, the automated affine registration and the visual assessment of the registered segmented images helped us validate our segmentation results and study the impact of moisturization on the skin's hydration in a comprehensive manner.

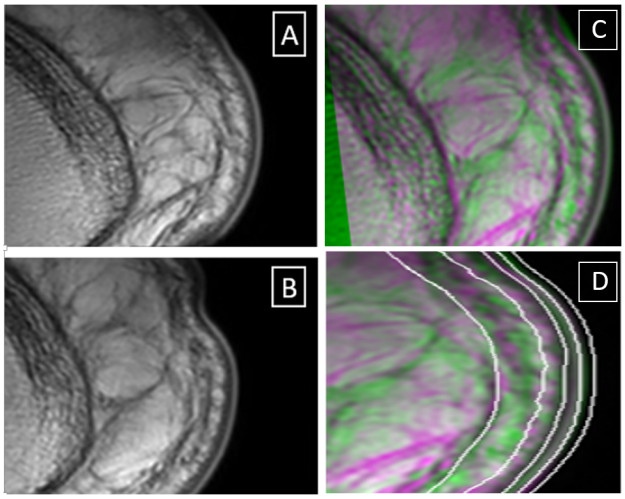

Figure 4.5.10: Registration. A, Second echo of the multi spin echo calculation T2-weighted sequence before moisturization. B, Second echo of the multi spin echo calculation T2-weighted sequence after moisturization.C, Registration of images A (fixed) and B (moving). D, highlighting the segmentation of B on image C.

4.5.4 Experiment 4: Artificial simulation of skin hydration phenomenon

In this experiment, we train the CNN model on pairs of images (input, output), where the input represents the MRI image before moisturization, and the output corresponds to the MRI image after moisturization. This setup allows the model to learn the transformation associated with the moisturization process. However, due to the nature of the auto encoder process, which requires a substantial amount of data to effectively capture underlying patterns, we have also implemented a data augmentation technique on our dataset. This augmentation process involves applying various transformations such as rotation, flipping, and scaling to the original images, effectively diversifying the dataset. This approach not only addresses the requirement for an extensive dataset but also aims to enhance the model's ability to generalize to different variations in moisturization effects. The practical impact of this augmentation can be seen in the comprehensive evaluation of the model's performance, as indicated in 4.5.11.

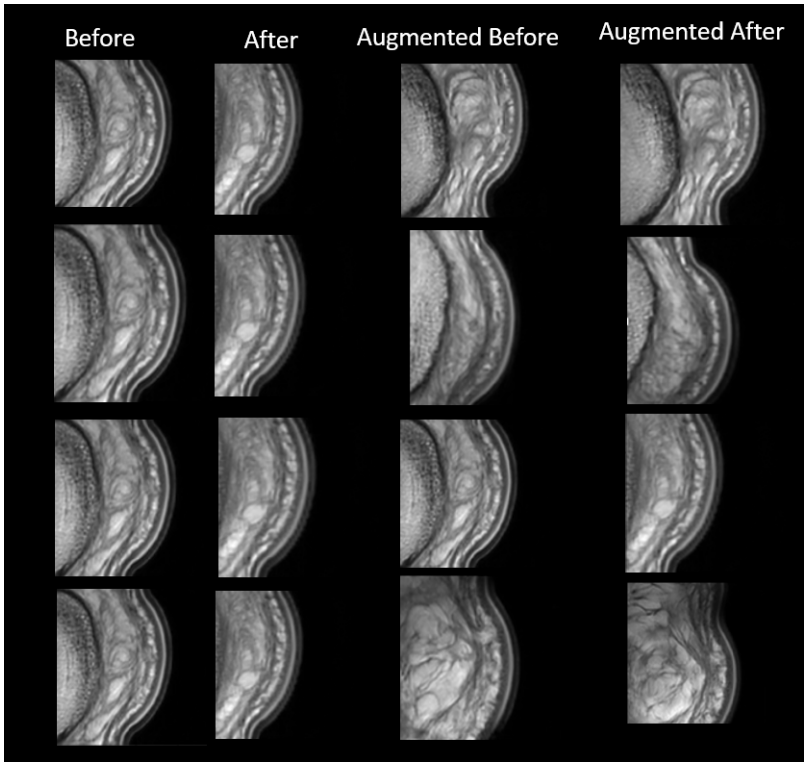

Figure 4.5.11: Auto encoder model

The primary concept is to enable the CNN auto-encoder model to learn the process of constructing MRI images after undergoing hydration, using labeled training data sets. Following the training phase, our model was subjected to testing, resulting in the generation of reconstructed images after moisturization. For the purpose of comparing the outcomes produced by the CNN auto-encoder model, we employed a method of enhancement (illustrated in figure 4.5.12 D). This enhancement was applied to the reconstructed image (depicted in figure 4.5.12 C), aligning it with the authentic image obtained after moisturization (shown in figure 4.5.12 E) from the auto-encoded image that was tested (represented in figure 4.5.12 A). Consequently, this highlighting technique serves to visualize and distinguish the distinct reconstructed skin layers as predicted by the CNN auto-encoder model. Evidently, our CNN auto-encoder model successfully reconstructs the image after hydration based on the image prior to the process. This underscores that our model has effectively grasped and emulated the skin hydration phenomenon, even when working with a relatively limited set of training data. However, it is important to note that the model's simulation results could potentially be enhanced further with a larger volume of training and validation data sets. The scalability of the training data

might likely lead to more accurate and realistic simulation outcomes.

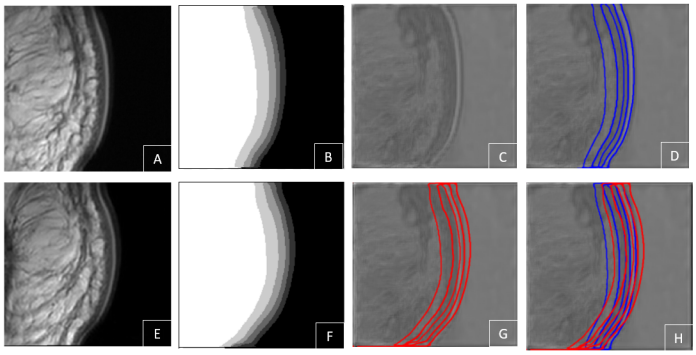

Figure 4.5.12: CNN model for hydration simulation : A: Second echo of the multi spin echo calculation T2-weighted sequence before moisturization, B U-net segmentation of A, C reconstructed image, D overlay of B on C, E: Second echo of the multi spin echo calculation T2-weighted sequence after moisturization. , F U-net segmentation of E, G overlay of F on C, H overlay of B (blue) and F(red) on C.

In terms of quantifying the accuracy of the model, we have relied on a distinct validation dataset that the network was not exposed to during the training process. As depicted in Figure 4.5.13, it is evident that the model converges effectively and demonstrates strong generalization capabilities. To evaluate the performance of the model, we employed the Kullback-Leibler Divergence loss function as a metric. This loss function measures the difference between the predicted and actual distributions, and we found it suitable for our purposes. Figure 4.5.13 illustrates the trajectory of both the validation loss and the training loss. Notably, these loss curves exhibit a synchronous behavior, indicative of a well-behaved model.

The convergence of both training and validation loss signifies that our model is not overfitting the training data. Specifically, the validation loss consistently decreases rather than increasing, and there is minimal disparity between the training and validation losses throughout the entire training phase. This outcome provides strong evidence that our model's generalization capability is robust, enabling it to accurately simulate the skin hydration phenomenon. In summary, the synchronization of training and validation loss, coupled with the model's effective convergence, validates the model's generalization prowess and its ability to successfully replicate the skin hydration phenomenon.

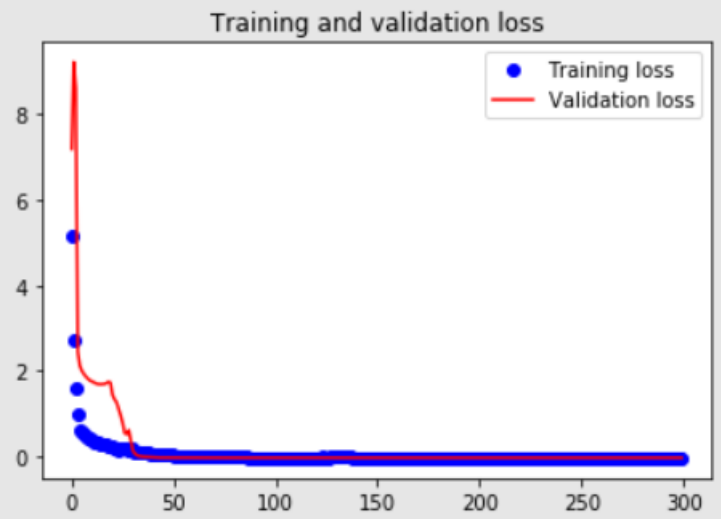

Figure 4.5.13: Training and validation loss of CNN model for hydration simulation.

4.6 Discussion

This study delves into the realm of skin hydration and moisturization, aiming to achieve a comprehensive understanding by quantifying hydration across distinct skin layers: the Stratum Corneum (SC), the Epidermis, and the Dermis. The segmentation of these skin layers was accomplished through the utilization of the **MedSeg** software, followed by manual T2 measurements for each layer using T2 mapping. However, the novel dimension of our work emerges from the incorporation of a deep learning Convolutional Neural Network (CNN) architecture, which enabled semantic segmentation of skin layers. This deep learning-driven approach was then juxtaposed with the established manual method for each skin layer. Despite the relatively modest size of the training dataset, the evaluation encompassed all MRI skin images, showcasing the model's aptitude for aligning with the intricate structural characteristics of the skin. The U-net model's training process, spanning 500 epochs, utilized augmented labeled data sets alongside a compact validation set. The yielded results were notably encouraging, boasting a commendable accuracy rate (up to 90%) coupled with a remarkably low loss percentage (below 10%). Visual validations, as depicted in Figure [insert Figure number], provided compelling evidence of the U-net model's effective learning as it generated masks closely mirroring their manual counterparts. To establish the extent of similarity, we employed the Dice similarity coefficient and the Hausdorff distance, revealing a strong agreement between labels and predicted output masks. As presented in Figure [insert Figure number], the Dice similar-

ity coefficient averages around 0.7 (CI:[0.66-0.88]), with a mean Hausdorff distance spanning from 0.1 to 0.2 mm. These metrics accentuate the model's capacity to faithfully reproduce the skin layer segmentation, demonstrating robust correlation across manual, automatic, and deep automatic methodologies. Following the segmentation of all data using the CNN model, mean T2 values before and after moisturization were computed for each segmented layer. The comprehensive results tabulated in Table 2 showcased consistent trends in T2 values before and after hydration. The observed increase in average T2 values post-hydration aligns with expectations. Importantly, the U-net model's generated values closely mirrored the manual reference, signifying its adeptness. Conversely, the results obtained through the Dense Net exhibited relatively more deviation from the manual reference (around 0.025%). On the other hand, the U-net model's results demonstrated remarkable consistency with the manual (approximately 0.001 %), validating the efficacy of our approach. It's worth noting that while various methods were explored, the focus here remained on U-net and Dense Net to primarily validate the chosen U-net architecture.

The application of the registration method enabled visualization of the hydration state and the segmented layers by overlaying MRI images before and after moisturization with segmentation outcomes, facilitating a comprehensive view of the moisture's impact. A pivotal challenge within this research was simulating the clinical hydration phenomenon with precision through deep learning, specifically employing the CNN model. The successful resolution of this challenge paved the way for generating artificial moisturization images from MRI data, as depicted in the figure. These images, synthesized by our CNN model, vividly capture the differentiation of skin layers, highlighting the profound potential of deep learning in such applications. Acknowledging that deep learning techniques can introduce noise, we emphasize that our exploration adds to the broader field of denoising methods, underscoring their relevance in varied tasks.

In conclusion, this study provides a holistic understanding of skin hydration through meticulous quantification and state-of-the-art segmentation techniques. The integration of deep learning, exemplified by U-net, not only showcases robust performance but also propels the field forward by offering an alternative to traditional manual methods.

4.7 Conclusion

Our deep learning approach for MRI skin segmentation exhibited robustness and yielded accurate T2 value representations, showcasing a high correlation with manual measurements. This was particularly evident when investigating the hydration of skin layers using high-resolution 3T MRI. The trio of segmentation methods we employed, all relying on T2 value calculations,

not only facilitated the quantification of water content within skin layers but also enabled the measurement of hydration levels within each layer. This ability proved essential for studying the effects of moisturization cream. In conclusion, this study successfully navigated the challenge of training efficient deep learning models with a limited dataset a common constraint in the medical domain. Moreover, our application of deep learning techniques allowed for the artificial simulation of the hydration phenomenon, a fundamental aspect of our investigation. It's important to note that deep learning methods do come with challenges, particularly concerning architecture depth selection. Given our modest dataset size, this issue posed a significant hurdle, but we adopted strategies like data augmentation and one-hot encoding to surmount it. U-net, being a deep learning model, can sometimes be perceived as a black box due to the complexity of interpreting its weights compared to other machine learning algorithms. Notably, our model's training and validation were executed on a relatively small training set consisting of 32 subjects, which may limit its generalizability for clinical routine applications. Furthermore, when contrasted with traditional machine learning approaches, deciphering the learned weights of neural networks remains a challenging task. This underlines the intricacies of deep learning interpretation as compared to more traditional techniques.

Conclusion and perspectives

This thesis represents a substantial stride forward in the domain of MRI-based skin analysis and hydration assessment. By meticulously exploring the capabilities of deep learning methodologies and conducting thorough validation procedures, this research has made notable contributions to both the understanding and application of advanced technologies in dermatological studies. The primary aim of this study was to develop a sophisticated framework capable of accurately segmenting skin layers and quantifying the impact of hydration using MRI data. Through the strategic adoption of Convolutional Neural Networks (CNNs) and the deployment of a U-net architecture, we achieved this objective with precision. The segmentation outcomes, which encompassed the intricate layers of the Stratum Corneum, Epidermis, and Dermis, underscored the potential of deep learning in effectively delineating complex anatomical structures within medical images. This accomplishment not only introduces a novel and non-invasive tool for assessing skin hydration but also validates the adaptability of CNN-based models in the demanding realm of medical image analysis. The robustness of our approach was demonstrated through meticulous validation against manual methods. The strong correlation observed between automated T2 measurements and manual assessments attests to the reliability and accuracy of our deep learning-driven technique. This validation process instills a sense of confidence in the clinical applicability of our methodology, empowering us to derive precise insights into the effects of various moisturization treatments. However, this achievement wasn't without its challenges. Addressing limited data sets, a common obstacle in medical image analysis, required innovative strategies. We harnessed the potential of data augmentation techniques and other methodologies to ensure meaningful results and the consistent performance of our models. While our approach successfully navigated these challenges, there remains ample opportunity for future research to optimize model architectures and address the interpretability concerns inherent in deep learning models. Looking forward, the implications of this research extend to promising directions for exploration. Expanding the dataset to encompass a broader spectrum of subjects and conditions could amplify the generalizability and clinical relevance of our approach. Additionally, delving into advanced interpretability techniques for deep learning models could enhance our understanding of their decision-making processes and augment trust

in their applications. In conclusion, this thesis stands as a testament to the potential of deep learning techniques to reshape the landscape of medical image analysis. Through the fusion of innovative methodologies and rigorous validation, we've demonstrated the capacity to precisely assess skin hydration and its multifaceted dynamics. As the study of skin health continues to evolve, this research provides a robust foundation for future advancements and innovations, propelling the field of dermatology research into an era characterized by data-driven insights and improved patient care.

Bibliography

[1] Stefanowska, J., Zakowiecki, D., and Cal, K. (2010). Magnetic resonance imaging of the skin. *Journal of the European Academy of Dermatology and Venereology*, 24(8), 875-880, 2010.

[2] Martinelli, D. (2022). Generative machine learning for de novo drug discovery: A systematic review. *Computers in Biology and Medicine*, 145, 105403.

[3] Kouanou, A. T., Tchiotsop, D., Kengne, R., Zephirin, D.T., Armele, N.M.A., Tchinda, R. (2018). An optimal big data workflow for biomedical image analysis. *Informatics in Medicine*, 11, 68-74.

[4] Shrivastava, A., Chakkaravathy, M., Shah, M.A. (2022). A Comprehensive Analysis of Machine Learning Techniques in Biomedical Image Processing Using Convolutional Neural Network. *2022 5th International Conference on Contemporary Computing and Informatics (IC3I)*, 22817211.

[5] Leite, M., Parreira, W.D., et al. (2022). A Comprehensive Analysis of Image Segmentation for Human Skin Detection. *Journal of Multidisciplinary Digital Publishing Institute*, 12(23), 12140.

[6] Farage, M.A., Han, S.S., et al. (2019). The Prevalence of Sensitive Skin. *Frontiers in Medicine*, 6, 98.

[7] Denis, A., Loustau, O., Chiavassa-Gandois, H., Vial, J., Lalande Champetier de Ribes, C., Railhac, J.J., Sans, N. (2008). IRM haute résolution de la peau : aspects normaux. *Journal de Radiologie, 2008*, 89(7-8), 873-879.

[8] Mirrashed, F., and Sharp, J.C. (2004). In vivo quantitative analysis of the effect of hydration (immersion and Vaseline treatment) in skin layers using high-resolution MRI and magnetisation transfer contrast. *Skin Research and Technology, 2004*, 10(1), 14-22.

[9] Stefanowska, J., Zakowiecki, D., and Cal, K. (2010). Magnetic resonance imaging of the skin. *Journal of the European Academy of Dermatology and Venereology, 2010*, 24(8), 875-880.

[10] Barcaui, E. de O., Carvalho, A. C. P., Pineiro-Maceira, J., Barcaui, C. B., and Moraes, H. (2015). Study of the skin anatomy with high-frequency (22 MHz) ultrasonography and histological correlation. *Radiologia Brasileira, 2015*, 48(5), 324-329.

[11] Bittoun, J., Querleux, B., and Darrasse, L. (2006). Advances in MR imaging of the skin. *NMR in Biomedicine, 2006*, 19(7), 723-730.

[12] Paus, R., Hamburg (2002). Controversies in Experimental Dermatology. *Experimental Dermatology, 2002*, 11(2), 159-187.

[13] Rodrigues, L., Palma, L., Tavares Marques, L., and Bujan Varela, J. (2015). Dietary water affects human skin hydration and biomechanics. *2015*, 413.

[14] Warner, R. R., Myers, M. C., and Taylor, D. A. (1988). Electron Probe Analysis of Human Skin: Determination of the Water Concentration Profile. *Journal of Investigative Dermatology, 1988*, 90(2), 218-224.

[15] Caspers, P. J., Bruining, H. A., Puppels, G. J., Lucassen, G. W., and Carter, E. A. (2001). In Vivo Confocal Raman Microspectroscopy of the Skin: Noninvasive Determination of Molecular Concentration Profiles. *Journal of Investigative Dermatology, 2001*, 116(3), 434-442.

[16] Verdier-Sévrain, S., and Bonté, F. (2007). Skin hydration: a review on its molecular mechanisms. *Journal of Cosmetic Dermatology, 2007*, 6(2), 75-82.

[17] Proksch, E., Folster-Holst, R., and Jensen, J.-M. (2006). Skin barrier function, epidermal proliferation and differentiation in eczema. *Journal of Dermatological Science, 2006*, 43(3), 159-169.

[18] Mirrashed, F., and Sharp, J. C. (2004). In vivo quantitative analysis of the effect of hydration (immersion and Vaseline treatment) in skin layers using high-resolution MRI and magnetisation transfer contrast. *Skin Research and Technology, 2004*, 10(1), 14-22.

[19] Stefanowska et al. (2010). Magnetic resonance imaging of the skin. *Journal of EADV, 2010*, 24(8), 875-880.

[20] Hendee, W., and Russell, E. (2003). Medical imaging physics. John Wiley & Sons.

[21] Bushberg, J. T., Seibert, J. A., Leidholdt, E. M., Boone, J. M., Mahesh, Mahadevappa. The Essential Physics of Medical Imaging, Third Edition. Medical Physics, 2013, 40(7), 077301.

[22] Plewes, D. B., and Kucharczyk, W. (2012). Physics of MRI: A primer. Journal of Magnetic Resonance Imaging, 35(5), 1038-1054.

[23] Beckmann, E. C. (2006). CT scanning the early days. The British Journal of Radiology, 79(937), 5-8.

[24] Chan, V. and Perlas, A. (2010). Basics of Ultrasound Imaging. In: Atlas of Ultrasound-Guided Procedures in Interventional Pain Management, 13-19.

[25] Bushberg, J. T., Seibert, J. A., et al. (2011). Comparison of the accuracy of human readers versus machine-learning algorithms for pigmented skin lesion classification. In: International Diagnostic Study, 2019.

[26] Bellazzi, R., Abu-Hanna, A., and Hunter, J. (Eds.) (2007). Artificial Intelligence in Medicine. Lecture Notes in Computer Science, 2007.

[27] Bellazzi, R., Abu-Hanna, A., and Hunter, J. (2007). Artificial Intelligence in Medicine. Lecture Notes in Computer Science, 4594, 978-1007.

[28] Plewes, D. B., and Kucharczyk, W. (2012). Physics of MRI: A primer. Journal of Magnetic Resonance Imaging, 35(5), 1038-1054.

[29] Lin DJ, Johnson PM, Knoll F, and Lui YW. (2020). Artificial Intelligence for MR Image Reconstruction: An Overview for Clinicians. Journal of Magnetic Resonance Imaging, 53(4), 1015-1028.

[30] Gaillard, F., Baba, Y., Bell, D., et al. (2023). MRI Sequences (Overview). Reference Article, Radiopaedia.org. Accessed on 24 May 2023.

[31] Yeung, J., Murphy, A., Bell, D., et al. (2023). Repetition Time. Reference Article, Radiopaedia.org. Accessed on 24 May 2023.

[32] Yeung, J., Jones, J., and Bell, D. (2023). Echo Time. Reference Article, Radiopaedia.org. Accessed on 24 May 2023.

[33] Wendt, M., and Melzer, A. (1999). Glossary: Magnetic resonance imaging. Minimally Invasive Therapy and Allied Technologies, 8(5), 343-346.

[34] Wild, J. M., Marshall, H., Bock, M., Schad, L. R., Jakob, P. M., Puderbach, M., and Biederer, J. (2012). MRI of the lung (1/3): methods. Insights into Imaging, 3(4), 345-353.

[35] Idy-Peretti, I. (2009). Évolution de límagerie par résonance magnétique. IRBM, 30(2), 53-59.

[36] Brandao, S., Seixas, D., Ayres-Basto, M., Castro, S., Neto, J., Martins, C., and Aboagye, E. O. (2013). Comparing T1-weighted and T2-weighted three-point Dixon technique with conventional T1-weighted fat-saturation and short-tau inversion recovery (STIR) techniques for the study of the lumbar spine in a short-bore MRI machine. Clinical Radiology, 68(11), 617-623.

[37] Maxime Descoteaux, D., Louis, C., and Kaleem, S. (2008). A geometric flow for segmenting vasculature in proton-density weighted MRI. Medical Image Analysis, 12(4), 497-513.

[38] Egger, J., Wild, D., Weber, M., et al. (2022). Studierfenster: an Open Science Cloud-Based Medical Imaging Analysis Platform. Digital Imaging Journal, 35, 340-355.

[39] Grover, V. P. B., Tognarelli, J. M., Crossey, M. M. E., Cox, I. J., Taylor-Robinson, S. D., and McPhail, M. J. W. (2015). Magnetic Resonance Imaging: Principles and Techniques: Lessons for Clinicians. Journal of Clinical and Experimental Hepatology, 5(3), 246-255.

[40] Goodwin, R. W., et al. (2007). MRI appearances of common benign soft-tissue tumours. Clinical Radiology, 62(9), 850-853.

[41] Alfageme Roldan, F. (2014). Ultrasound Skin Imaging. Actas Dermo-Sifiliograficas (English Edition), 105(10), 891-899.

[42] Humphreys, T. R., et al. (2017). The role of imaging in the management of patients with nonmelanoma skin cancer. Journal of the American Academy of Dermatology, 76(4), 591-607.

[43] Dias M, Hadgraft J, Glover PM, et al. (2003). Stray field magnetic resonance imaging: a preliminary study of skin hydration. Journal of Physics D: Applied Physics, 36, 364-368.

[44] Salter, D. C., Hodgson, R. J., Hall, L. D., Carpenter, T. A., and Ablett, S. (1993). Moisturization processes in living human skin studied by magnetic resonance imaging microscopy. International Journal of Cosmetic Science, 15(5), 219-226.

[45] Barral, J. K., Bangerter, N. K., Hu, B. S., and Nishimura, D. G. (2010). In vivo high-resolution magnetic resonance skin imaging at 1.5 T and 3 T. Magnetic Resonance in Medicine, 63(3), 790-796.

[46] Kim, R. H., and Armstrong, A. W. (2012). Nonmelanoma Skin Cancer. Dermatologic Clinics, 30(1), 125-139.

[47] van Zijl, P., Eleff, S., Ulatowski, J., et al. (1998). Quantitative assessment of blood flow, blood volume, and blood oxygenation effects in functional magnetic resonance imaging. Nature Medicine Journal, 4, 159-167.

[48] Bernheim, K. A. (2004). Functional and structural magnetic resonance imaging of humans and macaques. California Institute of Technology.

[49] Liao, Y., Oros-Peusquens, A. M., Lindemeyer, J., et al. (2019). An MR technique for simultaneous quantitative imaging of water content, conductivity, and susceptibility, with application to brain tumors using a 3T hybrid MR-PET scanner. Scientific Reports, 9(88).

[50] Stéphanie R, Bernard Q, et al. (1991). In-vivo proton relaxation times analysis of the skin layers by magnetic resonance imaging. Journal of Investigative Dermatology, 97(1), 120-125.

[51] Franconi F, Akoka S, Guesnet J, et al. (1995). Measurement of epidermal moisture content by magnetic resonance imaging: assessment of hydration cream. British Journal of Dermatology, 132(6), 913-917.

[52] Bernard Q, Bittoun J, et al. (1996). Measurement of epidermal moisture content. British Journal of Dermatology, 135(1), 144-5.

[53] Stéphanie R, Bernard Q, et al. (1996). Characterization of the Skin In Vivo by High Resolution Magnetic Resonance Imaging: Water Behavior and Age-Related Effects. Journal of Investigative Dermatology, 100(5), 705-709.

[54] Mesrar. J., Ognard.J., Garetier. M., et al. (2017). In vivo skin moisturizing measurement by high resolution 3 Tesla magnetic resonance imaging. Skin Research and Technology, 23, 289-294.

[55] Hockings, P. D., Hare, J. F., Reid, D. G., Dias, M., Hadgraft, J., and Glover, P. M.(2000). MRI instrumentation. In: Academic Press, London / San Diego, CA, 2000, 1372-1380.

[56] Kinsey, S.T., Moerland, T.S., McFadden, L., et al. (2000). Spatial resolution of transdermal water mobility using NMR microscopy. *Magn Reson Imaging, 1997*, 15, 939-947.

[57] Szayna, M., Kuhn, W. (1998). In vivo and in vitro investigations of hydration effects of beauty care products by high-field MRI and NMR microscopy. *J Eur Acad Dermatol Venereol, 1998*, 11, 122-128.

[58] Lohrke, J., Frenzel, T., Endrikat, J., et al. (2016). 25 Years of Contrast-Enhanced MRI: Developments, Current Challenges and Future Perspectives. *Advances in Therapy, 2016*, 33(1), 1-28.

[59] Nageotte, SJ., Lederman, RJ., Ratnayaka, K. (2020). MRI Catheterization: Ready for Broad Adoption. *Pediatric Cardiology, 2020.*

[60] Capelle-Laizé, AS. (2003). Segmentation des images IRM multi-échos tridimensionnelles pour la détection des tumeurs cérébrales par la théorie de l'évidence.
2003.

[61] Paulson, E. S., Erickson, B., Schultz, C., and Allen Li, X. (2015). Comprehensive MRI simulation methodology using a dedicated MRI scanner in radiation oncology for external beam radiation treatment planning. Medical Physics, 42(1), 28-39.

[62] Cho, S., Jones, D., Reddick, W. E., Ogg, R. J., and Steen, R. G. (1997). Establishing norms for age-related changes in proton T1 of human brain tissue in vivo. *Magnetic Resonance Imaging, 1997*, 15(10), 1133-1143.

[63] Susan M. N, Galen D. R., et al. (2010). Post-processing correction of the endorectal coil reception effects in MR spectroscopic imaging of the prostate. *Journal of Magnetic Resonance Imaging, 2010*, 32(3), 654-662.

[64] Ballester. M. A. G., Zisserman. A. P, Brady. M. (2002). Estimation of the partial volume effect in MRI. *Medical Image Analysis, 2002*, 6(4), 389-405.

[65] Barthel, H., Wilson, H., Collingridge, D. R., Brown, G., Osman, S., Luthra, S. K. Aboagye, E. O. (2004). In vivo evaluation of [18] fluoroetanidazole as a new marker for imaging tumour hypoxia with positron emission tomography. *British Journal of Cancer, 2004*, 90(11), 2232-2242.

[66] Hinton, G. E., Srivastava, N., Krizhevsky, A., et al. (2012). Improving neural networks by preventing co-adaptation of feature detectors. Department of Computer Science, University of Toronto.

[67] Long, J., Shelhamer, E., Darrell, T. (2015). Fully Convolutional Networks for Semantic Segmentation. Proceedings of the IEEE Conference on Computer Vision and Pattern Recognition (CVPR), 3431-3440.

[68] Laith, A., Zhang, J., Humaidi, A.J., et al. (2021). Review of deep learning: concepts, CNN architectures, challenges, applications, future directions. Journal of Big Data.

[69] Gu, J., Sun, B., et al. (2018). Consortium Blockchain-based Malware Detection in Mobile Devices. IEEE Access.

[70] Amrit, C., Paauw, T., Aly, R., and Lavric, M. (2017). Identifying child abuse through text mining and machine learning. Expert Systems with Applications, 88, 402-418.

[71] Hubel DH, and Wiesel TN. (1968). Receptive fields and functional architecture of monkey striate cortex. *J Physiol, 1968*, 195:215-243.

[72] Lecun, Y., Bottou, L., Bengio, Y.,and Haffner, P. (1998). Gradient-based learning applied to document recognition. *Proceedings of the IEEE, 1998*, 86(11):2278-2324.

[73] Deng, J., et al. (2009). ImageNet: A Large-Scale Hierarchical Image Database. *In 2009 IEEE Conference on Computer Vision and Pattern Recognition (CVPR), 2009*, 248-255.

[74] Glorot, X., and Bengio, Y. (2010). Understanding the difficulty of training deep feedforward neural networks. *In Proceedings of the Thirteenth International Conference on Artificial Intelligence and Statistics (AISTATS 2010)*, 249-256.

[75] He, K., Zhang, X., Ren, S., and Sun, J. (2015). Delving deep into rectifiers: Surpassing human-level performance on ImageNet classification. *In Proceedings of the IEEE International Conference on Computer Vision (ICCV 2015)*, 1026-1034.

[76] Bottou, L., Curtis, F. E., and Nocedal, J. (2018). *Optimization Methods for Large-Scale Machine Learning. SIAM Review*, 60(2), 223-311.

[77] Scherer, D., MÃŒller, A., and Behnke, S. (2010). *Evaluation of pooling operations in convolutional architectures for object recognition. International Conference on Artificial Neural Network, 2010*, 92-101.

[78] Glorot, X., Bordes, A., and Bengio, Y. (2011). *Deep Sparse Rectifier Neural Networks. In Proceedings of the Fourteenth International Conference on Artificial Intelligence and Statistics.*

[79] C. Luo, X. Li, L. Wang, J. He, D. Li, and J. Zhou (2018). *"How Does the Dataset Affect CNN-based Image Classification Performance?". In 5th International Conference on Systems and Informatics (ICSAI).* 361-366, doi: 10.1109/ICSAI.2018.8599448.

[80] Muhammad, I., and Yan, Z. (2015). *"SUPERVISED MACHINE LEARNING APPROACHES: A SURVEY." ICTACT Journal on Soft Computing, 5*(3).

[81] LeCun, Y., Jackel, L. D., Bottou, L., Cortes, C., Denker, J. S., et al. (1995). *Learning algorithms for classification: a comparison on handwritten digit recognition. Neural Netw Stat Mech Perspect, 1995*, 261-276.

[82] Krizhevsky, A., Sutskever, I., and Hinton, G. E. (2017). *Imagenet classification with deep convolutional neural networks. Commun ACM, 2017*, 60(6), 84-90.

[83] He, K., Zhang, X., Ren, S., and Sun, J. (2016). "Deep residual learning for image recognition." In Proceedings of the IEEE conference on computer vision and pattern recognition (pp. 770-778).

[84] Ronneberger, O., Fischer, P., and Brox, T. (2015). "U-net: Convolutional networks for biomedical image segmentation." In Medical Image Computing and Computer-Assisted Intervention-MICCAI 2015: 18th International Conference, Munich, Germany, October 5-9, 2015, Proceedings, Part III (pp. 234-241). Springer International Publishing.

[85] Kendall, A., Badrinarayanan, V., and Cipolla, R. (2015). "Bayesian segnet: Model uncertainty in deep convolutional encoder-decoder architectures for scene understanding." *arXiv preprint arXiv:1511.02680.*

[86] Huang, G., Liu, Z., Van Der Maaten, L., and Weinberger, K. Q. (2017). "Densely connected convolutional networks." In Proceedings of the IEEE conference on computer vision and pattern recognition (pp. 4700-4708).

[87] Tajbakhsh, N., Shin, J. Y., et al. (2016). *Convolutional Neural Networks for Medical Image Analysis: Full Training or Fine Tuning?. IEEE Transactions on Medical Imaging, 2016*, 35(5), 1299-1312.

[88] Cullell-Dalmau, M., Otero-Vinas, M., and Manzo, C. (2020). *Research Techniques Made Simple: Deep Learning for the Classification of Dermatological Images. Journal of Investigative Dermatology, 2020*, 140(3), 507-514.

[89] Narla, A., Kuprel, B., Sarin, K., Novoa, R., and Ko, J. (2018). *Automated Classification of Skin Lesions: From Pixels to Practice. Journal of Investigative Dermatology, 2018*, 138(10), 2108-2110.

[90] Codella, N., Gutman, D., et al. (2018). "Skin Lesion Analysis Toward Melanoma Detection: A Challenge at the 2017 International Symposium on Biomedical Imaging (ISBI), Hosted by the International Skin Imaging Collaboration (ISIC)." *Computer Vision and Pattern Recognition.*

[91] Codella, N., Junjie, C., Mani, A., et al. (2015). "Deep Learning, Sparse Coding, and SVM for Melanoma Recognition in Dermoscopy Images." *Machine Learning in Medical Imaging, 2015*, 9352, 118-126.

[92] Cullell-Dalmau, M., NoE.S, et al. (2021). *Convolutional Neural Network for Skin Lesion Classification: Understanding the Fundamentals Through Hands-On Learning. Frontiers in Medicine, 2021*, 8.

[93] Codella, N. C. F., Gutman, D., Celebi, M., et al. (2018). "Skin lesion analysis toward melanoma detection: A challenge at the 2017 International symposium on biomedical imaging (ISBI), hosted by the international skin imaging collaboration (ISIC)." *IEEE 2018 IEEE 15th International Symposium on Biomedical Imaging - Washington, DC, USA, 2018*, 168-172.

[94] Tschandl, P; Codella, N, Akay, B. N, et al. (2019). "The Essential Physics of Medical Imaging (3rd ed.)." *Lippincott Williams & Wilkins, 2011.*

[95] Goyal, M., Oakley, A., Bansal, et al. (2020). "Skin Lesion Segmentation in Dermoscopic Images With Ensemble Deep Learning Methods." *IEEE Access, 2020*, 8, 4171-4181.

[96] Kawahara, J., AND Hamarneh, G. (2019). "Visual diagnosis of dermatological disorders: human and machine performance." *arXiv preprint arXiv:1906.01256.*

[97] Goyal, M., Knackstedt, T., Yan, S., and Hassanpour, S. (2020). "Artificial intelligence-based image classification methods for diagnosis of skin cancer: Challenges and opportunities." *Computers in Biology and Medicine*, 127, 104065.

[98] Zhang, X., Pan, W., et al. (2018). *In-Vivo Skin Capacitive Image Classification Using AlexNet Convolutional Neural Network. IEEE 3rd International Conference on Image, Vision and Computing (ICIVC), 2018.*

[99] Drozdzal, M., Vorontsov, E., Chartrand, G., Kadoury, S., Pal, C. (2016). "The importance of skip connections in biomedical image segmentation." In: DLMIA. Vol. 10008 of Lect Notes Comput Sci, 179-187.

[100] Baghersalimi, S., Bozorgtabar, B., et al (2019). "DermoNet: densely linked convolutional neural network for efficient skin lesion segmentation." *J Image Video Proc, 2019.*

[101] Goyala, S., Bozorgtabar, B., et al. (2019). "Skin Lesion Segmentation in Dermoscopic Images with Ensemble Deep Learning Methods." *arXiv preprint arXiv*, 206-210.

[102] Yading Y, Yeh-Chi L, et al. (2017). "Improving Dermoscopic Image Segmentation With Enhanced Convolutional-Deconvolutional Networks." *IEEE Journal of Biomedical and Health Informatics*, 519-526.

[103] Lei, B., Dagan, F., and Jinman, K. (2018). "Improving Automatic Skin Lesion Segmentation using Adversarial Learning based Data Augmentation." *Computer Vision and Pattern Recognition, 2023.*

[104] Mirikharaji, Z., Abhishek, K., et al. (2023). "A survey on deep learning for skin lesion segmentation." *Medical Image Analysis, 2023*, 88, 102863.

[105] Bozorgtaba et al. (2017). "Investigating deep side layers for skin lesion segmentation." *IEEE International Symposium on Biomedical Imaging, 2017.*

[106] Pathana, S., Prabhub, G., et al. (2018). "Techniques and algorithms for computer aided diagnosis of pigmented skin lesions - A review." *Biomedical Signal Processing and Control, 2018*, 237-262.

[107] Hasan, M. D., et al. (2021). "DSNet: Automatic dermoscopic skin lesion segmentation." *Computers in Biology and Medicine, 2021.*

[108] Lameski, J., Jovanov, A., et al. (2019). "Skin lesion segmentation with deep learning." *IEEE EUROCON 2019 - 18th International Conference on Smart Technologies, 2019.*

[109] Jafari, M. H., Karimi, M., et al. (2016). "Skin lesion segmentation in clinical images using deep learning." *International Conference on Pattern Recognition, 2016.*

[110] Mishra, R., Daescu, O. (2017). "Deep learning for skin lesion segmentation." *IEEE International Conference on Bioinformatics and Biomedicine (BIBM), 2017.*

[111] Vesal, S., Ravikumar, N., et al. (2018). "SkinNet: A Deep Learning Framework for Skin Lesion Segmentation." *IEEE Symposium on Nuclear Science (NSS/MIC), 2018.*

[112] Tang, Peng, et al. (2019). "SkinNet: Efficient skin lesion segmentation using separable-U-net with stochastic weight averaging." *Computer Methods and Programs in Bio-medicine, 2019.*

[113] Al Nazi, Z., Azad, T., et al. (2019). "Automatic Skin Lesion Segmentation and Melanoma Detection: Transfer Learning Approach with U-Net and DCNN-SVM." *Proceedings of International Joint Conference on Computational Intelligence, 2019.*

[114] Phan, T., Kim, S., et al. (2021). "Skin Lesion Segmentation by U-Net with Adaptive Skip Connection and Structural Awareness." *Appl. Sci, 2019.*

[115] Yue, Z., et al. (2022). "Feature Fusion for Segmentation and Classification of Skin Lesions." *IEEE International Symposium on Biomedical Imaging, 2022.*

[116] Zhang, X., Pan, W., and Xiao, P. (2018). "In-vivo skin capacitive image classification using AlexNet convolution neural network." In *2018 IEEE 3rd International Conference on Image, Vision and Computing (ICIVC)* (pp. 439-443). IEEE.

[117] Zhang, X., Pan, W., Bontozoglou, C., Chirikhina, E., Chen, D., and Xiao, P. (2019). "Skin Capacitive Imaging Analysis Using Deep Learning GoogLeNet." In *Proceedings of the Computing Conference, London, UK, 16-17 July 2019.*

[118] Liaqat, S., Dashtipour, K., Zahid, A., et al. (2021). "A review and comparison of the state-of-the-art techniques for atrial fibrillation detection and skin hydration." *Frontiers in Communications and Networks, 2*, 679502.

[119] Darlenski, R., Sassning, S., Tsankov, N., and Fluhr, J. W. (2009). "Non-invasive in vivo methods for investigation of the skin barrier physical properties." *European Journal of Pharmaceutics and Biopharmaceutics, 72(2)*, 295-303.

[120] Han, S. S., and al. "Augmented intelligence dermatology: Deep neural networks empower medical professionals in diagnosing skin cancer and predicting treatment options for 134 skin disorders." *Journal of Invest Dermatol, 2020.*

[121] Mirdehghan, A., Nosraty, H., Shokrieh, M. M., Ghasemi, R., and Akhbari, M. (2019). "Micromechanical modelling of the compression strength of three-dimensional integrated woven sandwich composites." *Journal of Industrial Textiles, 48(9)*, 1399-1419.

[122] Li, J., Garfinkel, J., Zhang, X., Wu, D., Zhang, Y., De Haan, K., ... and Ozcan, A. (2021). "Biopsy-free in vivo virtual histology of skin using deep learning." *Light: Science & Applications, 10(1)*, 233.

[123] Wang, Q., Jin, Y., Deng, X., Liu, H., Pang, H., Shi, P., and Zhan, Z. (2015). "Second-harmonic generation microscopy for assessment of mesenchymal stem cell-seeded acellular dermal matrix in wound-healing."

[124] Ognard, J., Mesrar,J., and Benhoumich, Y.Edge detector based automatic segmentation of the skin layers and application to moisturization in high-resolution 3 Tesla magnetic resonance imaging. Skin Research and Technology,2018. 25 (3)-346.

[125] Weibin, R. , Zhanjing, li. , et al. An improved Canny edge detection algorithm . IEEE International Conference on Mechatronics and Automation.,2014 *Biomaterials, 53*, 659-668.

[126] D. P. Huttenlocher, G. A. Klanderman, and W. J. Rucklidge, "Comparing images using the Hausdorff distance," *IEEE Transactions on Pattern Analysis and Machine Intelligence*, vol. 15, no. 9, pp. 850–863, 1993.

Abstract: In the ever-advancing biomedical field, the acquisition of medical imaging data has reached unprecedented levels. However, the increasing volume of clinical data poses challenges in terms of manual analysis and interpretation. To address this issue, computerized approaches can be employed to automate tasks, aid in decision-making, and expedite examinations. Artificial Intelligence (AI) has emerged as a powerful tool in clinical applications, offering accuracy, speed, reliability, and interpretability. This thesis aims to tackle the challenge of employing AI in the biomedical field by analyzing existing work and proposing innovative techniques for skin MRI image analysis using Deep Learning (DL) networks.

Our approach involves utilizing real skin MRI data to achieve two main objectives. The first objective focuses on skin hydration measurements, specifically quantifying the hydration level of the feet before and after the application of moisturizing cream. This is accomplished through T2 mapping cartography, combining semantic segmentation of MRI skin images into different layers using U-Net and Dense-Net architectures. The second objective utilizes a CNN auto-encoder network to simulate the skin hydration phenomena, enabling the creation of an artificial hydration process. Additionally, we visualize and present the results of our experiments using image registration methods. The outcomes of our study demonstrate significant improvements in skin hydration experiments. By harnessing DL networks such as U-Net, Dense Net, and CNN auto-encoders, our proposed approaches contribute to the advancement of skin MRI image analysis and provide valuable insights into the dynamics of skin hydration. The integration of AI techniques in skin MRI image analysis has the potential to automate laborious tasks, assist physicians in decision-making, and enhance the efficiency of examinations. This thesis addresses the challenges involved in deploying AI in the biomedical field, paving the way for high-quality healthcare applications that prioritize accuracy, speed, reliability, and interpretability.

Résumé : Dans le domaine biomédical en constante évolution, l'acquisition de données d'imagerie médicale a atteint des niveaux sans précédent. Cependant, le volume croissant de données cliniques pose des défis en termes d'analyse manuelle et d'interprétation. Pour résoudre ce problème, des approches informatisées peuvent être utilisées pour automatiser les tâches, aider à la prise de décision et accélérer les examens. L'intelligence artificielle (IA) s'est révélée être un outil puissant dans les applications cliniques, offrant précision, rapidité, fiabilité et interopérabilité. Cette thèse vise à relever le défi d'utiliser l'IA dans le domaine biomédical en analysant les travaux existants et en proposant des techniques innovantes pour l'analyse d'images d'IRM cutanée en utilisant des réseaux d'apprentissage profond (Deep Learning - DL).Notre approche consiste à utiliser de véritables données d'IRM cutanée pour atteindre deux objectifs principaux. Le premier objectif se concentre sur les mesures d'hydratation de la peau, en quantifiant spécifiquement le niveau d'hydratation des pieds avant et après l'application d'une crème hydratante. Cela est accompli grâce à la cartographie T2, en combinant la segmentation sémantique des images d'IRM de la peau en différentes couches à l'aide des architectures U-Net et Dense Net. Le deuxième objectif utilise un réseau auto-encodeur de type CNN pour simuler les phénomènes d'hydratation de la peau, permettant ainsi de créer un processus artificiel d'hydratation. De plus, nous visualisons et présentons les résultats de nos expériences à l'aide de méthodes d'enregistrement d'images. Les résultats de notre étude démontrent des améliorations significatives dans les expériences d'hydratation de la peau. En utilisant des réseaux DL tels qu'U-Net, Dense Net et les auto-encodeurs CNN, nos approches proposées contribuent à l'avancement de l'analyse d'images d'IRM cutanée et fournissent des informations précieuses sur la dynamique de l'hydratation de la peau. L'intégration des techniques d'IA dans l'analyse d'images d'IRM cutanée a le potentiel d'automatiser les tâches laborieuses, d'aider les médecins dans la prise de décision et d'améliorer l'efficacité des examens. Cette thèse aborde les défis liés au déploiement de l'IA dans le domaine biomédical, ouvrant la voie à des applications de soins de santé de haute qualité qui privilégient la précision, la rapidité, la fiabilité et l'interopérabilité.

ملخص: في المجال الطبي الذي يتقدم باستمرار، وصل اكتساب بيانات التصوير الطبي إلى مستويات غير مسبوقة. ومع ذلك، تشكل الزيادة في حجم البيانات السريرية تحديًا فيما يتعلق بالتحليل اليدوي والتفسير. للتعامل مع هذه المشكلة، يمكن استخدام النهج المحوسب لتوطين المهام، والمساعدة في اتخاذ القرار، وتسريع الفحوص. يعد الذكاء الاصطناعي أداة قوية في التطبيقات السريرية، مما يقدم الدقة والسرعة والموثوقية وقابلية التفسير. تهدف هذه الأطروحة إلى معالجة التحدي المتمثل في استخدام الذكاء الاصطناعي في المجال الطبي عن طريق تحليل الأعمال الموجودة واقتراح تقنيات مبتكرة لتحليل صور الرنين المغناطيسي للجلد باستخدام شبكات التعلم العميق. تشتمل طريقتنا على استخدام بيانات واقعية لتحقيق هدفين رئيسيين. يركز الهدف الأول على قياس ترطيب الجلد، وتحديدًا قياس مستوى الترطيب للأقدام قبل وبعد وضع كريم الترطيب. يتم ذلك من خلال رسم الخرائط، ودمج تجزئة صور الرنين المغناطيسي للجلد إلى طبقات مختلفة باستخدام هندسيات التعلم العميق. يستخدم الهدف الثاني شبكة ترميز تلقائية لمحاكاة ظواهر ترطيب الجلد، مما يسمح بإنشاء عملية ترطيب اصطناعية. بالإضافة إلى ذلك، نعرض نتائج تجاربنا باستخدام طرق تسجيل الصور.

تظهر نتائج دراستنا تحسينات معتبرة في تجارب ترطيب الجلد. من خلال استغلال شبكات التعلم العميق وتساهم الطرق المقترحة ايضا في تحليل صور الرنين المغناطيسي للجلد وتقديم نظرة قيمة على ديناميكيات ترطيب الجلد. إن دمج تقنيات الذكاء الاصطناعي في تحليل صور الرنين المغناطيسي للجلد لديه القدرة على أتمته المهام المرهقة ومساعدة الأطباء في اتخاذ القرار وتعزيز كفاءة الفحوص. في هذا النطاق تعالج هذه الأطروحة التحديات المتعلقة باستخدام الذكاء الاصطناعي في المجال الطبي، مما يمهد الطريق لتطبيقات الرعاية الصحية عالية الجودة التي تعطي الأولوية للدقة والسرعة والموثوقية وقابلية التفسير.